Journal of Pathology and Translational Medicine

J Pathol Transl Med
pISSN: 2383-7837
eISSN: 2383-7845

Volume 49, Number 1, January 2015

CONTENTS

CONTENTS CONTINUED

Instructions for Authors for *Journal of Pathology and Translational Medicine* are available at http://jpatholtm.org/authors/authors.php.

Journal of Pathology and Translational Medicine 2015; 49: 1-4
http://dx.doi.org/10.4132/jptm.2014.11.17

TdT+ T-Lymphoblastic Proliferation in Castleman Disease

Chang Gok Woo · Jooryung Huh

Department of Pathology, Asan Medical Center, University of Ulsan College of Medicine, Seoul, Korea

The concept of indolent T-lymphoblastic proliferation (iT-LBP) was introduced by Velankar *et al.*[1] as the proliferation of immature terminal deoxynucleotidyl transferase (TdT)+ T cells in extrathymic tissue without the involvement of bone marrow or peripheral blood.[2] Although the histopathologic features and the immunophenotype are similar to T-lymphoblastic lymphoma (T-LBL), iT-LBP is a benign proliferation of thymocytes that requires no treatment.[1-3]

Here, we report a case of iT-LBP in association with hyaline vascular-type Castleman disease in the retroperitoneum of a Korean female. A 37-year-old woman presented with right lower quadrant pain. Abdominal computed tomography scan demonstrated a well-defined homogeneous enhancing mass in the retroperitoneum (Fig. 1A). Laparotomy was performed and the mass was resected. Grossly, the resected mass (6.3×4.8×3.1 cm) was well-demarcated, round, and rubbery-firm. The cut surface was pinkish-yellow and fleshy, exhibiting central fibrosis (Fig. 1B). Microscopically, there was a small amount of proliferation of follicles of various shapes and sizes, and expansion of the interfollicular regions with sinus obliteration (Fig. 1C). Follicles demonstrated expanded mantle zones with onion skinning, regressed germinal centers with hyperplastic follicular dendritic cells reactive for CD21, radially penetrating blood vessels, and few follicle center cells (Fig. 1D–F). Many follicles contained more than one germinal center. The interfollicular region was filled with hyperplastic high endothelial venules, hyalinizing fibrosis, and an admixture of plasma cells, eosinophils, immunoblasts, plasmacytoid dendritic cells, and lymphocytes. In addition, there were multiple nodular and diffuse areas of lymphoid cell infiltration in the interfollicular and perifollicular regions, which were composed of small- to medium-sized cells with a high nuclear/cytoplasmic ratio and slightly irregular nuclei with open chromatin and inconspicuous nucleoli (Fig. 2A, B). These cells were immunoreactive for TdT, CD3, CD4, and CD8, but negative for CD20 (Fig. 2C, D). The Ki-67 labeling index was also high (Fig. 2F). Some of the large cells in the interfollicular and perifollicular area appeared similar to dysplastic follicular dendritic cells; consequently, follicular dendritic cell sarcoma was considered. However, these cells were negative for CD21, CD23, or CD35. Systemic work-up revealed no evidence of lymphoma involvement. Polymerase chain reaction study of the T-cell receptor gamma genes using BIOMED-2 primers (Invivoscribe, San Diego, CA, USA) failed to produce evidence of monoclonal rearrangement (Fig. 2G). A provisional diagnosis of iT-LBP associated with hyaline vascular-type Castleman disease was established and the patient was observed without any further treatment. On three-month follow-up, the patient was free from disease.

A total of ten cases of iT-LBP associated with Castleman disease have been reported in the literature, with or without follicular dendritic cell tumor (FDCT) and various caricinomas. iT-LBP most commonly involves the lymph nodes, where it invades interfollicular/parafollicular areas without effacement of the architecture.[2-5] The cells are small to medium sized with blastic chromatin, and exhibit frequent mitotic figures without significant atypia or prominent nucleoli. The typical immunophenotype involves immature cortical thymocytes, expression of CD3 and TdT, coexpression of CD4 and CD8, and variable expression of other T-cell antigens (CD2, CD5, and CD7). iT-LBP may also exhibit CD10, CD99, and CD1a expression, but

Corresponding Author
Jooryung Huh, M.D.
Department of Pathology, Asan Medical Center, University of Ulsan College of Medicine, 88 Olympic-ro 43-gil, Songpa-gu, Seoul 138-736, Korea
Tel: +82-3010-4553, Fax: +82-472-7898, E-mail: jrhuh@amc.seoul.kr

Received: September 5, 2014 **Revised:** October 24, 2014
Accepted: November 17, 2014

pISSN 2383-7837
eISSN 2383-7845

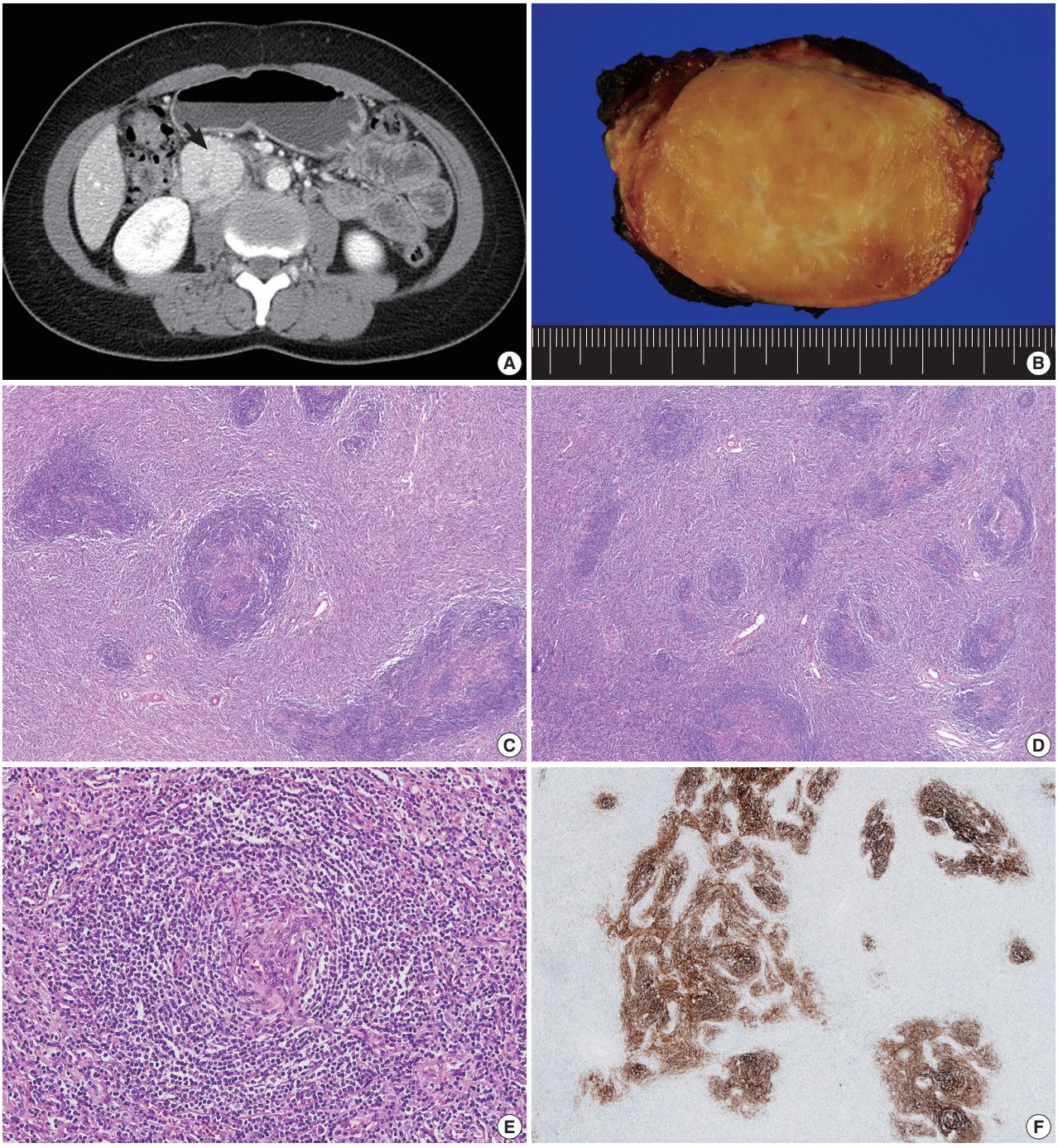

Fig. 1. Hyaline vascular-type Castleman disease. (A) Abdominal computed tomography demonstrates a well-defined homogeneous enhancing mass (arrow) in the retroperitoneum. (B) The mass exhibits a fleshy cut surface with central fibrosis. (C) Variably-sized follicles with multiple germinal centers are present. The interfollicular compartment is expanded with vascular proliferation. (D) Follicular structures appear smaller due to the regression of germinal centers. (E) Mantle zone lymphocytes have a laminated appearance, similar to onion skin. The vessel penetrating the atrophic follicle has a lollipop-like appearance. (F) Hyperplastic follicular dendritic cells are stained with CD21.

lacks CD34 or B-cell markers. The Ki-67 labeling index is high. The possibility of ectopic thymic tissue can be ruled out by the absence of cytokeratin-staining epithelial cells. Ohgami *et al.*[3] reported that the presence of TdT-positive T cells is not rare in lymph nodes with Castleman disease, FDCT, and angioimmunoblastic T-cell lymphoma, and that these cells are rarely noticeable on hematoxylin and eosin sections, although they are usually present at low density in a scattered distribution. Occa-

http://dx.doi.org/10.4132/jptm.2014.11.17

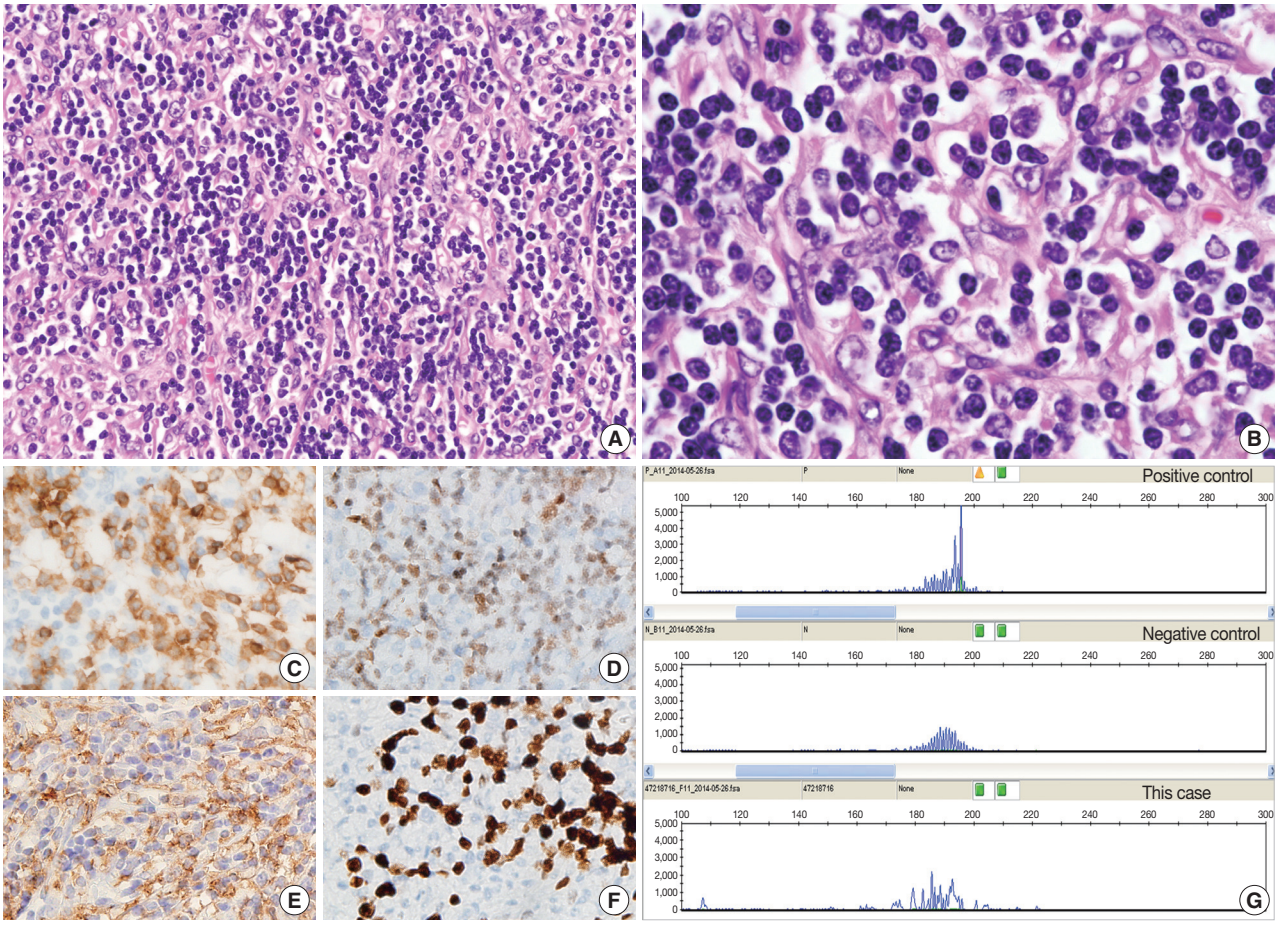

Fig. 2. Indolent T-lymphoblastic proliferation (iTLBP). (A) Nodular and diffuse areas of monotonous lymphoid cell infiltration in the interfollicular and perifollicular regions. (B) The cells show blastic nuclei with open chromatin and inconspicuous nuclei. (C–F) Cells are immunopositive for CD3 (C), terminal deoxynucleotidyl transferase (D), and CD33 (E), and have an increased Ki-67 labeling index (F). (G) Polymerase chain reaction study of the T-cell receptor gamma genes using BIOMED-2 primers shows no evidence of monoclonality.

sionally, they will form dense patches or tumors, and may mimic T-LBL with TdT positivity and a high Ki-67 labeling index. In contrast to T-LBL, which is a malignant monoclonal process that may involve peripheral blood, bone marrow, and the thymus, with tissue effacement, iT-LBP does not involve peripheral blood, bone marrow, or the thymus. In lymph nodes, iT-LBP does not lead to the tissue effacement typical of lymphomatous growth. A recent study indicated that iT-LBP could involve multiple lymph nodes and show partial CD33 expression.[5] In this case, immunopositivity for CD33 was also observed (Fig. 2E); however, node effacement as absent and the structure was preserved.

How immature lymphocytes localize and proliferate outside the context of thymic epithelial support remains unclear.[3,4] We suppose that immature T cells released from the thymus travel via the peripheral blood and eventually reach the lymph nodes. In a state of immune system dysfunction, these immature cells may proliferate like mature lymphocytes.

It is essential that clinicians are aware of this entity in order to avoid a misdiagnosis of T-LBL and consequent unnecessary treatment. Careful examination of morphologic features, immunochemical staining, molecular study, extent of involvement, and clinical course can contribute to the differentiation of iT-LBP from T-LBL.

Conflicts of Interest

No potential conflict of interest relevant to this article was reported.

REFERENCES

1. Velankar MM, Nathwani BN, Schlutz MJ, *et al.* Indolent T-lymphoblastic proliferation: report of a case with a 16-year course without cytotoxic therapy. Am J Surg Pathol 1999; 23: 977-81.

2. Ohgami RS, Arber DA, Zehnder JL, Natkunam Y, Warnke RA. Indolent T-lymphoblastic proliferation (iT-LBP): a review of clinical and pathologic features and distinction from malignant T-lymphoblastic lymphoma. Adv Anat Pathol 2013; 20: 137-40.
3. Ohgami RS, Zhao S, Ohgami JK, *et al.* TdT+ T-lymphoblastic populations are increased in Castleman disease, in Castleman disease in association with follicular dendritic cell tumors, and in angioimmunoblastic T-cell lymphoma. Am J Surg Pathol 2012; 36: 1619-28.
4. Qian YW, Weissmann D, Goodell L, August D, Strair R. Indolent T-lymphoblastic proliferation in Castleman lymphadenopathy. Leuk Lymphoma 2009; 50: 306-8.
5. Ohgami RS, Sendamarai AK, Atwater SK, *et al.* Indolent T-lymphoblastic proliferation with disseminated multinodal involvement and partial CD33 expression. Am J Surg Pathol 2014; 38: 1298-304.

http://dx.doi.org/10.4132/jptm.2014.11.17

Journal of Pathology and Translational Medicine 2015; 49: 5-12
http://dx.doi.org/10.4132/jptm.2014.10.24

■ REVIEW ■

Molecular Imaging in the Era of Personalized Medicine

Kyung-Ho Jung · Kyung-Han Lee

Department of Nuclear Medicine, Samsung Medical Center, Sungkyunkwan University School of Medicine, Seoul, Korea

Received: October 24, 2014
Accepted: October 24, 2014

Corresponding Author
Kyung-Han Lee, M.D.
Department of Nuclear Medicine, Samsung Medical Center, 81 Irwon-ro, Gangnam-gu, Seoul 135-710, Korea
Tel: +82-2-3410-2630
Fax: +82-2-3410-2639
E-mail: khnm.lee@samsung.com

Clinical imaging creates visual representations of the body interior for disease assessment. The role of clinical imaging significantly overlaps with that of pathology, and diagnostic workflows largely depend on both fields. The field of clinical imaging is presently undergoing a radical change through the emergence of a new field called molecular imaging. This new technology, which lies at the intersection between imaging and molecular biology, enables noninvasive visualization of biochemical processes at the molecular level within living bodies. Molecular imaging differs from traditional anatomical imaging in that biomarkers known as imaging probes are used to visualize target molecules-of-interest. This ability opens up exciting new possibilities for applications in oncologic, neurological and cardiovascular diseases. Molecular imaging is expected to make major contributions to personalized medicine by allowing earlier diagnosis and predicting treatment response. The technique is also making a huge impact on pharmaceutical development by optimizing preclinical and clinical tests for new drug candidates. This review will describe the basic principles of molecular imaging and will briefly touch on three examples (from an immense list of new techniques) that may contribute to personalized medicine: receptor imaging, angiogenesis imaging, and apoptosis imaging.

Key Words: Molecular imaging; Individualized medicine; Receptor; Angiogenesis; Apoptosis

CLINICAL IMAGING AND PATHOLOGY

Clinical imaging is the art (and technique) of creating visual representations of the interior of a body for clinical assessment of disease. Although distinctly separate disciplines, clinical imaging and pathology actually overlap substantially in their roles in medical practice, i.e., both are used to detect and diagnose diseases, identify therapeutic targets, and predict treatment responses and patient outcomes. As such, the routine diagnostic workflows for patients with various diseases are deeply dependent on both imaging and pathology. The hallmark of the pathologist's trade is to reveal abnormalities in tissues removed from the body using a microscope. Similarly, medical imaging specialists visualize and assess abnormal lesions in living bodies using specialized instruments. Depending on the type of signal picked up from the body interior, these instruments include computed tomography (CT), magnetic resonance imaging (MRI), ultrasonography, gamma scintigraphy, and positron emission tomography (PET).

Imaging and pathology contribute substantially to clinical practice by providing diagnoses and monitoring disease progression. Today, we are witnessing a radical shift in the way diseases are managed: from the present one-fits-all approach to one that delivers medical care tailored to the needs of individual patients.[1] This includes the detection of disease predisposition, early diagnosis, prognosis assessment, measurement of drug efficacy and disease monitoring. A crucial key for the success of this new healthcare paradigm is powerful molecular diagnostics.[2] Thus, the introduction of personalized medicine is creating an unprecedented opportunity for new technology development in fields of diagnostic medicine including pathology and imaging. The essence of diagnostic medicine in the context of personalized medicine lies in the use of biomarkers, objective indicators of pathogenic processes or pharmacologic effects that can be incorporated to predict or monitor treatment responses. Whereas markers have come mostly from patient tissues or serum, the location and activity of important markers can also be tracked with new imaging technologies. Such imaging tests may characterize diseases and assess treatment efficacy, with the added advantage of noninvasive longitudinal monitoring at multiple time points. The recent explosion of molecular biology and imaging technologies is now allowing quantitative characterization of biological processes inside the body at the molecular and genetic level. This exciting new field is envisioned to trans-

pISSN 2383-7837
eISSN 2383-7845

form the future of medicine on a massive scale and have an enormous impact on the advancement of targeted therapies for individualized medicine. This innovative new technique is referred to as "molecular imaging."

EMERGENCE OF MOLECULAR IMAGING

Molecular imaging emerged amidst the overflowing innovations from new discoveries made in the field of molecular biotechnology. Unlike conventional imaging that relies on visualizing late consequences of pathologic alterations, molecular imaging interrogates the very molecular events that drive disease processes.[3,4] It can thus be defined as "noninvasive imaging and quantification of molecular and biochemical events that occur at the cellular and molecular level in tissues in their normal surroundings inside living bodies." Noninvasive examination of cells inside living subjects by molecular imaging is critically dependent on biomarker probes that target key proteins linked to disease processes. This is analogous to the dependence of immunohistochemical staining of extracted tissue on special antibodies that bind to proteins-of-interest. In both situations, biomarker probes are used to identify key molecules that provide a more complete diagnostic picture for the referring physician (Fig. 1).

The clinical benefits of molecular imaging are immense. At the top of the list is the promise of early disease detection and prediction of treatment response, which will lead to optimal therapies for individual patients. Molecular imaging is already having a substantial impact on therapeutic decisions made by clinicians, and this will be even more apparent as individualized treatment becomes the norm of clinical practice. Another important contribution will be in drug development, which typically requires expensive and prolonged preclinical and clinical trials to bring new drugs to market. Molecular imaging has the ability to noninvasively monitor the pharmacokinetic properties and pharmacodynamic changes of candidate drugs in the living body.[5] This can substantially shorten the development phase of drug production for the pharmaceutical industry by assessing drug response substantially earlier than by using anatomic criteria.

MOLECULAR IMAGING PROBES

Deriving noninvasive information regarding molecular events within the body can be done by tracking the temporal and spatial distribution of a marker probe that has high target specificity and behaves favorably *in vivo*. Therefore, the first and most pivotal step in molecular imaging research is the design and synthesis of superior probes that can interrogate important molecular targets.[6] Such probes are fundamentally different from contrast agents that are used in conventional imaging, which are nonspecific agents that increase the contrast of the blood pool. Molecular imaging probes are beacons that depict and enhance epitopes of key proteins that would otherwise be impos-

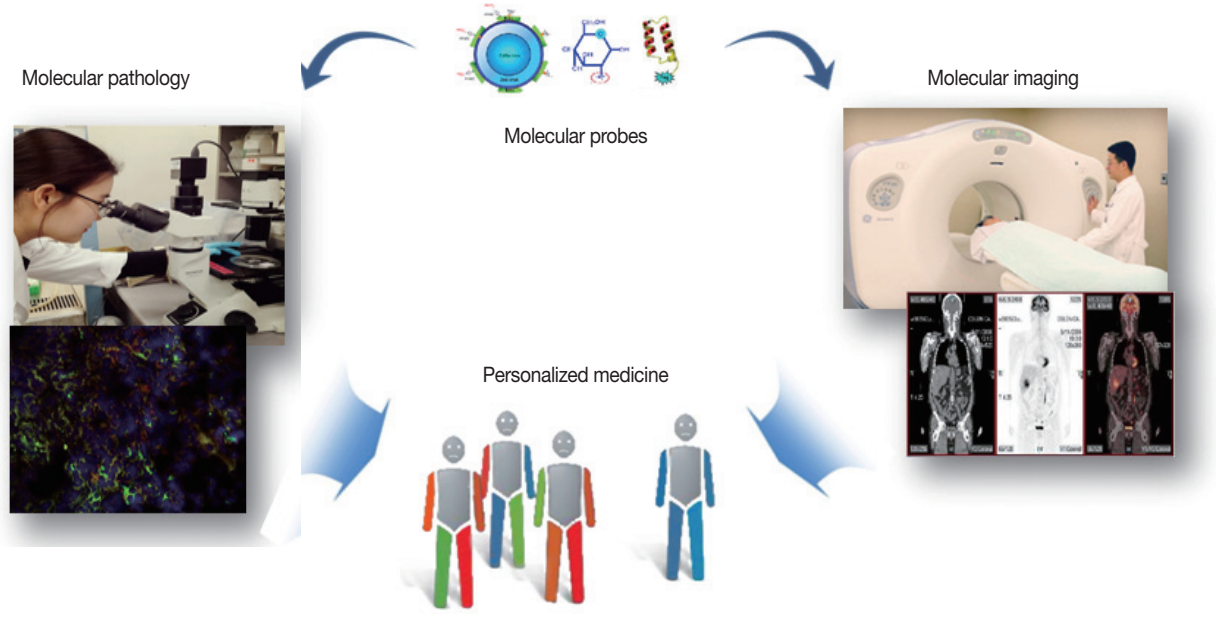

Fig. 1. Similarity of molecular imaging and pathology in utilizing probes to contribute to personalized medicine.

http://dx.doi.org/10.4132/jptm.2014.10.24

sible to distinguish from surrounding tissue. Molecular imaging probes thus consist of a targeting component and a signaling component. Targeting moieties have traditionally been based on small molecules. More recently, however, advancements have introduced new classes of molecular imaging probes, including peptides, proteins, antibodies, aptamers, affibodies, and nanoparticles. Direction of the moieties to target molecules is provided by specific ligands that are included as part of the agents or are surface-decorated. A signaling component is conjugated or labeled to the moieties so that they can be detected from outside of the body. Signals emitted can be radioactive, magnetic, echogenic, luminescent or fluorescent (Fig. 2A). Ideal molecular imaging probes should have low nonspecific binding, high selectivity for the process-of-interest, high *in vivo* stability, and favorable *in vivo* pharmacokinetics. They should also have a good safety profile so that clinical translation is possible.

MOLECULAR IMAGING INSTRUMENTS

The second requirement for molecular imaging is specialized instruments that detect signals from probes in sensitive and accurate manners. Depending on the type of signal, modalities used in the clinic include CT, MRI, ultrasonography, optical imaging devices, gamma scintigraphy, and PET (Fig. 2B). Among these, clinical molecular imaging has traditionally been the domain of nuclear medicine. Indeed, molecular imaging has been in clinics for some time in the form of radionuclide imaging. Radioactive probes can track specific molecules in living bodies in a safe and hyper-sensitive manner. PET is already an indispensable clinical imaging tool and is the most mature molecular imaging technique in routine clinical use.[7]

PET has superior sensitivity and spatial resolution over gamma scintigraphy. It also has quantitative capabilities and high tissue penetration depth, making it the preferred molecular imaging modality in the clinic. The signaling component of PET probes is composed of positron-emitting radioisotopes including ^{18}F, ^{11}C, and ^{15}O, which are the major constituents of the building blocks of life. The positrons decay with a relatively short physical half-life of minutes to hours, and immediately collide with an electron to annihilate into two photons. These two photons proceed in exactly opposite trajectories but with identical energies, which makes it possible to pinpoint their location with high accuracy. Unlike PET, gamma scintigraphy detects probes that emit gamma-ray photons. Although more affordable than PET, it is less sensitive and has lower spatial resolution. Because PET can provide truly quantitative molecular information and is readily applicable to humans, it is a major driver of personalized medicine.[7]

Other imaging modalities are also speedily entering into molecular imaging research. Magnetic resonance (MR) is a versatile modality that uses powerful magnets and radiofrequency signals to provide images with high temporal and spatial resolution. MR images have excellent tissue contrast with an unlimited depth of tissue penetration and can simultaneously acquire anatomical structure and physiological function information. Limitations include weak magnetic signals and relatively low sensitivity, which requires administration of contrast agents and signal amplification strategies. Ferromagnetic agents such as super-paramagnetic iron oxide reduce signals in T2-weighted images (negative contrast), whereas paramagnetic agents such as gadolinium–diethylenetriamine pentaacetic acid increase signals in T1-weighted images (positive contrast). MR probes have

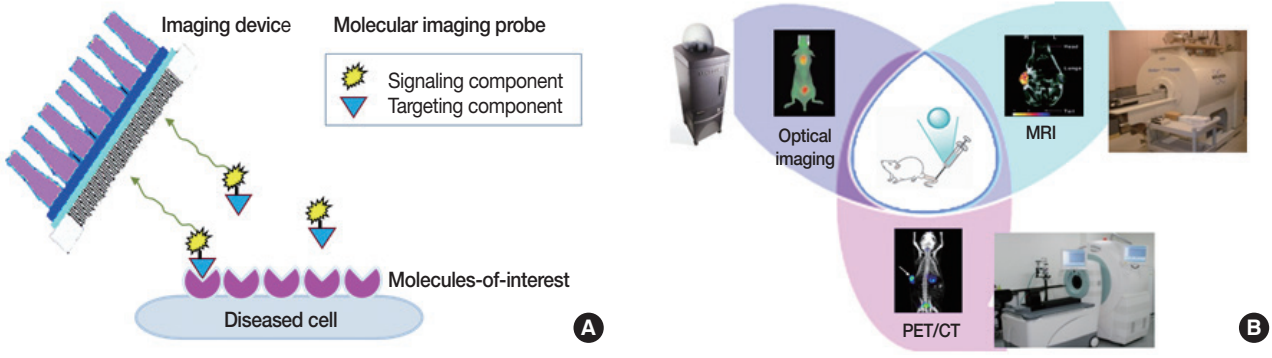

Fig. 2. Basic principles of molecular imaging. (A) Molecular imaging probes containing targeting components that interact with molecules-of-interest and signaling components that allow detection from outside of the body. (B) Representative small animal-dedicated molecular imaging devices that visualize signals emitted from probes within the living bodies of animal models. PET-CT, positron emission tomography–computed tomography; MRI, magnetic resonance imaging.

been developed that can interrogate molecular processes in a small number of cells.[8] A major problem for clinical translation of most of these techniques, however, is the issue of potential toxicity that arises from the relatively large doses of probe administration required.

CT provides 3-dimensional X-ray images of structural anatomy. Although iodinated contrast agents improve soft tissue contrast, they require large quantities and are not target-specific. In this sense, CT does not fit in the list of bonafide molecular imaging methods. However, recent small animal dedicated micro-CT instruments have provided ultra-high resolution, and have transformed preclinical CT from visualization of the organ level to the molecular level.[9] CT is usually combined with PET for molecular imaging. Recent developments in CT contrast agents offer increasing potential, but further studies will be required to explore its molecular imaging capability.

Optical imaging is based on light signals emitted from fluorescent or bioluminescent probes. It is safe, has high sensitivity, and is widely available. The main disadvantage is that low photon energies limit the penetration depth to a few centimeters, which makes it unsuitable for clinical use except for surface targets. However, this is not a problem for small experimental animals, where it is widely used for preclinical research and drug development.[10] Bioluminescence imaging exploits photons produced by enzymatic reaction of luciferase with its substrate. Several types of enzymes, including Firefly, Renilla and Gaussia luciferase, each require different conditions for reaction. Since mammalian tissues do not have endogenous bioluminescence, luminescent imaging has excellent signal to background ratios. Fluorescence imaging takes advantage of fluorescent signals that are typically emitted from genetically encoded reporter proteins. A celebrated example is the Nobel-prize winning green fluorescence protein reporter. Fluorescence imaging can also be employed by administering fluorophore-tagged probes to visualize molecular events in living cells. The strengths of fluorescence imaging include low cost, potential for multiplexed imaging, and, in the case of reporter protein, no need for probe administration.

EXAMPLES OF MOLECULAR IMAGING TECHNIQUES

While a vast number of molecular imaging techniques are in preclinical development or in the process of clinical translation, several have already entered the clinical arena. These techniques tend to use radiolabeled probes, which is due to their superior sensitivity and high safety profile. PET using radiolabeled fluorodeoxyglucose (FDG), a glucose analogue avidly taken up by cancer cells, is by far the most widely employed clinical molecular imaging test. FDG PET has virtually revolutionized cancer management, including tumor diagnosis, staging, and monitoring of treatment response.[7] Other examples include PET using radiolabeled ^{18}F-fluorothymidine, a thymine analogue biomarker of cell proliferation, and PET using radiolabeled Pittsburgh compound B, a biomarker of amyloid plaques in Alzheimer's disease.

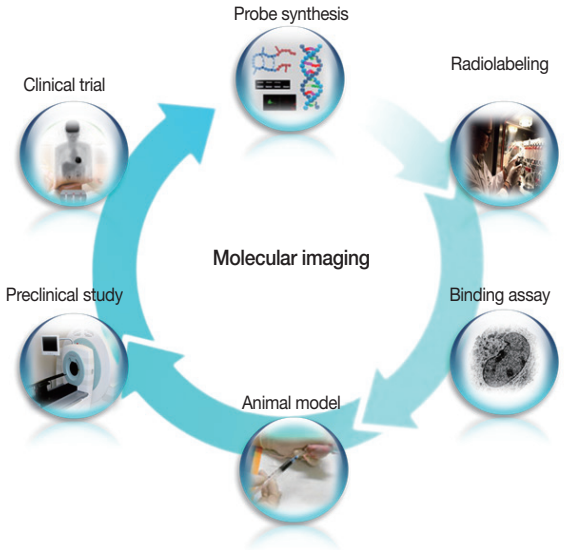

Fig. 3. The overall process of molecular imaging research, which is similar to that of new drug development.

In addition, a vast list of newer molecular imaging techniques are in the process of clinical translation for evaluation of malignant, neurologic, cardiovascular, and inflammatory diseases. In keeping with the overall molecular imaging development process illustrated in Fig. 3, various novel imaging targets have been identified for which arrays of imaging biomarkers are being designed and synthesized. Following verification of target-specific binding and favorable *in vivo* pharmacokinetics, the probes are then tested for efficacy in preclinical animal models and finally in human subjects. As it is impossible to touch on all of these new techniques, which number in the hundreds, we will briefly look at just three examples among the many new molecular imaging techniques that are anticipated to contribute to personalized medicine. For other areas of molecular imaging, readers are asked to refer to the many excellent reviews on specific subjects.

Tumor receptor imaging

The next decade will see an individual's tumor biology char-

http://dx.doi.org/10.4132/jptm.2014.10.24

acterized at the molecular level by noninvasive imaging applications. An example is imaging of tumor receptor expression to identify promising therapeutic targets and delineate pharmacologic effects. The ability to measure receptor expression by imaging rather than by histologic inspection has the advantages of noninvasiveness, ability to assess sites difficult to sample, and potential for serial monitoring over time or after drug treatment. Importantly, it also allows assessment of the entire disease burden and avoids sampling errors from biopsies when receptor expression is heterogeneous. Overexpression of growth factor receptors in cancers leads to aberrant stimulation of growth signaling pathways, and their evaluation may thus help predict the efficacy of targeted drugs.

Growth receptors have high binding affinities and can become saturated by even small molar quantities of binding ligands. Therefore, imaging probes need to have especially high signal density. The most success has been achieved with probes based on receptor-specific ligands or antibodies.[11] In comparison, probes based on tyrosine kinase inhibitors are challenging due to the ubiquity of tyrosine kinase expression and the requirement for intracellular transport. Radiolabeled fragments of trastuzumab have shown feasibility for imaging regional HER2 expression in animal models.[12] Our group demonstrated high-contrast epidermal growth factor (EGF) receptor imaging using a quantum dot probe multiplexed with EGF as a ligand for high affinity binding and radiolabels for scintigraphic imaging.[13] The technique was able to discriminate high from low receptor expression and monitor tumor response to targeted treatment (Fig. 4). Other studies include imaging of estrogen receptors and somatostatin receptors.[11] Similar technologies may be transferable to human subjects in the near future to monitor the adequacy of targeted anti-cancer therapies.

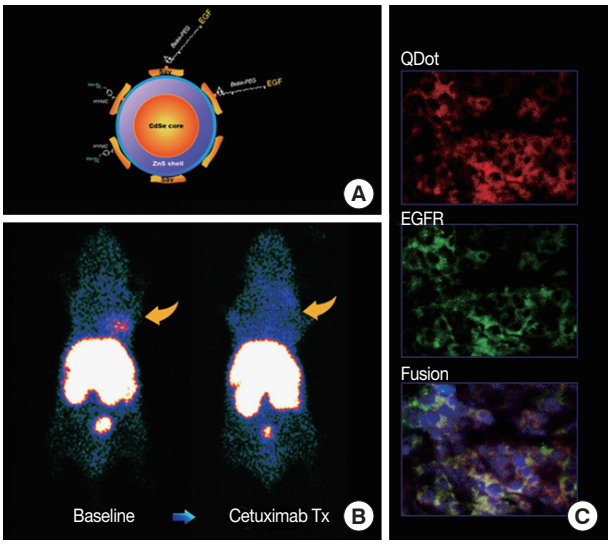

Fig. 4. Example of tumor receptor imaging. (A) Quantum dot (QDot) probe surface-conjugated with epidermal growth factor (EGF) for targeting and radioisotopes for signaling. (B) A human breast cancer xenograft shows high probe uptake at baseline that is blocked by cetuximab therapy (Tx). (C) Tumor tissue sections show co-localization of fluorescent signals from the QDot with that from fluorescent-conjugated antibodies against EGF receptors (EGFR), indicating receptor-specific probe targeting.

Angiogenesis imaging

Many pathologic processes involve inflammatory and ischemic responses that stimulate signaling for angiogenesis and apoptosis. Progression of tumor growth is highly dependent on remodeling of the vascular network through angiogenesis, as is the healing process following ischemic injury. As such, angiogenesis is receiving a large amount of attention as a potential target for treating tumors as well as ischemic diseases. Because the response to such targeted therapies cannot be readily assessed by conventional methods, there is a need for an imaging biomarker that can visualize and monitor changes in angiogenesis over time.

Potential biologic targets for angiogenesis imaging include markers of activated endothelial cells and extracellular matrix.[14,15] Among various targets, including vascular endothelial growth factor receptors and matrix metalloproteinases, the most successful to date is the αvβ3 integrin receptor, a member of a family of heterodimeric cell-surface receptors highly up-regulated at sites of neovascularization. These receptors recognize the tripeptide Arg-Gly-Asp (RGD) sequence as their binding motif. Hence, a large series of cyclic RGD-containing peptide compounds have been synthesized, labeled with different radioisotopes or fluorophores, and characterized as probes for angiogenesis imaging.[14,15] Our lab developed a radiolabeled RGD probe with high affinity binding to αvβ3 integrin, and imaging in mice showed high contrast tumor uptake that was reduced by anti-angiogenic treatment in a manner correlating to reduced integrin expression and tumor growth retardation.[16] In addition, we were among the first to show that RGD imaging can also monitor angiogenic responses of ischemic limbs[17] and myocardial tissue (Figs. 5, 6). More recently, RGD PET has been moving toward clinical translation,[15] with clinical studies taking place in Europe that are showing the feasibility and safety of radiolabeled galacto-RGD and AH111585 for delineating integrin-positive tumors. Furthermore, clinical studies with radiolabeled FPPRGD2 have demonstrated good lesion contrast in cancer patients.

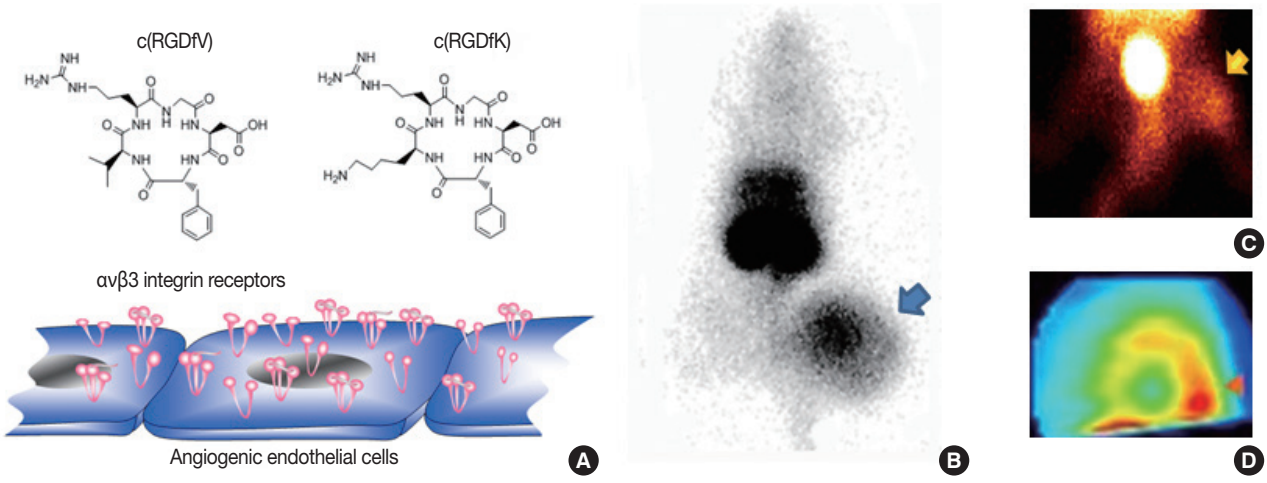

Fig. 5. Example of angiogenesis imaging. (A) Cyclic Arg-Gly-Asp (RGD) peptide probes can interrogate αvβ3 integrin receptors overexpressed on activated endothelial cells. (B–D) Examples of a xenografted tumor-bearing mouse model (B), a hindlimb ischemia mouse model (C), and a myocardial infarction rat model (D) showing increased uptake of radiolabeled RGD probes in lesions with angiogenesis.

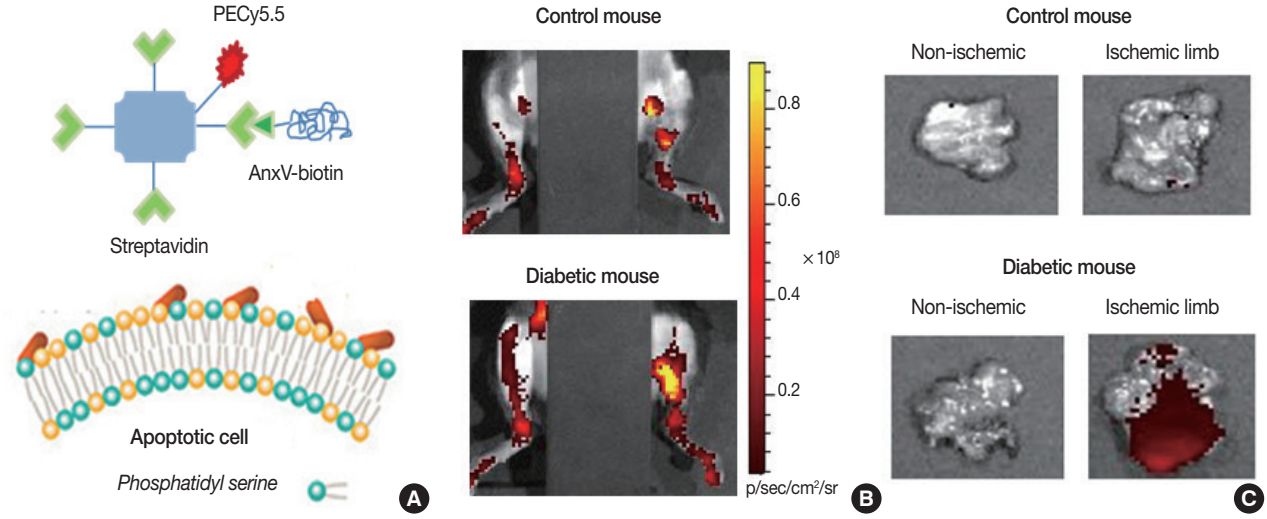

Fig. 6. Example of apoptosis imaging. (A) Annexin-V (AnxV) based probes target phosphatidyl serine exposed to the surface of cells that are undergoing apoptotic death. Here, AnxV is bound to streptavidin conjugated with PECy5.5 for fluorescent signaling. (B, C) *In vivo* fluorescent images of hindlimbs of living mice (supine with torso covered to block background signals; B) and *ex vivo* images of extracted tissue (C). Probe uptake is significantly increased in the ischemic hindlimb of the diabetic mouse due to apoptosis.

Apoptosis imaging

Apoptosis is a fine-tuned biological process of programmed cell death that can be triggered by anticancer drugs and ionizing radiation as well as by various disease processes including ischemic injury. It is therefore being increasingly evaluated as a prognostic biomarker of treatment outcomes. Among several probes being investigated, the most extensively investigated is annexin-V, a peptide with high-affinity binding to phosphatidylserine.[18] This target normally resides in the inner leaflet of the plasma membrane, but scramblase activation by apoptotic stimuli flips it to the outer leaflet, exposing it to binding by annexin-V.

Radiolabeled annexin-V compounds have been shown to enable imaging of apoptotic cells in animal models of anti-cancer therapy, allograft rejection, myocardial infarction, and infectious disease. Our group showed that fluorescent-conjugated annexin-V probes can image ischemia-induced apoptosis in a mouse model of diabetic limb ischemia.[19] Annexin-V imaging has also been applied in clinical trials of cancer patients receiving chemotherapy, where its predictive potential was indicated by the

http://dx.doi.org/10.4132/jptm.2014.10.24

increased probe accumulation in cases that later showed remission.[20] A limitation for annexin-V imaging is the possible difficulty in discriminating necrotic cell death, because phosphatidylserine of disrupted plasma membranes may also become accessible for binding.

Other early changes in the apoptotic membrane, including loss of membrane potential, membrane acidification and activation of scramblase, may also serve as imaging targets. ML-10 shows promise as a PET probe for apoptotic imaging of tumors following therapy, where uptake correlated with breakdown of mitochondrial membrane potential and caspase activation. ML-10 PET was recently evaluated in human patients with brain metastases, and a significant correlation was found between early tumor uptake and late anatomical response.[21] Several groups have also developed PET probes that target caspase-3 activation, but found limited sensitivity despite specific caspase binding. Further studies are needed to evaluate the applicability of these apoptotic markers in clinical practice.

FUTURE PERSPECTIVES AND CONCLUSION

Molecular imaging enables dynamic and quantitative visualization of specific biochemical and molecular events in living bodies. In recent years, this new technology has seen progress in early diagnosis, curative effect monitoring, and drug development. Many of these roles are similar to those pursued by molecular pathology, indicating significant overlap in mission and research agenda. Therefore, reinforcement of this trend may offer substantial synergic collaboration between pathologists and molecular imaging specialists, and pooling resources and strategic goals will have a powerful multiplier effect on future medicine.

In conclusion, molecular imaging has emerged as a young but powerful new discipline. This paradigm shift in clinical imaging requires the rapid implementation of new validated imaging biomarkers. Although many aspects of molecular imaging are still in the early stages of development, the long-range idea is that medical professionals will be able to utilize the techniques to improve diagnoses, make better treatment choices, and predict patient outcomes. We foresee that the next decade will see even greater technological advances in molecular imaging methods, which in turn, will have a large impact on personalized medicine.

Conflicts of Interest

No potential conflict of interest relevant to this article was reported.

Acknowledgments

This work was supported by the Samsung Biomedical Research Institute Grant # SMX1131891.

REFERENCES

1. Hamburg MA, Collins FS. The path to personalized medicine. N Engl J Med 2010; 363: 301-4.
2. Hoggatt J. Personalized medicine: trends in molecular diagnostics: exponential growth expected in the next ten years. Mol Diagn Ther 2011; 15: 53-5.
3. Herschman HR. Molecular imaging: looking at problems, seeing solutions. Science 2003; 302: 605-8.
4. Kircher MF, Hricak H, Larson SM. Molecular imaging for personalized cancer care. Mol Oncol 2012; 6: 182-95.
5. Willmann JK, van Bruggen N, Dinkelborg LM, Gambhir SS. Molecular imaging in drug development. Nat Rev Drug Discov 2008; 7: 591-607.
6. Reynolds F, Kelly KA. Techniques for molecular imaging probe design. Mol Imaging 2011; 10: 407-19.
7. Weber WA, Grosu AL, Czernin J. Technology Insight: advances in molecular imaging and an appraisal of PET/CT scanning. Nat Clin Pract Oncol 2008; 5: 160-70.
8. Gore JC, Manning HC, Quarles CC, Waddell KW, Yankeelov TE. Magnetic resonance in the era of molecular imaging of cancer. Magn Reson Imaging 2011; 29: 587-600.
9. Ritman EL. Molecular imaging in small animals: roles for micro-CT. J Cell Biochem Suppl 2002; 39: 116-24.
10. Hellebust A, Richards-Kortum R. Advances in molecular imaging: targeted optical contrast agents for cancer diagnostics. Nanomedicine (Lond) 2012; 7: 429-45.
11. Mankoff DA, Link JM, Linden HM, Sundararajan L, Krohn KA. Tumor receptor imaging. J Nucl Med 2008; 49 Suppl 2: 149S-63S.
12. Smith-Jones PM, Solit DB, Akhurst T, Afroze F, Rosen N, Larson SM. Imaging the pharmacodynamics of HER2 degradation in response to Hsp90 inhibitors. Nat Biotechnol 2004; 22: 701-6.
13. Jung KH, Choe YS, Paik JY, Lee KH. 99mTc-Hydrazinonicotinamide epidermal growth factor-polyethylene glycol-quantum dot imaging allows quantification of breast cancer epidermal growth factor receptor expression and monitors receptor downregulation in response to cetuximab therapy. J Nucl Med 2011; 52: 1457-64.
14. Choe YS, Lee KH. Targeted *in vivo* imaging of angiogenesis: present status and perspectives. Curr Pharm Des 2007; 13: 17-31.
15. Iagaru A, Gambhir SS. Imaging tumor angiogenesis: the road to clinical utility. AJR Am J Roentgenol 2013; 201: W183-91.
16. Jung KH, Lee KH, Paik JY, *et al.* Favorable biokinetic and tumor-tar-

geting properties of 99mTc-labeled glucosamino RGD and effect of paclitaxel therapy. J Nucl Med 2006; 47: 2000-7.
17. Lee KH, Jung KH, Song SH, *et al.* Radiolabeled RGD uptake and alphav integrin expression is enhanced in ischemic murine hindlimbs. J Nucl Med 2005; 46: 472-8.
18. Yang TJ, Haimovitz-Friedman A, Verheij M. Anticancer therapy and apoptosis imaging. Exp Oncol 2012; 34: 269-76.
19. Jung KH, Lee JH, Park JW, *et al.* Annexin V imaging detects diabetes-accelerated apoptosis and monitors the efficacy of benfotiamine treatment in ischemic limbs of mice. Mol Imaging 2014; 13: 1-7.
20. Kartachova M, van Zandwijk N, Burgers S, van Tinteren H, Verheij M, Valdés Olmos RA. Prognostic significance of 99mTc Hynic-rh-annexin V scintigraphy during platinum-based chemotherapy in advanced lung cancer. J Clin Oncol 2007; 25: 2534-9.
21. Allen AM, Ben-Ami M, Reshef A, *et al.* Assessment of response of brain metastases to radiotherapy by PET imaging of apoptosis with ^{18}F-ML-10. Eur J Nucl Med Mol Imaging 2012; 39: 1400-8.

http://dx.doi.org/10.4132/jptm.2014.10.24

Journal of Pathology and Translational Medicine 2015; 49: 13-22
http://dx.doi.org/10.4132/jptm.2014.12.26

■ REVIEW ■

Genomic Landscapes of Pancreatic Neoplasia

Laura D. Wood · Ralph H. Hruban

The Sol Goldman Pancreatic Cancer Research Center, Johns Hopkins University School of Medicine, Baltimore, MD, USA

Received: December 26, 2014
Accepted: December 26, 2014

Corresponding Author
Laura D. Wood, M.D.
The Sol Goldman Pancreatic Cancer Research Center, Johns Hopkins University School of Medicine, CRB 2 Room 345, 1550 Orleans Street, Baltimore, MD 21231, USA
Tel: +1-410-955-3511
Fax: +1-410-614-0671
E-mail: ldwood@jhmi.edu

Pancreatic cancer is a deadly disease with a dismal prognosis. However, recent advances in sequencing and bioinformatic technology have led to the systematic characterization of the genomes of all major tumor types in the pancreas. This characterization has revealed the unique genomic landscape of each tumor type. This knowledge will pave the way for improved diagnostic and therapeutic approaches to pancreatic tumors that take advantage of the genetic alterations in these neoplasms.

Key Words: Pancreatic neoplasms; Cancer genomics; Cancer mutation

Decades of cancer research have shown that cancer is a genetic disease caused by the accumulation of somatic, and in some cases inherited, mutations in oncogenes and tumor suppressor genes. Pancreatic neoplasms are some of the best characterized at the genomic level. Some of the key genetic drivers in pancreatic neoplasia have been known for years, but the introduction of high throughput sequencing has led to a more complete understanding of pancreatic cancer genomes. The exomes of all of the major tumor types in the pancreas have been analyzed by whole exome sequencing. This systematic genomic characterization has identified unique genetic signatures in each morphologically defined pancreatic tumor type, demonstrating that each type of neoplasm is driven by a distinct set of genetic alterations. A huge opportunity now exists to translate this new knowledge to improve patient care.

PANCREATIC DUCTAL ADENOCARCINOMA AND ITS VARIANTS

Pancreatic ductal adenocarcinoma (PDAC) is the most common pancreatic malignancy, and with a 5-year survival of only 6%, it is one of the deadliest of all human cancers. The *KRAS* gene, which encodes a small GTPase that mediates downstream signaling from growth factor receptors, is the most commonly mutated oncogene in PDAC.[1-3] Missense mutations in *KRAS* cluster in specific hotspots (most commonly codon 12), consistent with its role as an oncogene—*KRAS* mutations occur in >90% of PDACs. In addition to hotspot mutations in the *KRAS* oncogene, three tumor suppressor genes are frequently mutated in PDAC. The tumor suppressor gene *P16/CDKN2A*, which encodes a critical cell cycle regulator, is inactivated in >90% of PDACs by several mechanisms, including intragenic mutation coupled with loss of heterozygosity, homozygous deletion, and promoter methylation.[4] Mutations in *TP53*, a key component of the cellular stress response, are also common in PDAC, reported in approximately 75% of PDACs, most commonly by small intragenic mutation coupled with loss of heterozygosity.[5,6] Mutations in *TP53* often result in strong diffuse nuclear expression of p53 protein which can be detected by immunohistochemistry (Fig. 1A). Somatic inactivation of *SMAD4*, a tumor suppressor gene that codes for a component of the transforming growth factor beta signaling pathway, occurs in approximately 55% of PDACs, usually by homozygous deletion or intragenic mutation coupled with loss of heterozygosity.[7,8] These mutations

pISSN 2383-7837
eISSN 2383-7845

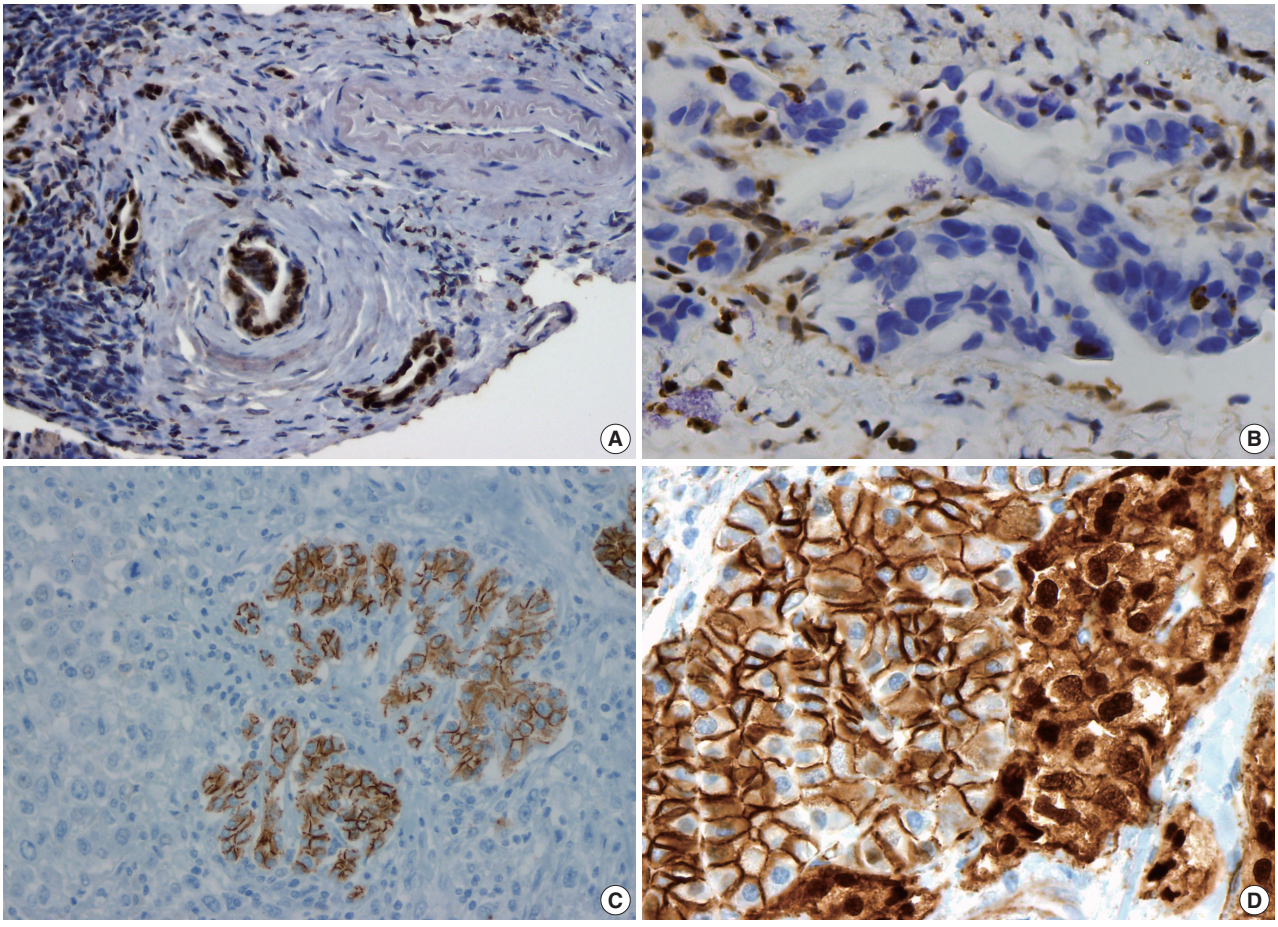

Fig. 1. Immunohistochemical correlates of somatic mutations in pancreatic neoplasms. (A) Mutation in *TP53* causes strong diffuse nuclear expression of the protein. (B) *SMAD4* mutation causes loss of protein expression in malignant glands, while expression is retained in non-neoplastic stromal and endothelial cells. (C) Undifferentiated carcinomas often lose E-cadherin expression. (D) Solid-pseudopapillary neoplasms show aberrant nuclear accumulation of β-catenin. The adjacent non-neoplastic pancreas shows normal membranous staining.

can also be detected by immunohistochemistry, as they cause loss of Smad4 protein expression (Fig. 1B). Mutations in *SMAD4* have potential clinical implications, as these mutations are associated with worse prognosis and widespread metastases (rather than local disease).[9,10] Although these four genes (often referred to as the four "mountains") are the most commonly mutated genes in pancreatic cancer (Table 1), only a minority of patients (37% in one study) have mutations in all four genes, highlighting the genetic heterogeneity of the disease.[11]

Mutations in these four driver genes were well described before the introduction of high throughput sequencing. However, multiple studies have now examined the whole exomes and whole genomes of large numbers of PDACs, and these studies have deepened our understanding of the pancreatic cancer in many ways.[6,12] First, these studies confirmed the importance of the four key driver genes (*KRAS*, *P16/CDKN2A, TP53*, and *SMAD4*) as the most frequently altered genes in PDAC. These studies also identified numerous other genes that are less commonly somatically mutated in PDACs—the average number of nonsynonymous genetic alterations ranged from 26 to 63 in the two key studies.[6,12] Several of these genes have known roles in tumorigenesis, including *MLL3, TGFBR2, ATM*, and *ARID1A*, and thus are likely to be drivers in pancreatic cancer in spite of their low mutation rate. However, many of the other infrequently mutated genes have no known role in cancer, and thus it is not possible to separate out driver mutations (which have a functional effect on tumorigenesis) from passenger mutations (which have no functional effect but instead accumulate randomly through repeated rounds of cell division within a tumor). Overall, these data highlight the heterogeneity at the gene level among different PDACs from different patients. However, although the individual genes altered are markedly heteroge-

 http://dx.doi.org/10.4132/jptm.2014.12.26

Table 1. Frequently altered genes in pancreatic neoplasms

Neoplasm	Gene(s)	Alteration prevalence (%)
PDAC	*KRAS*	95
	P16/CDKN2A	95
	TP53	75
	SMAD4/DPC4	55
IPMN	*KRAS*	80
	RNF43	60
	GNAS	60
	PIK3CA	10
	P16/CDKN2A	Only in HGD/carcinoma
	TP53	Only in HGD/carcinoma
	SMAD4/DPC4	Only in HGD/carcinoma
MCN	*KRAS*	80
	RNF43	40
	TP53	Only in HGD/carcinoma
	P16/CDKN2A	Only in HGD/carcinoma
	SMAD4/DPC4	Only in HGD/carcinoma
SCA	*VHL*	50
SPN	*CTNNB1*	95
PanNET	*MEN1*	45
	DAXX/ATRX	45
	mTOR pathway	15
ACC	Numerous genes with nonsynonymous point mutations	0–30
	RAF rearrangements	25
PB	*CTNNB1*	55
	APC	10
	11p loss (gene unknown)	85

PDAC, pancreatic ductal adenocarcinoma; IPMN, intraductal papillary mucinous neoplasm; HGD, high-grade dysplasia; MCN, mucinous cystic neoplasm; carcinoma, invasive carcinoma; SCA, serous cystadenoma; SPN, solid-pseudopapillary neoplasm; PanNET, well-differentiated pancreatic neuroendocrine tumor; mTOR, mammalian target of rapamycin; ACC, acinar cell carcinoma; PB, pancreatoblastoma.

neous, PDACs share many similarities when mutated genes are not considered at the individual gene level, but instead are considered as components of their larger biological pathways: there are several core processes and pathways that are genetically altered in the majority of carcinomas sequenced. These commonly altered pathways, which include *KRAS* signaling, DNA damage control, and cell adhesion, represent shared features of pancreatic tumorigenesis. In addition to these pathways with clear links to processes critical to tumor formation, one study also identified frequent mutations in genes in the axon guidance pathway as promising potential drivers in PDAC.[12]

Somatic mutations have also been used to understand metastasis and model the time course of pancreatic tumorigenesis. Studies of somatic mutations in matched primary tumors and metastases did not identify any genetic alterations that were specific to metastasis.[13] Instead, the vast majority of the mutations identified in metastases were present in a subclonal population of the primary tumor. Modeling based on these data suggests a time period of approximately 15 years between the occurrence of the initiating mutation in PDAC and the acquisition of metastatic ability.[13] These data are encouraging, as they suggest a broad time window for early detection of PDAC while it is still curable by surgery.[14]

Although the contribution of protein-altering somatic mutations is well documented in PDAC, it is likely that other genetic and epigenetic alterations also play a role in pancreatic tumorigenesis. This idea is supported by the observation that copy number alterations and promoter methylation affect known drivers of PDAC.[15] Many studies have identified copy number gains and losses as well as complex karyotypes in PDAC, and several studies have examined differential expression of microRNAs.[16-21] However, because of difficulties in determining the target genes and functional effects of these types of alterations, it is much more challenging to separate out driver and passenger alterations when analyzing large chromosomal alterations as well as differences in gene and microRNA expression.

There are several uncommon variants of PDAC—most of these are genetically similar to PDAC with respect to mutations in key driver genes (*KRAS*, *P16/CDKN2A, TP53*, and *SMAD4*). However, some variants also have unique genetic alterations. For example, in addition to mutations in previously known drivers, adenosquamous carcinoma has frequent somatic mutations in *UPF1*, which encodes a crucial component of the RNA degradation pathway of nonsense mediated decay.[22,23] The mutations in *UPF1* cause aberrant splicing of the mRNA, eliminating essential protein domains and potentially conferring dominant negative activity.[22] Colloid carcinomas, which are characterized by large pools of stromal mucin and are associated with intestinal-type intraductal papillary mucinous neoplasms (IPMNs, see below), have somatic mutations in *GNAS* (which are not typically seen in PDAC), as well as *KRAS* and *TP53*.[24] Medullary carcinomas exhibit a high prevalence of microsatellite instability,[25,26] and undifferentiated carcinomas show frequent loss of E-cadherin protein expression[27] (Fig. 1C). Although no somatic mutations in *CDH1* have been reported in undifferentiated carcinomas, promoter methylation has been reported and may explain the loss of E-cadherin protein expression.[27]

FAMILIAL PANCREATIC CANCER GENES

A number of genes have been identified that increase the risk of developing PDAC when altered in the germline (Table 2). These genes are important to recognize for three reasons. First, the risk of developing pancreatic cancer can be quantified when the gene is known; this knowledge can help guide patient care

Table 2. Genes with germline alterations causing increased risk of pancreatic neoplasia

Gene	Syndrome	Neoplasm
BRCA2 and *BRCA1*	Familial breast cancer	PDAC
PALB2 (*FANCN*)	Familial breast cancer	PDAC
P16/CDKN2A	Familial atypical multiple mole melanoma syndrome (FAMMM)	PDAC
STK11/LKB1	Peutz-Jeghers syndrome (PJS)	PDAC, IPMN
PRSS1, SPINK1	Hereditary pancreatitis	PDAC
hMSH2, hMLH1, hPMS1, hPMS2, hMSH6/GTB	Lynch syndrome/hereditary non-polyposis colorectal cancer (HNPCC)	PDAC (medullary variant)
ATM	Ataxia-Telangiectasia	PDAC
VHL	von Hippel-Lindau syndrome (VHL)	SCA, PanNET
MEN1	Multiple endocrine neoplasia type 1 (MEN1)	PanNET
TSC1, TSC2	Tuberous sclerosis complex (TSC)	PanNET
NF1	Neurofibromatosis type 1 (NF1)	PanNET
Unknown	Beckwith-Wiedemann syndrome (BWS)	PB

PDAC, pancreatic ductal adenocarcinoma; IPMN, intraductal papillary mucinous neoplasm; SCA, serous cystadenoma; PanNET, well-differentiated pancreatic neuroendocrine tumor; PB, pancreatoblastoma.

and research screening. For example, germline mutations in *PRSS1* cause chronic pancreatitis and greatly increase the risk of pancreatic cancer.[28] Some of these individuals, particularly those with a nonfunctioning pancreas from years of chronic pancreatitis, choose prophylactic pancreatectomy to reduce their risk of developing PDAC.[29] Second, the risk of developing extra-pancreatic malignancies can be quantified when the gene is known. For example, germline *P16/CDN2KA* mutations increase the risk of both PDAC and melanoma and lives can be saved by screening carriers of a germline *P16/CDN2KA* mutation and their biological relatives for melanoma.[30,31] Third, some of the germline mutations result in changes in the PDACs that are potentially therapeutically targetable. For example, germline *BRCA2* mutations increase the risk of ovarian, breast and pancreatic cancer, and the pancreatic cancers that arise in patients with a germline *BRCA2* mutation may be particularly sensitive to poly (ADP-ribose) polymerase (PARP) inhibitors and to DNA cross-linking agents such as cisplatinum.[32,33]

PRECURSORS TO PANCREATIC DUCTAL ADENOCARCINOMA: PANCREATIC INTRAEPITHELIAL NEOPLASIAS

PDACs arise from histologically well-defined precursor lesions. The majority of PDACs arise from pancreatic intraepithelial neoplasia (PanIN), which are microscopic intraductal lesions and too small to be detected using currently available imaging technologies. However, a significant minority of PDACs arise from cystic precursors that can be identified with currently available imaging technologies—these cystic precursor lesions include IPMNs and mucinous cystic neoplasms (MCNs). Although some alterations are shared among these precursor lesions, there are genetic features that distinguish PanINs, IPMNs, and MCNs.

PanINs, which are categorized based on the morphological grade of dysplasia as low-grade (PanIN-1 and PanIN-2) and high-grade (PanIN-3), sequentially acquire the driver gene mutations that characterize PDAC. *KRAS* mutations are an early event in PanIN formation, occurring in >90% of even the lowest grade PanINs.[34] *P16/CDKN2A* mutations also occur in PanIN-1, though far less frequently than *KRAS* mutations, and the prevelance of *P16/CDKN2A* mutations increase with PanIN grade.[34] However, loss of Smad4 expression and *TP53* alterations are late events. Smad4 loss has been reported only in high-grade PanIN (PanIN-3) and invasive carcinoma—the same pattern has been reported for *TP53* alterations.[35,36] In addition to mutations in these driver genes, telomere shortening is a very early event in PanINs, occurring in approximately 90% of PanIN-1s.[37] More extensive genetic characterization of PanINs is complicated by several factors. First, these lesions are small and thus only yield enough DNA for specific targeted genetic analyses. Second, as these lesions are only visible microscopically, it is very difficult to prospectively identify them and harvest fresh tissue; thus, the vast majority of PanIN lesions are only available from formalin-fixed paraffin-embedded tissue. The study of high-grade PanIN (PanIN-3) is particularly difficult. Because PDAC can invade into and then spread along the duct system, it can be impossible to distinguish true PanIN-3 from the intraductal spread of invasive carcinoma. In spite of these difficulties, one study has reported whole exome sequencing of PDAC and associated PanINs.[38] This study found that approximately two-thirds of the somatic mutations were shared between PanINs and associated invasive carcinoma, while 10% were unique to the invasive carcinoma and 25% were unique to the PanINs. This study con-

 http://dx.doi.org/10.4132/jptm.2014.12.26

firms the genetic relationship between PanINs and invasive carcinoma but also suggests additional genetic evolution with clinical progression of the disease.

PRECURSORS TO PANCREATIC DUCTAL ADENOCARCINOMA: IPMNS AND MCNS

Cystic pancreatic cancer precursors, IPMNs and MCNs, can also give rise to PDAC. Both are cystic lesions but have distinct clinical and morphological differences. IPMNs are more common in the head of the pancreas and involve the pancreatic duct system. MCNs are more common in the tail of the pancreas, occur almost exclusively in women, do not involve the duct system, and have a characteristic ovarian-type stroma. Like PanINs, IPMNs and MCNs are also classified by their grade of dysplasia (low, intermediate, or high). In addition, IPMNs are also classified by the direction of differentiation of the neoplastic epithelium into gastric, intestinal, pancreatobiliary, and oncocytic subtypes.

IPMNs share mutations in the four key drivers of invasive PDAC (Table 1). *KRAS* mutations are prevalent in IPMNs and are present in up to 80% of tumors, occurring even in IPMNs with low-grade dysplasia.[24,39] Loss of p16 expression occurs in both noninvasive IPMNs and in IPMN associated invasive carcinomas, but it is much more common in invasive carcinomas (100% of invasive carcinomas vs 10% of noninvasive IPMNs in one study).[40] Similarly, Smad4 loss is rare in noninvasive IPMNs but occurs in about one-third of IPMN-associated invasive carcinomas, identifying this as a late alteration in IPMN associated tumorigenesis.[40,41] *TP53* mutations and protein overexpression are also limited to areas of high-grade dysplasia or invasive carcinoma in IPMNs.[42-45]

In addition to these drivers shared with conventional PDAC, IPMNs also have alterations in genes not typically targeted in PDAC (Table 1). Approximately 60% of IPMNs have somatic mutations in the oncogenic hotspot of *GNAS*, which encodes a protein that couples transmembrane receptors to their downstream signaling proteins.[24] These mutations occur in all grades of dysplasia and are most prevalent in intestinal-type IPMNs.[39,46] Other genetic alterations that underlie the morphological differences between the IPMN subtypes remain unknown. In addition, inactivating mutations in *RNF43*, a gene coding for an ubiquitin ligase, occur in approximately 60% of IPMNs.[47] The mutations in *GNAS* and *RNF43* are striking in their prevalence as well as mutation types. The mutations in *GNAS* cluster at a single oncogenic hotspot codon, unequivocally establishing this gene as an oncogene. In contrast, the mutations in *RNF43* are striking enriched for nonsense and other inactivating mutations, indicating that this is a tumor suppressor gene. Other potential driver genes that are mutated in IPMN but not PDAC include *PIK3CA* (10% of IPMNs) and *STK11/LKB1* (5% of IPMNs).[48,49] Whole exome sequencing of IPMNs revealed an average of 26 nonsynonymous somatic mutations per tumor, far fewer than in PDAC.[47]

Like IPMNs, MCNs share mutations in the four key drivers of PDAC—*KRAS* mutation is an early event, while tumor suppressor gene mutations (*TP53, SMAD4, P16/CDKN2A*) occur in MCNs with high-grade dysplasia or associated invasive carcinomas (Table 1). However, unlike IPMNs, *GNAS* mutations have not been identified in MCNs. Inactivating *RNF43* mutations do occur in MCNs, but at a lower prevalence than in IPMNs.[47] Whole exome sequencing revealed an average of 16 nonsynonymous somatic mutations per IPMN.[47]

OTHER CYSTIC NEOPLASMS

In addition to the cystic precursors to pancreatic cancer (IPMNs and MCNs), serous cystadenomas (SCAs) are clinically, pathologically, and genetically distinct from IPMNs and MCNs. SCAs are important to recognize because they are benign neoplasms with negligible risk of malignant behavior—these neoplasms are only resected if they cause symptoms due to mass effect or if there is clinical/radiologic concern for an IPMN. They are not precursors to invasive cancer. Whole exome sequencing of SCAs revealed an average of only 10 nonsynonymous somatic mutations per tumor, far fewer than in PDAC or its cystic precursors.[47] Only *VHL* was identified as a definite tumor suppressor gene in this tumor type, with somatic mutation in 50% and loss of heterozygosity in 90% of tumors (Table 1).[47] SCAs occur as part of the clinical syndrome in von Hippel–Lindau syndrome, which results in clear cell neoplasms in various organs and is caused by germline mutations in *VHL* on chromosome 3—as such, the occurrence of somatic *VHL* mutations in sporadic SCAs is not surprising. Taken together, these data support the assertion that *VHL* is the major tumor suppressor responsible for the formation of both familial and sporadic SCAs. In addition, recent data show that vascular endothelial growth factor, a downstream target of VHL, is a marker of SCAs in pancreatic cyst fluid.[50] No mutations have been identified in PDAC or IPMN/MCN driver genes in SCAs. In addition to frequent loss of heterozygosity on chromosome 3p (the *VHL* locus), allelic loss of chromosome 10q has also been reported in 50% of cases and losses in several

other chromosomes have been reported in multiple SCAs; however, no target genes for these losses has been identified.[51]

SOLID-PSEUDOPAPILLARY NEOPLASMS

Solid-pseudopapillary neoplasms (SPNs) are uncommon pancreatic neoplasms with low malignant potential—although surgical resection is curative for most patients, metastases can rarely occur.[52,53] Activating somatic mutations in *CTNNB1* occur in almost all cases, leading to abnormal nuclear accumulation of β-catenin which can be detected with immunohistochemistry (Fig. 1D).[54,55] Importantly, this nuclear accumulation of β-catenin on immunohistochemical stains can be used to support the histological diagnosis of SPN. Whole exome sequencing of SPNs revealed shockingly few somatic mutations, an average of only three nonsynonymous somatic mutations per tumor.[47] Some tumors in this sequencing study had only one somatic mutation, but all SPNs had a somatic mutation in *CTNNB1*. This demonstrates a unique feature of SPNs: a remarkably low number of somatic mutations, lower than any tumor type described to date, including pediatric tumors. Additional studies are required to determine whether tumorigenesis in this tumor type is driven by other types of alterations, such as large chromosomal translocations or epigenetic events.

PANCREATIC NEUROENDOCRINE TUMORS

Pancreatic neuroendocrine tumors (PanNETs), also known as islet cell tumors, are a distinct pancreatic neoplasm with neuroendocrine differentiation, as demonstrated by morphology or immunohistochemistry. They are classified as "syndromic" if they express hormones that result in a clinical syndrome, and as "familial" if they arise in a patient with a genetic predisposition. PanNETs are graded based on their proliferation rate, as assessed by mitotic count or Ki67 labeling index.[56] Tumors with >20 mitoses per high power field or Ki67 index >20% are considered neuroendocrine carcinomas, and neuroendocrine carcinomas can be further subdivided into large cell and small cell carcinomas.

Whole exome sequencing of sporadic low-grade PanNETs identified an average of only 16 nonsynonymous somatic mutations per tumor.[57] Several driver genes unique to this tumor type were identified (Table 1). Somatic mutations in the *MEN1* gene were identified in 45% of sporadic PanNETs.[57,58] Considering PanNETs are a major clinical manifestation of multiple endocrine neoplasia type 1 syndrome caused by germline mutation in *MEN1*, the presence of somatic mutations in this gene in sporadic PanNETs is not surprising. In addition, mutually exclusive somatic mutations in the chromatin remodeling genes *ATRX* and *DAXX* were identified in 45% of sporadic PanNETs.[57] These genes, which were enriched for inactivating mutations in PanNETs, function as part of a complex that is important for telomere maintenance—inactivation of *ATRX* and *DAXX* is associated with the telomerase independent telomere maintenance mechanism known as alternative lengthening of telomeres.[59] Studies in patients with MEN1 syndrome identified loss of *ATRX* and *DAXX* expression only in large PanNETs, suggesting that alterations in these genes are late events in pancreatic neuroendocrine tumorigenesis.[60] Somatic mutations in genes in the mammalian target of rapamycin cell signaling pathway (including *PIK3CA, PTEN*, and *TSC2*) occur in approximately 15% of sporadic PanNETs.[57] These alterations carry clinical significance, as drugs targeting this pathway have been developed for clinical use, and one such drug (Everolimus) has shown promise in PanNETs.[61] PanNETs lack frequent genetic alterations in major driver genes of PDAC—rare *TP53* mutations have been reported, but no mutations in *KRAS* or *P16/CDKN2A* have been reported.[57,62] However, *P16/CDKN2A* promoter hypermethylation has been reported to be frequent in gastrinomas.[62] Although *SMAD4* mutations were reported in one small study of nonfunctional PanNETs, this finding was not replicated in the whole exome sequencing study of PanNETs.[57,63]

Intriguingly, high-grade neuroendocrine carcinomas are genetically distinct from low-grade PanNETs. Neuroendocrine carcinomas retain expression of *ATRX* and *DAXX* and instead have alterations of *P53* and *RB1*.[64]

NEOPLASMS WITH ACINAR DIFFERENTIATION

Two rare neoplasms of the pancreas exhibit acinar differentiation: acinar cell carincoma and pancreatoblastoma. While acinar cell carcinoma typically occurs in adults, pancreatoblastoma is more common in children and can occur in patients with Beckwith-Wiedemann syndrome, a disorder associated with imprinting dysregulation of chromosome 11p leading to overgrowth of various organs and predisposition to embryonal tumors.[65]

Acinar cell carcinomas are characterized by striking genomic instability at both the base pair and chromosomal level. In a recent whole exome sequencing study, each carcinoma had an average of 119 nonsynonymous somatic mutations, a larger number than any other pancreatic neoplasm.[66] Approximately 10%

 http://dx.doi.org/10.4132/jptm.2014.12.26

of acinar cell carincomas had microsatellite instability and a very large number of somatic mutations. Chromosomal instability was demonstrated by high fractional allelic losses in acinar cell carcinomas—sites of frequent loss included chromosome 11p (which was previously reported to be lost in a large proportion of acinar cell carcinomas) as well as tumor suppressor loci on chromosome 17p (*TP53*) and 18q (*SMAD4*).[67] There was also a striking diversity in the genes altered by small somatic mutations in the whole exome sequencing—no single gene was altered in more than 30% of the acinar cell carcinomas sequenced. Mutations were identified in genes known to be drivers of PDAC (*SMAD4* and *TP53*), cystic neoplasms (*GNAS* and *RNF 43*), and PanNET (*MEN1*), as well as genes known to be drivers in other extrapancreatic tumor types. The mutations identified in *APC* and *CTNNB1* confirmed previously reported findings of the importance of the Wnt signaling pathway in acinar cell carcinomas.[67] Other intriguing driver gene mutations identified in small subsets of acinar cell carcinomas included *JAK1, BRAF, RB1, PTEN, ARID1A, MLL3*, and *BAP1*. Importantly, these data suggest that therapies targeting mutations in *JAK1* and *BRAF* could show promise in patients with acinar cell carcinoma. Many other genes were also mutated in 10%–20% of acinar cell carcinomas in the whole exome sequencing study, but further functional studies are required to determine the role of these mutations (if any) in tumorigenesis. Recent genetic studies have also identified frequent genomic rearrangements involving RAF genes (*BRAF* and *RAF1*) in almost one-fourth of acinar cell carcinomas.[68] Functional studies of the most frequently formed fusion gene *SND1-BRAF* show that it activates the mitogen-activated protein kinase pathway and confers sensitivity to MEK inhibition, pointing to a promising targeted therapy for a subset of patients with acinar cell carcinoma.[68] This study also confirmed the observation in the whole exome sequencing data of frequent mutations in DNA repair genes, suggesting potential utility for platinum-based chemotherapy or PARP inhibitors.

Loss of chromosome 11p is the most frequent genetic alteration in pancreatoblastomas, occurring in >80% of tumors.[69] Like acinar cell carcinomas, pancreatoblastomas also have mutations in Wnt pathway genes: activating *CTNNB1* mutations are more common than inactivating *APC* mutations in pancreatoblastoma, although both can occur.[69] Pancreatoblastomas lack frequent mutations in the key PDAC driver genes. Although at least a subset of pancreatoblastomas contain large chromosomal alterations, these alterations are difficult to interpret since no target genes in these alterations have been identified.[70-73] Recent whole exome sequencing studies included two pancreatoblastomas, and although the number of tumors sequenced is small, a few observations can be made.[66] First, these tumors contained far fewer mutations than the acinar cell carcinomas—17 and 18 nonsynonymous somatic mutations per pancreatoblastoma. Second, both pancreatoblastomas had somatic mutations in *CTNNB1*, supporting previous studies demonstrating the importance of Wnt pathway alterations in this tumor type.

CONCLUSION

Although the genetic alterations underlying pancreatic neoplasms have been studied for decades, the recent development of high throughput sequencing has enabled systematic characterization of the genomes of all the major tumor types in the pancreas. These studies have confirmed previously identified drivers of pancreatic neoplasia as well as identified previously unknown genes that likely play a crucial role in tumorigenesis. Each type of pancreatic neoplasm has a unique genetic profile, and many potential therapeutic targets have been identified. As we enter into the era of genomic medicine, knowledge of the molecular alterations in pancreatic neoplasms will become a critical component of clinical care, as these alterations will likely form the basis for early detection strategies and targeted therapeutic approaches. This has the potential to lead to great improvements in the lives of patients with pancreatic neoplasms, as diagnostic and therapeutic approaches will be targeted to an individual patient's tumor.

Conflicts of Interest

Dr. Hruban receives royalty payments from Myriad Genetics for the PALB2 invention.

Acknowledgments

Supported by the Kaya Tuncer Career Development Award in GI Cancer Prevention; the AGA-Bernard Lee Schwartz Research Scholar Award in Pancreatic Cancer; Sigma Beta Sorority; Joseph C. Monastra Fundation; Michael Rolfe Pancreatic Cancer Foundation; Sol Goldman Pancreatic Cancer Research Center; NIH grant CA62924.

REFERENCES

1. Almoguera C, Shibata D, Forrester K, Martin J, Arnheim N, Perucho M. Most human carcinomas of the exocrine pancreas contain mutant c-K-ras genes. Cell 1988; 53: 549-54.

2. Smit VT, Boot AJ, Smits AM, Fleuren GJ, Cornelisse CJ, Bos JL. *KRAS* codon 12 mutations occur very frequently in pancreatic adenocarcinomas. Nucleic Acids Res 1988; 16: 7773-82.
3. Hruban RH, van Mansfeld AD, Offerhaus GJ, *et al.* K-ras oncogene activation in adenocarcinoma of the human pancreas: a study of 82 carcinomas using a combination of mutant-enriched polymerase chain reaction analysis and allele-specific oligonucleotide hybridization. Am J Pathol 1993; 143: 545-54.
4. Schutte M, Hruban RH, Geradts J, *et al.* Abrogation of the Rb/p16 tumor-suppressive pathway in virtually all pancreatic carcinomas. Cancer Res 1997; 57: 3126-30.
5. Rozenblum E, Schutte M, Goggins M, *et al.* Tumor-suppressive pathways in pancreatic carcinoma. Cancer Res 1997; 57: 1731-4.
6. Jones S, Zhang X, Parsons DW, *et al.* Core signaling pathways in human pancreatic cancers revealed by global genomic analyses. Science 2008; 321: 1801-6.
7. Iacobuzio-Donahue CA, Song J, Parmiagiani G, Yeo CJ, Hruban RH, Kern SE. Missense mutations of *MADH4*: characterization of the mutational hot spot and functional consequences in human tumors. Clin Cancer Res 2004; 10: 1597-604.
8. Wilentz RE, Su GH, Dai JL, *et al.* Immunohistochemical labeling for dpc4 mirrors genetic status in pancreatic adenocarcinomas: a new marker of DPC4 inactivation. Am J Pathol 2000; 156: 37-43.
9. Blackford A, Serrano OK, Wolfgang CL, *et al. SMAD4* gene mutations are associated with poor prognosis in pancreatic cancer. Clin Cancer Res 2009; 15: 4674-9.
10. Iacobuzio-Donahue CA, Fu B, Yachida S, *et al. DPC4* gene status of the primary carcinoma correlates with patterns of failure in patients with pancreatic cancer. J Clin Oncol 2009; 27: 1806-13.
11. Yachida S, White CM, Naito Y, *et al.* Clinical significance of the genetic landscape of pancreatic cancer and implications for identification of potential long-term survivors. Clin Cancer Res 2012; 18: 6339-47.
12. Biankin AV, Waddell N, Kassahn KS, *et al.* Pancreatic cancer genomes reveal aberrations in axon guidance pathway genes. Nature 2012; 491: 399-405.
13. Yachida S, Jones S, Bozic I, *et al.* Distant metastasis occurs late during the genetic evolution of pancreatic cancer. Nature 2010; 467: 1114-7.
14. Lennon AM, Wolfgang CL, Canto MI, *et al.* The early detection of pancreatic cancer: what will it take to diagnose and treat curable pancreatic neoplasia? Cancer Res 2014; 74: 3381-9.
15. Sato N, Fukushima N, Maitra A, *et al.* Discovery of novel targets for aberrant methylation in pancreatic carcinoma using high-throughput microarrays. Cancer Res 2003; 63: 3735-42.
16. Bloomston M, Frankel WL, Petrocca F, *et al.* MicroRNA expression patterns to differentiate pancreatic adenocarcinoma from normal pancreas and chronic pancreatitis. JAMA 2007; 297: 1901-8.
17. Lee EJ, Gusev Y, Jiang J, *et al.* Expression profiling identifies microRNA signature in pancreatic cancer. Int J Cancer 2007; 120: 1046-54.
18. Szafranska AE, Davison TS, John J, *et al.* MicroRNA expression alterations are linked to tumorigenesis and non-neoplastic processes in pancreatic ductal adenocarcinoma. Oncogene 2007; 26: 4442-52.
19. Griffin CA, Hruban RH, Morsberger LA, *et al.* Consistent chromosome abnormalities in adenocarcinoma of the pancreas. Cancer Res 1995; 55: 2394-9.
20. Iacobuzio-Donahue CA, van der Heijden MS, Baumgartner MR, *et al.* Large-scale allelotype of pancreaticobiliary carcinoma provides quantitative estimates of genome-wide allelic loss. Cancer Res 2004; 64: 871-5.
21. Birnbaum DJ, Adélaïde J, Mamessier E, *et al.* Genome profiling of pancreatic adenocarcinoma. Genes Chromosomes Cancer 2011; 50: 456-65.
22. Liu C, Karam R, Zhou Y, *et al.* The UPF1 RNA surveillance gene is commonly mutated in pancreatic adenosquamous carcinoma. Nat Med 2014; 20: 596-8.
23. Brody JR, Costantino CL, Potoczek M, *et al.* Adenosquamous carcinoma of the pancreas harbors *KRAS2*, *DPC4* and *TP53* molecular alterations similar to pancreatic ductal adenocarcinoma. Mod Pathol 2009; 22: 651-9.
24. Wu J, Matthaei H, Maitra A, *et al.* Recurrent *GNAS* mutations define an unexpected pathway for pancreatic cyst development. Sci Transl Med 2011; 3: 92ra66.
25. Wilentz RE, Goggins M, Redston M, *et al.* Genetic, immunohistochemical, and clinical features of medullary carcinoma of the pancreas: a newly described and characterized entity. Am J Pathol 2000; 156: 1641-51.
26. Goggins M, Offerhaus GJ, Hilgers W, *et al.* Pancreatic adenocarcinomas with DNA replication errors (RER+) are associated with wild-type K-ras and characteristic histopathology. Poor differentiation, a syncytial growth pattern, and pushing borders suggest RER+. Am J Pathol 1998; 152: 1501-7.
27. Winter JM, Ting AH, Vilardell F, *et al.* Absence of E-cadherin expression distinguishes noncohesive from cohesive pancreatic cancer. Clin Cancer Res 2008; 14: 412-8.
28. Whitcomb D, Greer J. Germ-line mutations, pancreatic inflammation, and pancreatic cancer. Clin Gastroenterol Hepatol 2009; 7(11 Suppl): S29-34.
29. Bellin MD, Freeman ML, Gelrud A, *et al.* Total pancreatectomy and islet autotransplantation in chronic pancreatitis: recommendations from PancreasFest. Pancreatology 2014; 14: 27-35.
30. van der Rhee JI, Boonk SE, Putter H, *et al.* Surveillance of second-

 http://dx.doi.org/10.4132/jptm.2014.12.26

degree relatives from melanoma families with a *CDKN2A* germline mutation. Cancer Epidemiol Biomarkers Prev 2013; 22: 1771-7.
31. Lynch HT, Fusaro RM, Lynch JF, Brand R. Pancreatic cancer and the FAMMM syndrome. Fam Cancer 2008; 7: 103-12.
32. Lowery MA, Kelsen DP, Stadler ZK, *et al.* An emerging entity: pancreatic adenocarcinoma associated with a known *BRCA* mutation: clinical descriptors, treatment implications, and future directions. Oncologist 2011; 16: 1397-402.
33. O'Sullivan CC, Moon DH, Kohn EC, Lee JM. Beyond breast and ovarian cancers: PARP inhibitors for *BRCA* mutation-associated and BRCA-like solid tumors. Front Oncol 2014; 4: 42.
34. Kanda M, Matthaei H, Wu J, *et al.* Presence of somatic mutations in most early-stage pancreatic intraepithelial neoplasia. Gastroenterology 2012; 142: 730-3.e9.
35. Wilentz RE, Iacobuzio-Donahue CA, Argani P, *et al.* Loss of expression of Dpc4 in pancreatic intraepithelial neoplasia: evidence that DPC4 inactivation occurs late in neoplastic progression. Cancer Res 2000; 60: 2002-6.
36. Maitra A, Adsay NV, Argani P, *et al.* Multicomponent analysis of the pancreatic adenocarcinoma progression model using a pancreatic intraepithelial neoplasia tissue microarray. Mod Pathol 2003; 16: 902-12.
37. van Heek NT, Meeker AK, Kern SE, *et al.* Telomere shortening is nearly universal in pancreatic intraepithelial neoplasia. Am J Pathol 2002; 161: 1541-7.
38. Murphy SJ, Hart SN, Lima JF, *et al.* Genetic alterations associated with progression from pancreatic intraepithelial neoplasia to invasive pancreatic tumor. Gastroenterology 2013; 145: 1098-109.e1.
39. Amato E, Molin MD, Mafficini A, *et al.* Targeted next-generation sequencing of cancer genes dissects the molecular profiles of intraductal papillary neoplasms of the pancreas. J Pathol 2014; 233: 217-27.
40. Biankin AV, Biankin SA, Kench JG, *et al.* Aberrant p16(INK4A) and DPC4/Smad4 expression in intraductal papillary mucinous tumours of the pancreas is associated with invasive ductal adenocarcinoma. Gut 2002; 50: 861-8.
41. Iacobuzio-Donahue CA, Klimstra DS, Adsay NV, *et al.* Dpc-4 protein is expressed in virtually all human intraductal papillary mucinous neoplasms of the pancreas: comparison with conventional ductal adenocarcinomas. Am J Pathol 2000; 157: 755-61.
42. Satoh K, Shimosegawa T, Moriizumi S, Koizumi M, Toyota T. K-ras mutation and p53 protein accumulation in intraductal mucin-hypersecreting neoplasms of the pancreas. Pancreas 1996; 12: 362-8.
43. Kawahira H, Kobayashi S, Kaneko K, Asano T, Ochiai T. p53 protein expression in intraductal papillary mucinous tumors (IPMT) of the pancreas as an indicator of tumor malignancy. Hepatogastroenterology 2000; 47: 973-7.
44. Chadwick B, Willmore-Payne C, Tripp S, Layfield LJ, Hirschowitz S, Holden J. Histologic, immunohistochemical, and molecular classification of 52 IPMNs of the pancreas. Appl Immunohistochem Mol Morphol 2009; 17: 31-9.
45. Lubezky N, Ben-Haim M, Marmor S, *et al.* High-throughput mutation profiling in intraductal papillary mucinous neoplasm (IPMN). J Gastrointest Surg 2011; 15: 503-11.
46. Dal Molin M, Matthaei H, Wu J, *et al.* Clinicopathological correlates of activating GNAS mutations in intraductal papillary mucinous neoplasm (IPMN) of the pancreas. Ann Surg Oncol 2013; 20: 3802-8.
47. Wu J, Jiao Y, Dal Molin M, *et al.* Whole-exome sequencing of neoplastic cysts of the pancreas reveals recurrent mutations in components of ubiquitin-dependent pathways. Proc Natl Acad Sci U S A 2011; 108: 21188-93.
48. Schönleben F, Qiu W, Ciau NT, *et al. PIK3CA* mutations in intraductal papillary mucinous neoplasm/carcinoma of the pancreas. Clin Cancer Res 2006; 12: 3851-5.
49. Sato N, Rosty C, Jansen M, *et al. STK11/LKB1* Peutz-Jeghers gene inactivation in intraductal papillary-mucinous neoplasms of the pancreas. Am J Pathol 2001; 159: 2017-22.
50. Yip-Schneider MT, Wu H, Dumas RP, *et al.* Vascular endothelial growth factor, a novel and highly accurate pancreatic fluid biomarker for serous pancreatic cysts. J Am Coll Surg 2014; 218: 608-17.
51. Moore PS, Zamboni G, Brighenti A, *et al.* Molecular characterization of pancreatic serous microcystic adenomas: evidence for a tumor suppressor gene on chromosome 10q. Am J Pathol 2001; 158: 317-21.
52. Reddy S, Cameron JL, Scudiere J, *et al.* Surgical management of solid-pseudopapillary neoplasms of the pancreas (Franz or Hamoudi tumors): a large single-institutional series. J Am Coll Surg 2009; 208: 950-7.
53. Law JK, Ahmed A, Singh VK, *et al.* A systematic review of solid-pseudopapillary neoplasms: are these rare lesions? Pancreas 2014; 43: 331-7.
54. Abraham SC, Klimstra DS, Wilentz RE, *et al.* Solid-pseudopapillary tumors of the pancreas are genetically distinct from pancreatic ductal adenocarcinomas and almost always harbor beta-catenin mutations. Am J Pathol 2002; 160: 1361-9.
55. Tanaka Y, Kato K, Notohara K, *et al.* Frequent beta-catenin mutation and cytoplasmic/nuclear accumulation in pancreatic solid-pseudopapillary neoplasm. Cancer Res 2001; 61: 8401-4.
56. McCall CM, Shi C, Cornish TC, *et al.* Grading of well-differentiated pancreatic neuroendocrine tumors is improved by the inclusion of both Ki67 proliferative index and mitotic rate. Am J Surg Pathol 2013; 37: 1671-7.

57. Jiao Y, Shi C, Edil BH, *et al.* DAXX/ATRX, MEN1, and mTOR pathway genes are frequently altered in pancreatic neuroendocrine tumors. Science 2011; 331: 1199-203.
58. Öberg K. The genetics of neuroendocrine tumors. Semin Oncol 2013; 40: 37-44.
59. Heaphy CM, de Wilde RF, Jiao Y, *et al.* Altered telomeres in tumors with *ATRX* and *DAXX* mutations. Science 2011; 333: 425.
60. de Wilde RF, Heaphy CM, Maitra A, *et al.* Loss of *ATRX* or *DAXX* expression and concomitant acquisition of the alternative lengthening of telomeres phenotype are late events in a small subset of MEN-1 syndrome pancreatic neuroendocrine tumors. Mod Pathol 2012; 25: 1033-9.
61. Yao JC, Shah MH, Ito T, *et al.* Everolimus for advanced pancreatic neuroendocrine tumors. N Engl J Med 2011; 364: 514-23.
62. Serrano J, Goebel SU, Peghini PL, Lubensky IA, Gibril F, Jensen RT. Alterations in the *p16INK4a*/*CDKN2A* tumor suppressor gene in gastrinomas. J Clin Endocrinol Metab 2000; 85: 4146-56.
63. Bartsch D, Hahn SA, Danichevski KD, *et al.* Mutations of the *DPC4*/*Smad4* gene in neuroendocrine pancreatic tumors. Oncogene 1999; 18: 2367-71.
64. Yachida S, Vakiani E, White CM, *et al.* Small cell and large cell neuroendocrine carcinomas of the pancreas are genetically similar and distinct from well-differentiated pancreatic neuroendocrine tumors. Am J Surg Pathol 2012; 36: 173-84.
65. Wood LD, Klimstra DS. Pathology and genetics of pancreatic neoplasms with acinar differentiation. Semin Diagn Pathol 2014; 31: 491-7.
66. Jiao Y, Yonescu R, Offerhaus GJ, *et al.* Whole-exome sequencing of pancreatic neoplasms with acinar differentiation. J Pathol 2014; 232: 428-35.
67. Abraham SC, Wu TT, Hruban RH, *et al.* Genetic and immunohistochemical analysis of pancreatic acinar cell carcinoma: frequent allelic loss on chromosome 11p and alterations in the *APC*/beta-catenin pathway. Am J Pathol 2002; 160: 953-62.
68. Chmielecki J, Hutchinson KE, Frampton GM, *et al.* Comprehensive genomic profiling of pancreatic acinar cell carcinomas identifies recurrent RAF fusions and frequent inactivation of DNA repair genes. Cancer Discov 2014; 4: 1398-405.
69. Abraham SC, Wu TT, Klimstra DS, *et al.* Distinctive molecular genetic alterations in sporadic and familial adenomatous polyposis-associated pancreatoblastomas : frequent alterations in the *APC*/beta-catenin pathway and chromosome 11p. Am J Pathol 2001; 159: 1619-27.
70. Wiley J, Posekany K, Riley R, *et al.* Cytogenetic and flow cytometric analysis of a pancreatoblastoma. Cancer Genet Cytogenet 1995; 79: 115-8.
71. Nagashima Y, Misugi K, Tanaka Y, *et al.* Pancreatoblastoma: a second report on cytogenetic findings. Cancer Genet Cytogenet 1999; 109: 178-9.
72. Barenboim-Stapleton L, Yang X, Tsokos M, *et al.* Pediatric pancreatoblastoma: histopathologic and cytogenetic characterization of tumor and derived cell line. Cancer Genet Cytogenet 2005; 157: 109-17.
73. Wang CL, Zhao WH, Yu J, Li S. Fluorescence *in situ* hybridization analysis of pancreatoblastoma. Pancreas 2009; 38: 223-4.

 http://dx.doi.org/10.4132/jptm.2014.12.26

Journal of Pathology and Translational Medicine 2015; 49: 23-29
http://dx.doi.org/10.4132/jptm.2014.10.08

■ ORIGINAL ARTICLE ■

PHH3 as an Ancillary Mitotic Marker in Gastrointestinal Stromal Tumors

Yooju Shin · Jiyeon Hyeon
Boram Lee · Sang Yun Ha
Min Eui Hong · In Gu Do
Kyoung-Mee Kim

Department of Pathology and Translational Genomics, Samsung Medical Center, Sungkyunkwan University College of Medicine, Seoul, Korea

Received: August 6, 2014
Revised: September 24, 2014
Accepted: October 8, 2014

Corresponding Author
Kyoung-Mee Kim, M.D.
Department of Pathology and Translational Genomics, Samsung Medical Center, Sunkyungkwan University School of Medicine, 81 Irwon-ro, Gangnam-gu, Seoul 135-710, Korea
Tel: +82-2-3410-2807
Fax: +82-2-3410-6396
E-mail: kkmkys@skku.edu

Background: Counting mitoses is subjective and time-consuming. The adjunctive diagnostic utility of a recently reported mitotic marker, phosphohistone H3 (PHH3), was investigated in gastrointestinal stromal tumors (GISTs). **Methods:** We reviewed 77 GISTs for several proliferative indices. These included the mitotic count per 50 high power fields (HPFs), the immunohistochemical Ki-67 labeling index and the immunohistochemical PHH3 mitotic index (MI). For comparison, Spearman's rank correlation and interclass correlation coefficient were used. **Results:** Mitotic counts ranged from 0–138 (mean, 7.57 ± 2.34) and the PHH3 MI ranged from 0–126 per 50 HPFs (mean, 9.61 ± 2.27). We found a positive correlation between mitotic counts and PHH3 MI ($r = 0.810$, $p < .001$). The inter-observer correlation coefficient for three participants was 0.975 for mitotic counts and 0.940 for the PHH3 MI. When using the PHH3 MI instead of mitotic counts in the Armed Forces Institute of Pathology (AFIP) stratification criteria, 10 cases were reclassified. In one patient with a mitotic count of 2 and a PHH3 MI of 6 per 50 HPFs, distant metastasis occurred. **Conclusions:** In GISTs, the PHH3 MI correlated adequately with mitotic counts and can be used as a useful adjunctive to count mitotic figures efficiently.

Key Words: Gastrointestinal stromal tumors; Mitosis; Ki-67; Biological marker

Gastrointestinal stromal tumors (GISTs) are the most common mesenchymal tumors of the gastrointestinal (GI) tract. GISTs can occur anywhere along the GI tract from the esophagus to the rectum, but most are located in the stomach (60%), jejunum and ileum (30%), and duodenum (5%).[1] The tumors have a wide spectrum of biological and clinical behaviors. Some GISTs rarely metastasize or recur, whereas others progress rapidly.[2] Great effort has been invested in establishing a histopathological classification that can predict aggressive behavior in GISTs. Franquemont[3] first described differentiation and risk assessment of GISTs in 1995. In 2002, the National Institutes of Health (NIH) consensus criteria used tumor size and mitotic counts as key prognostic factors.[4] Recently, data from the Armed Forces Institute of Pathology (AFIP) revealed that small intestinal GISTs have higher malignant potential than gastric GISTs[5,6] and the AFIP risk stratification is used widely to predict prognosis of patients with GIST.[1]

The most important prognostic indicator in GISTs is the mitotic count. However, counting mitoses is time-consuming and subjective which leads to high inter-observer variability.[7,8] Moreover, mitotic figures are indistinguishable from apoptotic figures. Phosphohistone 3 (PHH3) is a mitotic specific marker recently evaluated in a wide array of different tumor types[9] and shown to be a useful tool for counting mitoses and predicting prognosis.[9-18] Several studies showed PHH3 enhanced rapid recognition of mitotic figures in meningiomas, which are classified based on the mitotic index (MI).[9-11] PHH3 was also very helpful in mitotic counting in breast carcinomas,[12] melanocytic lesions,[13] uterine smooth muscle tumors[14] and pulmonary neuroendocrine carcinomas.[15] Furthermore, PHH3 expression was reported to be an independent prognostic factor in gastric adenocarcinoma[16] and esophageal squamous cell carcinoma.[17] Recently, Kim *et al.*[19] reported PHH3 staining primarily supported grading by facilitating mitotic counting and might have prognostic value in GISTs. However, inter-observer agreement in quantifying mitoses and the PHH3 MI has not been established. Moreover, the difference in the risk of tumor progression observed between mitotic counts and the PHH3 MI has not been thoroughly explored. The aim of this study was to determine the difference, if any, in the risk of tumor progression when

pISSN 2383-7837
eISSN 2383-7845

using the PHH3 MI instead of mitotic counts in the established AFIP risk stratification criteria. Additionally, inter-observer agreement between mitotic counts and the PHH3 MI was assessed.

MATERIALS AND METHODS

Seventy-seven patients with KIT (CD117)-positive primary GISTs who underwent surgical resection at Samsung Medical Center between 2012 and 2013 were selected for this study. Patients who received neoadjuvant Gleevec therapy were excluded. The medical records of patients were reviewed for tumor size and tumor location. Mitotic figures were counted at the highest proliferative region and the mitotic counts were recorded as the number of mitoses per 50 high power fields (HPFs).

The formalin-fixed, paraffin-embedded tumor tissue from resected specimens was cut into 3-μm sections and mounted on slides. The tissue section slides were then deparaffinized and immunostained using the Leica Bond-Max automatic stainer (Leica Microsystems, Bannockburn, IL, USA). All hematoxylin and eosin (H&E)–stained slides were reviewed and a representative slide was chosen containing the most mitotically-active area. Immunohistochemical staining was then performed using monoclonal antibodies against Ki-67 (1:300, Dako, Glostrup, Denmark) and polyclonal antibodies against PHH3 (1:4,000, Ser10, Millipore, Billerica, MA, USA). The Ki-67 labeling index (LI) was assessed manually as the percentage of positively stained cells out of at least 1,000 tumor cells within the highest proliferative area. The number of PHH3-positive nuclei was calculated per 50 HPFs to attain the PHH3 MI. Three different pathologists independently reviewed the H&E-stained slides to assess the mitotic count, the Ki-67 and the PHH3-immunostained slides for the Ki-67 LI and the PHH3 MI, respectively.

Statistical analysis was performed using IBM SPSS Statistics ver. 20 (IBM Co., Armonk, NY, USA). The Spearman rank correlation test was used to compare relationships between the mitotic count, the Ki-67 LI and the PHH3 MI. The inter-observer agreement for mitotic counts and PHH3 MI was calculated using the interclass correlation coefficient. A $p < .05$ was considered to indicate statistical significance.

Table 1. Clinicopathological characteristics of the 77 patients with GIST

Variable	n (%)
Median age (range, yr)	57 (28-86)
Gender	
Female	28 (36.4)
Male	49 (63.6)
Tumor size (cm)	
≤2	8 (10.4)
>2 and ≤5	52 (67.5)
>5 and ≤10	12 (15.6)
>10	5 (6.5)
Tumor location	
Stomach	54 (70.1)
Duodenum	12 (15.6)
Jejunum/ileum	10 (13.0)
Rectum	1 (1.3)
Mitosis	
≤5/50HPFs	62 (80.5)
6–10/50HPFs	4 (5.2)
>10/50HPFs	11 (14.3)
Ki-67 LI (%)	
≤5	59 (76.6)
6–10	10 (13.0)
>10	8 (10.4)
PHH3 MI	
≤5/50HPFs	51 (66.2)
6–10/50HPFs	11 (14.3)
>10/50HPFs	15 (19.5)

GIST, gastrointestinal stromal tumor; HPFs, high power fields; Ki-67 LI, Ki-67 labeling index; PHH3 MI, phosphohistone H3 mitotic index.

RESULTS

Table 1 summarizes the clinicopathological characteristics of the 77 patients. The median age of the patients was 57 years (range, 28 to 86 years) and 49 (63.6%) were males. The tumor locations included the stomach (n = 54), duodenum (n = 12), jejunum/ileum (n = 10), and rectum (n = 1). Mean tumor size was 4.39 cm (range, 1 to 36 cm). Mitotic counts ranged from 0–138 per 50 HPFs (mean, 7.57 ± 2.34; median, 2). The Ki-67 LI ranged from 1%–25% (mean, 4.83 ± 0.61; median, 3). The PHH3 MI ranged from 0–126 per 50 HPFs (mean, 9.61 ± 2.27; median, 4). The risk of aggressive behavior stratified according to the NIH criteria[4] and the AFIP criteria[1] of the 77 tumors is described in Table 2.

A limited positive correlation was found between mitotic counts and the Ki-67 LI ($r = 0.605$, $p < .001$) and a significant positive correlation was found between mitotic counts and the

Table 2. Risk of aggressive behavior in GISTs stratified according to the NIH and AFIP criteria

Risk subgroup	NIH criteria	AFIP criteria
Very low	4 (5.2)	36 (46.9)
Low	48 (62.3)	22 (28.6)
Intermediate/moderate	9 (11.7)	12 (15.6)
High	16 (20.8)	7 (9.1)

Values are presented as number (%).
GISTs, gastrointestinal stromal tumors; NIH, National Institutes of Health; AFIP, Armed Forces Institute of Pathology.

http://dx.doi.org/10.4132/jptm.2014.10.08

Table 3. Clinicopathological characteristics of the 10 cases stratified before and after the PHH3 MI replaced mitotic counts in the AFIP criteria

Patient No.	Sex/Age (yr)	Location	Size	Mitosis	Ki-67 LI	PHH3 MI	Risk of tumor progression (%)	
							AFIP criteria	PHH3 MI applied
1	M/51	Duodenum	4.5	2	10	14	Low (8.3)	High (50)
2	M/48	Jejunum	3.0	2	4	6	Low (4.3)	High (73)
3	M/47	Ileum	3.9	2	8	10	Low (4.3)	High (73)
4	M/56	Rectum	2.1	4	3	7	Low (8.5)	High (52)
5	M/67	Stomach	3.0	1	4	8	Very low (1.9)	Moderate (16)
6	M/57	Stomach	2.5	2	3	7	Very low (1.9)	Moderate (16)
7	M/57	Stomach	4.5	3	6	6	Very low (1.9)	Moderate (16)
8	F/67	Stomach	2.9	4	5	10	Very low (1.9)	Moderate (16)
9	M/64	Stomach	2.7	5	5	14	Very low (1.9)	Moderate (16)
10	M/64	Stomach	2.2	5	3	6	Very low (1.9)	Moderate (16)

PHH3 MI, phosphohistone H3 mitotic index; AFIP, Armed Forces Institute of Pathology; Ki-67 LI, Ki-67 labeling index.

PHH3 MI ($r = 0.810$, $p < .001$). Mitotic counts correlated with both the Ki-67 LI and PHH3 MI, but the correlation with PHH3 MI was slightly higher. The PHH3 MI also correlated with Ki-67 LI ($r = 0.703$, $p < .001$). The inter-observer agreement among the three participating pathologists was high for both the mitotic count (interclass correlation coefficient, 0.974; 95% confidence interval [CI], 0.962 to 0.983) and the PHH3 MI (interclass correlation coefficient, 0.940; 95% CI, 0.912 to 0.961). When the PHH3 MI replaced mitotic counts in the AFIP risk restratification analysis, the PHH3 MI imposed a higher risk among the 10 cases compared to using mitotic counts in the risk stratification (Table 3); 4 of these 10 cases were from extragastric sites (duodenum, jejunum, ileum, and rectum). This change in risk tended to be greater in extragastric GISTs when compared to gastric GISTs.

In all 10 discrepant cases, the H&E- and PHH3-immunostained slides were thoroughly reviewed. In case No. 1, the highest proliferative area on the H&E- and the PHH3-immunostained slides were not well matched. In cases Nos. 3, 5, 6, and 8, many inflammatory cells were admixed with tumor cells which may have artifactually inflated the PHH3 MI. In cases Nos. 7, 9, and 10, diffuse degeneration of tumor cells was observed on the H&E-stained slides rendering mitoses difficult to identify. In contrast, on the PHH3-immunostained slides, the darkly stained PHH3-positive cells were easy to identify even at low magnification (Fig. 1). Degenerated mitotic tumor cells, which are difficult to identify on H&E-immunostained slides, were also highlighted as dark brown figures on the PHH3-immunostained slides (Fig. 2). The last case (case No. 2) was stratified in the low risk of aggressive behavior group by both the NIH and the AFIP criteria when diagnosed in 2012. In 2014, the patient was found to have a metastasis in the liver. The primary tumor was located in the jejunum with a size of 3 cm and a mitotic count of 2 per 50 HPFs. The PHH3 MI for this case was 6 per 50 HPFs and the mean PHH3 MI among the three observers was 7 per 50 HPFs (Fig. 3) placing this tumor into the high risk group in the restratification of the AFIP criteria using the PHH3 MI. This correlates with an approximately 73% chance of malignant behavior.

DISCUSSION

To explore the diagnostic utility of the PHH3 immunohistochemical stain as an ancillary mitotic marker in GIST, a comparison was made between mitotic counts, Ki-67 LI and PHH3 MI in 77 primary GISTs. The PHH3 MI correlated very well with mitotic counts and the inter-observer correlation coefficient among the 3 pathologists was also high. However, in cases with poor fixation, abundant lymphocytes, or degeneration of tumor cells, a discrepancy between risk categorization based on mitotic counts and the PHH3 MI was observed. This study supports the use of PHH3 as a helpful adjunct strategy for the efficient analysis of mitotic figures in GISTs.

Ki-67 has been widely used as a proliferative marker in many different tumors, including GISTs.[19-21] However, Ki-67 is expressed throughout the cell cycle except in the G0 phase. Therefore, there is no assurance that Ki-67–positive cells are actually undergoing mitosis.[22] In contrast, PHH3, a recently introduced mitosis-specific marker, only highlights cells in the late G2 and M phases.[23,24] Discrepancies have been found in the correlation between PHH3 and Ki-67 expression in various tumors for the above reason.[16,17] The robust positive correlation between PHH3 and mitotic counts has been well established in many different tumors and benign tissues.[9-11,14,15,18,25]

In the present study, the PHH3 MI showed a higher correlation with mitotic counts than Ki-67 LI. The PHH3 MI also

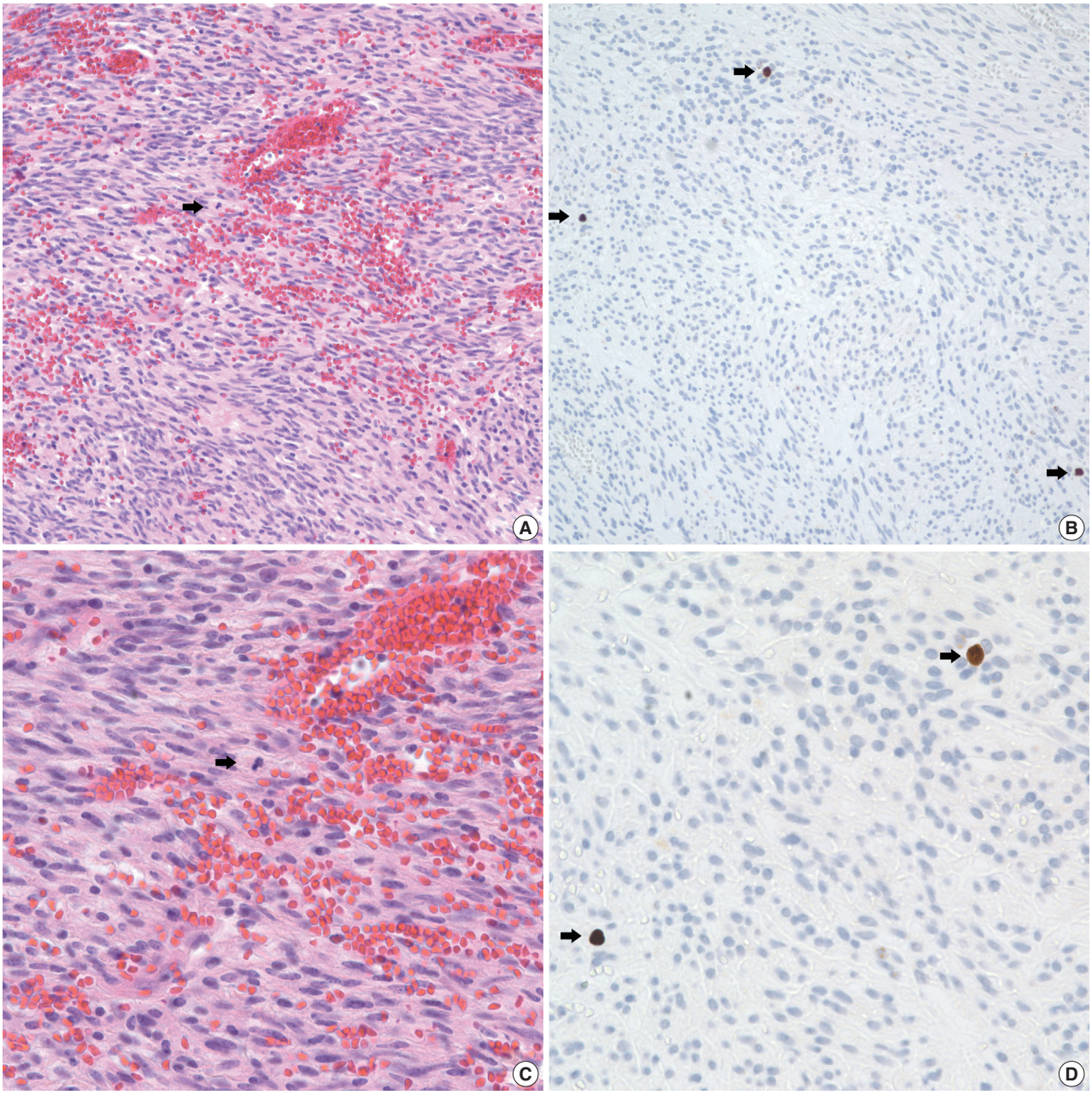

Fig. 1. A comparison of hematoxylin and eosin (A, C) and phophohistone H3 (PHH3) immunohistochemistry (B, D) in mitotic detection (arrows). Mitotic figures (arrows) are easily and quickly recognized with PHH3 immunohistochemistry.

correlated with Ki-67 LI in the current study. Interclass correlation coefficients among 3 observers for counting mitoses with either staining method were high. The interclass correlation coefficient was slightly higher for counting mitoses than for PHH3 MI in this study. In a series of 92 thin melanoma cases, inter-observer agreement was higher using the PHH3 MI than with mitotic counts.[26] In the present study, in some cases with poor fixation the immunoreactivity of the PHH3 antibody had variable staining intensity making accurate quantification of PHH3 MI difficult. Higher inter-observer agreement for PHH3 MI may be achieved with a standardized high quality immunostaining method and by consensus.

To assess the substitutability of PHH3 analysis for mitotic counts, the cases were restratified according to the PHH3 MI in accordance with the established AFIP criteria. Considering recent data suggesting tumor location can affect the malignant

 http://dx.doi.org/10.4132/jptm.2014.10.08

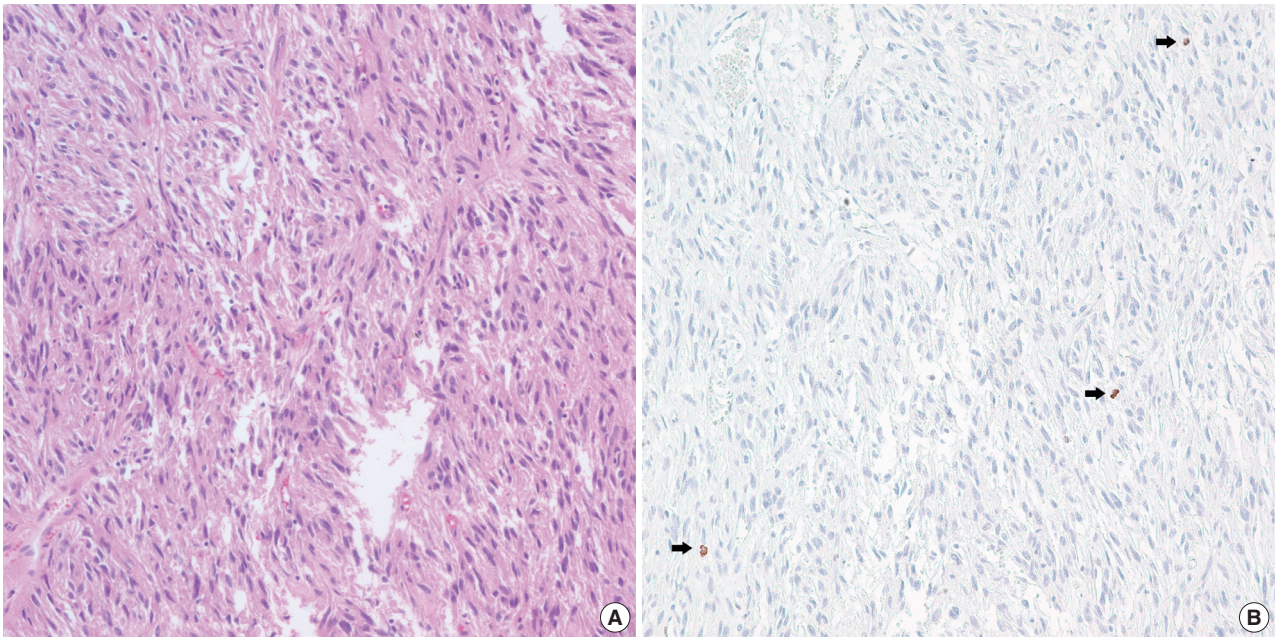

Fig. 2. Hematoxylin and eosin (H&E) (A) and phophohistone H (PHH3) immunohistochemistry (B) in a case with delayed fixation. H&E shows no mitotic figures whereas PHH3 shows three mitotic figures in the same field (arrows).

potential of GISTs, the AFIP criteria were used to analyze all cases. The 10 cases showing a change in risk stratification after applying the PHH3 MI were reviewed. The use of the PHH3 MI led to a higher risk categorization when compared to the use of mitotic counts in all 10 cases. These cases showed poor specimen fixation, abundant lymphocytes, or degeneration of tumor cells. Poor fixation of tumor cells causes difficulty in counting mitotic figures precisely. Abundant lymphocytes around tumor cells may also confuse pathologists. PHH3 is positive in mitotic tumor cells and in interphase nuclei and mitotic lymphocytes. Therefore, careful counting is needed and pathologists may overestimate the PHH3 MI in cases with abundant lymphocytic infiltration. In fact, several published reports indicate the PHH3 MI is higher than mitotic counts in various tumor types likely due to this reason.[7,9,11,14,15,26] The PHH3 immunostain highlights mitotic cells as distinct dark brown figures rendering their identification much simpler and easier than searching for mitotic figures and allows rapid detection of the most proliferative area of a lesion.

In the current study, a direct relationship between the PHH3 MI and disease-free survival was not proven. Kim *et al.*[19] demonstrated a significant correlation between recurrence-free survival and PHH3 MI, but failed to prove the independent prognostic significance of the PHH3 MI in GISTs. Interestingly, we found a case of a jejunum GIST stratified as low risk of malignant potential according to both the NIH and AFIP criteria. However, this lesion metastasized to the liver 2 years after the initial diagnosis. The mitotic count of the primary GIST was 2 per 50 HPFs and the PHH3 MI and mean PHH3 MI among the 3 observers was 6 per 50 HPFs and 7 per 50 HPFs, respectively. When the PHH3 MI was applied to risk stratification in place of mitotic counts, the case was reclassified into the high risk group (73% chance of malignant behavior). Therefore, more attention should be given to cases with a higher PHH3 MI. These cases may warrant risk recategorization. To obtain reliable results regarding the PHH3 MI as an independent prognostic factor in GISTs, a large-scale study is needed with a prolonged follow-up period.

In summary, the PHH3 MI correlated satisfactorily with mitotic counts even when compared to the Ki-67 LI in GISTs. Overall, inter-observer agreement for mitotic counts and the PHH3 MI was both high. The PHH3 immunostain enables pathologists to identify mitotic figures easily and quickly. Furthermore, in cases with inadequate fixation, quantification of the PHH3 MI was superior to counting mitotic figures. We believe the PHH3 MI is a viable adjunct strategy to use when assessing the mitotic rates in GISTs.

Conflicts of Interest

No potential conflict of interest relevant to this article was reported.

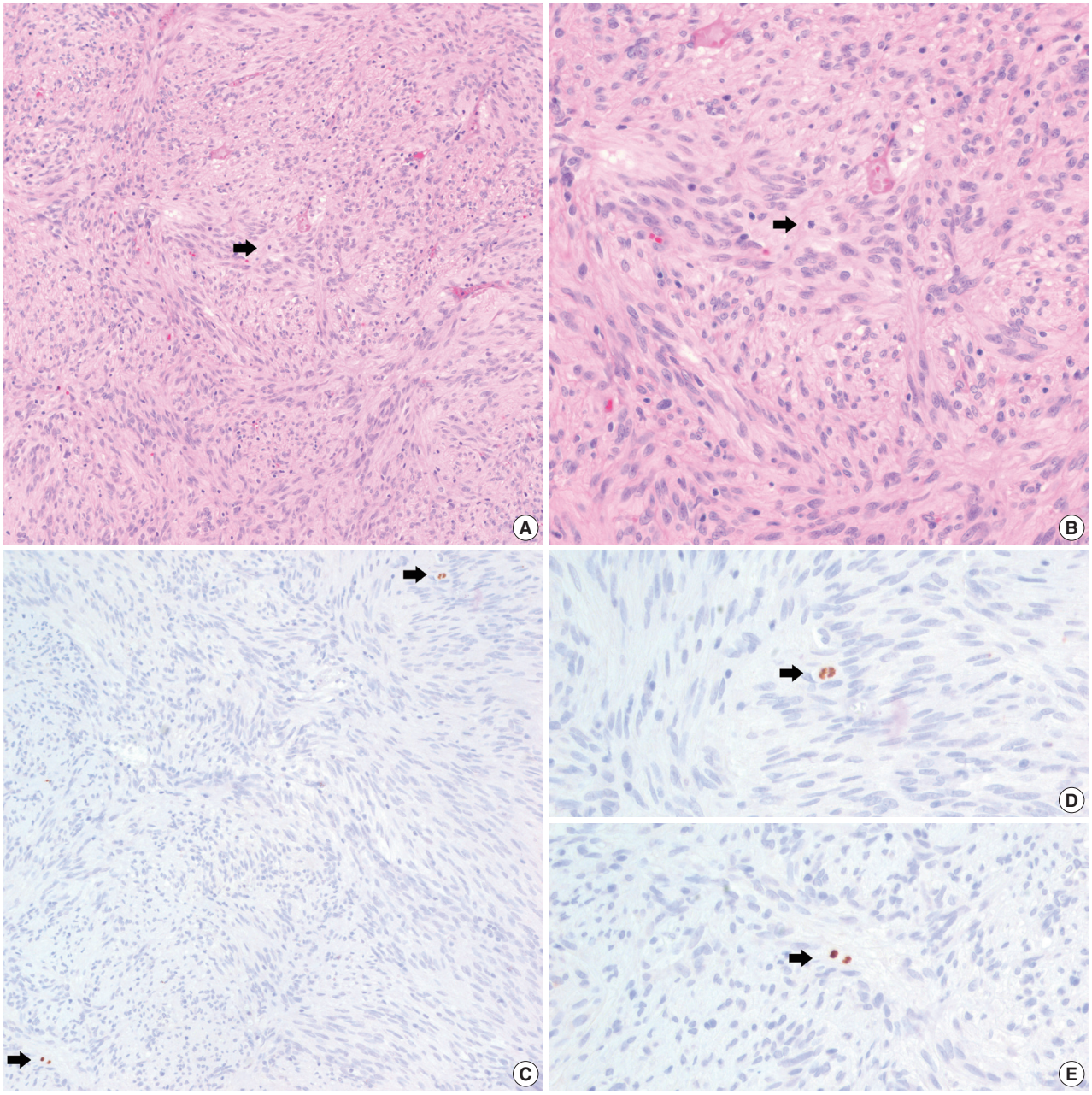

Fig. 3. Mitosis and PHH3 positive cells in a patient with distant metastasis. Hematoxylin and eosin (H&E) staining shows a single mitotic figure. (B) H&E at higher magnification. (C) Phophohistone H3 (PHH3) immunohistochemistry highlights two mitotic figures in the same field (arrows). (D, E) PHH3 at higher magnification.

REFERENCES

1. Miettinen M, Lasota J. Gastrointestinal stromal tumors: review on morphology, molecular pathology, prognosis, and differential diagnosis. Arch Pathol Lab Med 2006; 130: 1466-78.
2. Corless CL, Fletcher JA, Heinrich MC. Biology of gastrointestinal stromal tumors. J Clin Oncol 2004; 22: 3813-25.
3. Franquemont DW. Differentiation and risk assessment of gastrointestinal stromal tumors. Am J Clin Pathol 1995; 103: 41-7.
4. Fletcher CD, Berman JJ, Corless C, *et al.* Diagnosis of gastrointestinal stromal tumors: a consensus approach. Hum Pathol 2002; 33: 459-65.
5. Miettinen M, Sobin LH, Lasota J. Gastrointestinal stromal tumors of the stomach: a clinicopathologic, immunohistochemical, and molecular genetic study of 1765 cases with long-term follow-up. Am J Surg Pathol 2005; 29: 52-68.

http://dx.doi.org/10.4132/jptm.2014.10.08

6. Miettinen M, Makhlouf H, Sobin LH, Lasota J. Gastrointestinal stromal tumors of the jejunum and ileum: a clinicopathologic, immunohistochemical, and molecular genetic study of 906 cases before imatinib with long-term follow-up. Am J Surg Pathol 2006; 30: 477-89.
7. Tapia C, Kutzner H, Mentzel T, Savic S, Baumhoer D, Glatz K. Two mitosis-specific antibodies, MPM-2 and phospho-histone H3 (Ser28), allow rapid and precise determination of mitotic activity. Am J Surg Pathol 2006; 30: 83-9.
8. Agaimy A. Gastrointestinal stromal tumors (GIST) from risk stratification systems to the new TNM proposal: more questions than answers? A review emphasizing the need for a standardized GIST reporting. Int J Clin Exp Pathol 2010; 3: 461-71.
9. Hendzel MJ, Wei Y, Mancini MA, *et al.* Mitosis-specific phosphorylation of histone H3 initiates primarily within pericentromeric heterochromatin during G2 and spreads in an ordered fashion coincident with mitotic chromosome condensation. Chromosoma 1997; 106: 348-60.
10. Ribalta T, McCutcheon IE, Aldape KD, Bruner JM, Fuller GN. The mitosis-specific antibody anti-phosphohistone-H3 (PHH3) facilitates rapid reliable grading of meningiomas according to WHO 2000 criteria. Am J Surg Pathol 2004; 28: 1532-6.
11. Kim YJ, Ketter R, Steudel WI, Feiden W. Prognostic significance of the mitotic index using the mitosis marker anti-phosphohistone H3 in meningiomas. Am J Clin Pathol 2007; 128: 118-25.
12. Fukushima S, Terasaki M, Sakata K, *et al.* Sensitivity and usefulness of anti-phosphohistone-H3 antibody immunostaining for counting mitotic figures in meningioma cases. Brain Tumor Pathol 2009; 26: 51-7.
13. Bossard C, Jarry A, Colombeix C, *et al.* Phosphohistone H3 labelling for histoprognostic grading of breast adenocarcinomas and computer-assisted determination of mitotic index. J Clin Pathol 2006; 59: 706-10.
14. Nasr MR, El-Zammar O. Comparison of pHH3, Ki-67, and survivin immunoreactivity in benign and malignant melanocytic lesions. Am J Dermatopathol 2008; 30: 117-22.
15. Veras E, Malpica A, Deavers MT, Silva EG. Mitosis-specific marker phospho-histone H3 in the assessment of mitotic index in uterine smooth muscle tumors: a pilot study. Int J Gynecol Pathol 2009; 28: 316-21.
16. Tsuta K, Liu DC, Kalhor N, Wistuba II, Moran CA. Using the mitosis-specific marker anti-phosphohistone H3 to assess mitosis in pulmonary neuroendocrine carcinomas. Am J Clin Pathol 2011; 136: 252-9.
17. Takahashi H, Murai Y, Tsuneyama K, *et al.* Overexpression of phosphorylated histone H3 is an indicator of poor prognosis in gastric adenocarcinoma patients. Appl Immunohistochem Mol Morphol 2006; 14: 296-302.
18. Nakashima S, Shiozaki A, Ichikawa D, *et al.* Anti-phosphohistone H3 as an independent prognostic factor in human esophageal squamous cell carcinoma. Anticancer Res 2013; 33: 461-7.
19. Kim A, Im DH, Kim K, *et al.* Usefulness of anti-phosphohistone H3 immunoreactivity to determine mitotic rate in gastrointestinal stromal tumors. Basic Appl Pathol 2012; 5: 91-7.
20. Carrillo R, Candia A, Rodriguez-Peralto JL, Caz V. Prognostic significance of DNA ploidy and proliferative index (MIB-1 index) in gastrointestinal stromal tumors. Hum Pathol 1997; 28: 160-5.
21. Toquet C, Le Neel JC, Guillou L, *et al.* Elevated (> or = 10%) MIB-1 proliferative index correlates with poor outcome in gastric stromal tumor patients: a study of 35 cases. Dig Dis Sci 2002; 47: 2247-53.
22. Filiz G, Yalçinkaya O, Gürel S, Yerci O, Memik F. The relationship between MIB-1 proliferative activity and mitotic index in gastrointestinal stromal tumors. Hepatogastroenterology 2007; 54: 438-41.
23. Gerdes J, Lemke H, Baisch H, Wacker HH, Schwab U, Stein H. Cell cycle analysis of a cell proliferation-associated human nuclear antigen defined by the monoclonal antibody Ki-67. J Immunol 1984; 133: 1710-5.
24. Juan G, Traganos F, James WM, *et al.* Histone H3 phosphorylation and expression of cyclins A and B1 measured in individual cells during their progression through G2 and mitosis. Cytometry 1998; 32: 71-7.
25. Brenner RM, Slayden OD, Rodgers WH, *et al.* Immunocytochemical assessment of mitotic activity with an antibody to phosphorylated histone H3 in the macaque and human endometrium. Hum Reprod 2003; 18: 1185-93.
26. Schimming TT, Grabellus F, Roner M, *et al.* pHH3 immunostaining improves interobserver agreement of mitotic index in thin melanomas. Am J Dermatopathol 2012; 34: 266-9.

Journal of Pathology and Translational Medicine 2015; 49: 30-36
http://dx.doi.org/10.4132/jptm.2014.10.23

■ ORIGINAL ARTICLE ■

Clinical and Prognostic Significances of Cytokeratin 19 and KIT Expression in Surgically Resectable Pancreatic Neuroendocrine Tumors

Eun-Mi Son · Joo Young Kim[1]
Soyeon An · Ki-Byung Song[2]
Song Cheol Kim[2] · Eunsil Yu
Seung-Mo Hong

Department of Pathology, Asan Medical Center, University of Ulsan College of Medicine; [1]Department of Pathology, Korea University Anam Hospital, Korea University College of Medicine; [2]Department of Surgery, Asan Medical Center, University of Ulsan College of Medicine, Seoul, Korea

Received: August 12, 2014
Revised: October 22, 2014
Accepted: October 23, 2014

Corresponding Author
Seung-Mo Hong, M.D.
Department of Pathology, University of Ulsan College of Medicine, Asan Medical Center, 88 Olympic-ro 43-gil, Songpa-gu, Seoul 138-736, Korea
Tel: +82-2-3010-4558
Fax: +82-2-472-7898
E-mail: smhong28@gmail.com

Background: Pancreatic neuroendocrine tumors (PanNETs) are malignant endocrine neoplasms that present diverse clinical behaviors. Therefore, identification of biomarkers of PanNETs is important for stratification of the prognosis of PanNET patients. Recently, cytokeratin 19 (CK19) and KIT expression were reported to have prognostic significance in PanNET patients. **Methods:** To identify their prognostic significance, CK19 and KIT protein expression were assessed in 182 surgically resected PanNETs and compared with clinicopathologic factors. **Results:** Of 182 PanNETs cases, CK19 and KIT expression was noted in 97 (53.3%) and 16 (8.8%) cases, respectively. PanNET patients with CK19 expression had larger tumors ($p=.006$), higher World Health Organization (WHO) grade ($p=.002$) and pT classification ($p<.001$), increased distant metastasis ($p=.004$), and lymphovascular ($p=.012$) and perineural ($p=.019$) invasion. Similarly, those with KIT expression had larger tumors ($p=.030$), higher WHO grade ($p=.001$), advanced pT classification ($p<.001$), distant metastasis ($p=.001$), and lymphovascular invasion ($p=.014$). The 5-year survival rate for PanNET patients with KIT expression was significantly lower (62%) than that of patients without KIT expression (77%, $p=.011$), as determined by univariate but not by multivariate analyses. **Conclusions:** CK19 and KIT expression correlate with higher metastatic potential and advanced disease stage, and KIT expression is associated with worse survival in PanNET patients.

Key Words: Pancreas; Neuroendocrine tumors; Keratin-19; KIT; Immunohistochemistry

Pancreatic neuroendocrine tumors (PanNETs) are malignant tumors of endocrine origin from the pancreas and comprise 1.3% to 2.8% of all pancreatic neoplasms.[1] The incidence and prevalence of PanNETs have increased over the past decades according to data from the Surveillance, Epidemiology, and End Results (SEER) study.[2] Compared with ductal adenocarcinoma of the pancreas, PanNETs are generally considered to have indolent behaviors with diverse clinical features ranging from benign to highly malignant.[3,4] Therefore, predicting the clinical behavior of PanNETs is very difficult.

A recent whole-exome sequencing study demonstrated unique driver mutations in PanNETs, such as *MEN1, ATRX*, and *DAXX*.[5] In addition, although the frequencies are low, several genes in the mammalian target of rapamycin pathway, including *PTEN, TSC2*, and *PIK3CA*, were also reported to be involved in the tumorigenesis of PanNETs.[5] The expression status of some of these proteins was shown to be related to the survival of PanNET patients. For example, the losses of *ATRX* and *DAXX* were associated with worse survival. On the other hand, loss of PTEN expression was associated with better survival in PanNET patients.[6,7]

The new World Health Organization (WHO) grading scheme and the TNM staging system from the American Joint Committee on Cancer (AJCC) and the International Union for Cancer Control (UICC) provide reliable guidelines for the prognosis and treatment of PanNET patients.[4,8] However, except for pathologic grade and TNM stage, few prognostic biomarkers for PanNETs have been reported. Hence, the identification of prognostic biomarkers for PanNETs will provide more precise information regarding PanNET patient survival after surgical resection.[2,9-13]

pISSN 2383-7837
eISSN 2383-7845

Several previous studies have reported the prognostic significance of cytokeratin 19 (CK19), KIT, cyclooxygenase 2, and CD99 in PanNET patients.[2,9-13] However, there have not been any validation studies for these markers, except for CK19 expression.[2,9,11,12] The aims of this study were to determine the clinical and prognostic significance of CK19 and KIT expression in surgically resected PanNET patients using tissue microarray immunohistochemical staining.

MATERIALS AND METHODS

After approval (2014-0580) from the Institutional Review Board, 182 patients with primary PanNETs who underwent surgical resection at our institution from 1995 to 2013 were selected from the files of the Department of Pathology. Medical records were reviewed to evaluate clinical data, such as age, sex, symptoms, and follow-up data. Pathologic information, including tumor size, extension, metastases to regional lymph nodes, distant metastases, and lymphovascular and perineural invasions were carefully reviewed. Hematoxylin and eosin–stained slides were independently reviewed by three pathologists (S.-M.H., J.Y.K., and E.-M.S.). All PanNET cases were confirmed by immunohistochemical staining using neuroendocrine markers, synaptophysin, chromogranin, and/or CD56. Immunohistochemical staining for synaptophysin and chromogranin was performed in 144 and 138 cases, respectively. All 144 cases (100%) were positive for synaptophysin, and 113 of 138 (81.9%) cases were positive for chromogranin. All PanNET cases were re-classified into grades 1, 2, or 3 based on mitotic counts (per 10 high-power fields) and the Ki-67 labeling index according to the scheme of the 2010 WHO classification.[8] Tumor extension was assessed based on the T classification of the 2010 AJCC/UICC cancer staging system.

Tissue microarrarys (TMAs) were constructed using three 2-mm-diameter tumor cores from donor blocks using a manual tissue microarryer (Uni TMA Co., Ltd., Seoul, Korea). The sections of TMAs were stained using an automatic immunohistochemistry staining device (Benchmark XT, Ventana Medical System, Tucson, AZ, USA). Briefly, 5-μm-thick formaldehyde-fixed paraffin-embedded tissue sections were transferred onto adhesive slides and dried at 62°C for 30 minutes. Standard heat epitope retrieval was performed for 30 minutes in ethylene diamine tetraacetic acid, pH 8.0, in the autostainer. The samples were then incubated with antibodies against KIT (1:400, DakoCytomation, Glostrup, Denmark) and CK19 (1:100, Cell Marque, Rocklin, CA, USA). The sections were subsequently incubated with biotinylated anti-mouse immunoglobulins, peroxidase-labeled streptavidin (LSAB kit, DakoCytomation), and 3,30-diaminobenzidine. Negative control samples were processed without the primary antibody. Slides were counterstained with Harris hematoxylin. Nuclear labeling of intra-tumoral mast cells was used as an internal positive control for KIT immunohistochemical staining. Normal pancreatic acinar cells, ductal epithelial cells, and islet cells were negative for KIT staining, while mast cells in the pancreatic parenchyma were positive (Fig. 1A). Membranous immunolabeling in normal pancreatic ductal epithelial cells and centroacinar cells was used as an internal positive control for CK19 staining. Normal pancreatic islet cells and acinar cells were negative for CK19 staining (Fig. 1B). Sections demonstrating >5% positivity for KIT- and CK19-labeled tumor cells were considered to be positive, as previously described.[2,13]

SPSS ver. 18.0 (SPSS, Chicago, IL, USA) was used for the statistical analysis. The overall survival time was calculated from the date of diagnosis of PanNET to that of death from any cause. The overall survival rate was calculated with the Kaplan-Meier method, and the associations between overall survival rate and clinicopathologic factors were compared using the log-rank test. Correlations between KIT and CK19 expression and other prognostic factors were analyzed using chi-square and Fisher exact tests. Possible prognostic factors associated with survival probability were calculated by the Cox's proportional hazard regression model. A $p < .05$ was considered statistically significant.

RESULTS

Of a total of 182 PanNET patients, 44.5% (81 cases) were men, 55.5% (101 cases) were women, and the mean age was 51.4±13.10 years. The mean tumor size was 3.06±2.31 cm. Tumors were classified as functional tumors if they were associated with the distinct clinical manifestations of hormonal alterations, including hypoglycemia, sweating, or syncope; 45 cases (24.7%) were consequently classified as functional PanNETs. There were 71 head (39.0%), 7 uncinate (3.8%), 29 body (15.9%), 67 tail (36.8%), 2 head to body (1.1%), and 6 body to tail (3.3%) tumors. Using the TNM staging system, PanNETs were classified as pT1 in 74 (40.7%), pT2 in 47 (25.8%), and pT3 in 61 (33.5%) cases. Because only surgically resected PanNETs were included in the study, pT4 tumors were not included. Lymphovascular and perineural invasion was noted in 48 (26.4%) and 27 (14.8%) cases, respectively. Evaluation of the lymph nodes was possible in 99 cases (54.4%), and lymph node metastasis

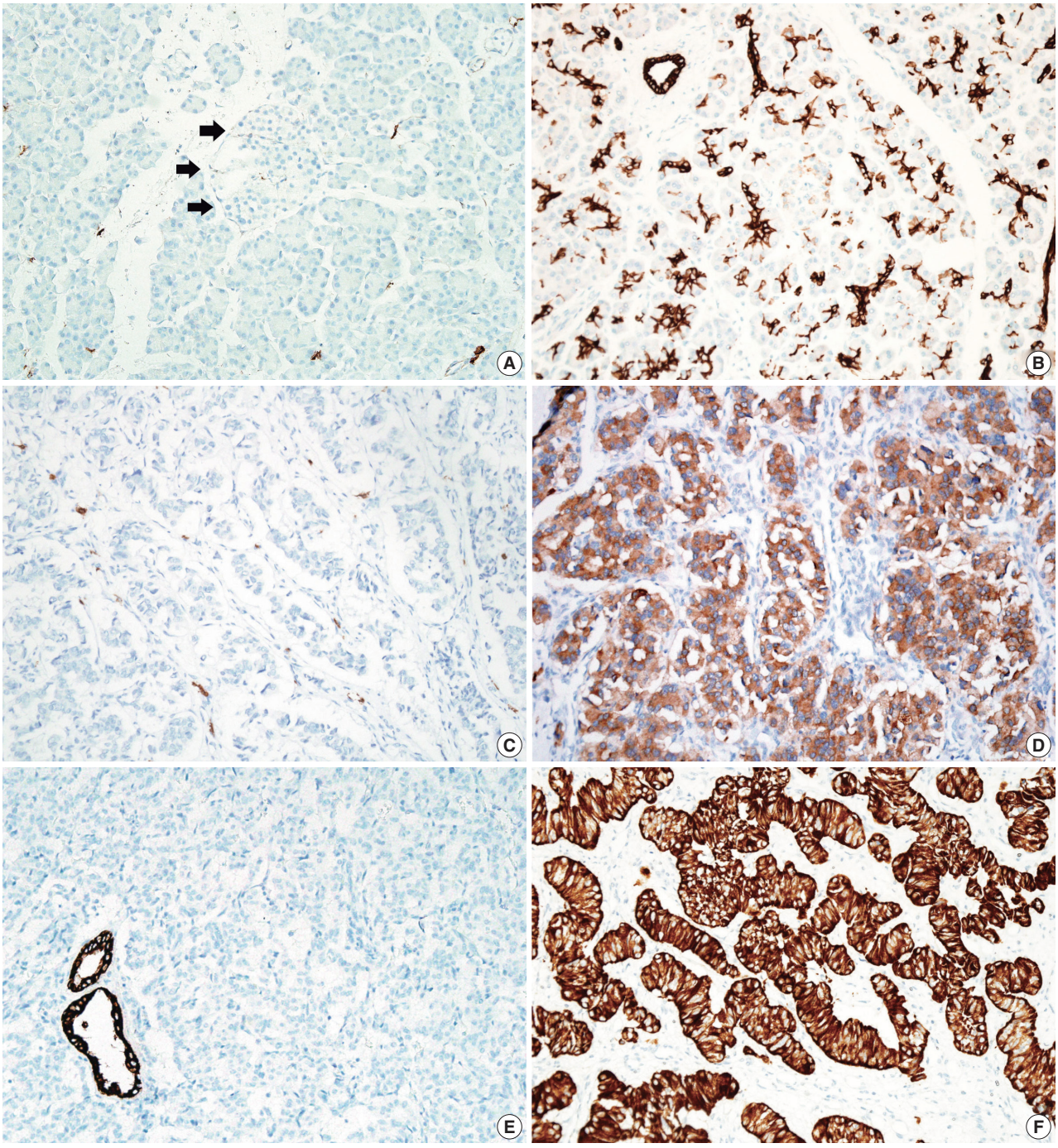

Fig. 1. Representative images of KIT and cytokeratin 19 (CK19) staining. (A) Normal acinar cell, ductal epithelial cells, and islet cells (arrows) of the pancreas are negative for KIT staining, while mast cells in the pancreatic parenchyma are positive for KIT staining. (B) Membranous CK19 immunolabeling is noted in the normal centroacinar cell and the ductal epithelial cells, while islet cells are not stained. Negative (C) and positive (D) KIT expression in a pancreatic neuroendocrine tumor. (E) Negative CK19 expression is observed in a pancreatic neuroendocrine tumor, while entrapped normal pancreatic ductal cells are positive for CK19. (F) Positive CK19 expression in a pancreatic neuroendocrine tumor.

was present in 29 cases (15.9%). Distant metastasis was observed in 36 cases (19.8%), and liver was the most common site of these distant metastases (32 cases, 88.9%). Adequate follow-up of survival information was available in 181 patients, with a median follow-up period of 30 months (range, 1 to 142 months), and 153 patients (84.1%) were alive and 28 patients (15.3%) had died; 9 of these patients died of an unrelated cause.

KIT expression was observed in 16 of 182 PanNETs (8.8%)

http://dx.doi.org/10.4132/jptm.2014.10.23

Table 1. Correlations between KIT or CK19 expression and clinicopathological factors

Parameter		Total	KIT expression		p-value	CK19 expression		p-value
			Positive	Negative		Positive	Negative	
Sex	Male	81	11 (13.6)	70 (86.4)	.063	49 (60.5)	32 (39.5)	.081
	Female	101	5 (5.0)	96 (95.0)		48 (47.5)	53 (52.5)	
Age (yr)	<60	127	11 (8.7)	116 (91.3)	1.000	68 (53.5)	59 (46.5)	.919
	≥60	55	5 (9.1)	50 (90.9)		29 (52.7)	26 (47.3)	
Function status	Functioning	45	1 (2.2)	44 (97.8)	.125	12 (26.7)	33 (73.3)	**<.001**
	Non-functioning	137	15 (10.9)	122 (89.1)		85 (62.0)	52 (38.0)	
Tumor size (cm)	≤2	81	3 (3.7)	78 (96.3)	**.030**	34 (42.0)	47 (58.0)	**.006**
	>2	101	13 (12.9)	88 (87.1)		63 (62.4)	38 (37.6)	
Extrapancreatic extension	Absent	120	4 (3.3)	116 (96.7)	**<.001**	52 (43.3)	68 (56.7)	**<.001**
	Present	62	12 (19.4)	50 (80.6)		45 (72.6)	17 (27.4)	
pT classification	pT1	74	1 (1.4)	73 (98.6)	**<.001**	30 (40.5)	44 (59.5)	**<.001**
	pT2	47	3 (6.3)	44 (93.6)		23 (48.9)	24 (51.1)	
	pT3	61	12 (19.7)	49 (80.3)		45 (71.4)	18 (28.6)	
Lymph node metastasis	Absent	89	24 (27.0)	65 (73.0)	.152	39 (63.9)	31 (81.6)	.061
	Present	10	5 (50.0)	5 (50.0)		31 (81.6)	7 (18.4)	
Distant metastasis	Absent	146	7 (4.8)	139 (95.2)	**.001**	70 (47.9)	76 (52.1)	**.004**
	Present	36	9 (25.0)	27 (75.0)		27 (75.0)	9 (25.0)	
WHO grade	Grade 1	125	6 (4.8)	119 (95.2)	**.001**	59 (47.2)	66 (52.8)	**.002**
	Grade 2	48	7 (14.6)	41 (85.4)		29 (60.4)	19 (39.6)	
	Grade 3	9	3 (33.3)	6 (66.7)		9 (90.9)	0	
Lymphovascular invasion	Absent	134	7 (5.2)	127 (94.8)	**.014**	64 (47.8)	70 (52.2)	**.012**
	Present	48	9 (18.8)	39 (81.3)		33 (68.8)	15 (31.3)	
Perineural invasion	Absent	155	11 (7.1)	144 (92.9)	.067	77 (49.7)	78 (50.3)	**.019**
	Present	27	5 (18.5)	22 (81.5)		20 (74.1)	7 (25.9)	

Values are presented as number (%).
CK9, cytokeratin 9; WHO, World Health Organization.

(Fig. 1D) and CK19 expression was noted in 97 cases (53.3%) (Fig. 1F). All 16 PanNET cases that showed KIT expression were also positive for CK19. The associations between KIT or CK19 expression and clinicopathological factors are summarized in Table 1. KIT expression was more frequently observed in larger PanNETs (p=.030), those with extrapancreatic extension (p<.001), advanced pT classification (p<.001), distant metastasis (p=.001), higher WHO grade (p=.001), and lymphovascular invasion (p=.014). There was no statistically significant correlation between KIT expression and sex, age, functional status, lymph node metastasis, expression of synaptophysin and chromogranin, or perineural invasion.

CK19 expression was more commonly observed in functioning PanNETs (p<.001), larger tumors (p=.006), extrapancreatic extension (p<.001), advanced pT classification (p<.001), lymph node metastasis (p=.009), distant metastasis (p=.004), higher WHO grade (p=.002), and lymphovascular (p=.012) and perineural (p=.019) invasion. There was no statistically significant correlation between CK19 expression and sex, age, or expression of synaptophysin and chromogranin. The overall survival rate of PanNET patients with KIT expression was significantly lower (5-year survival rate, 62%) than that of patients without KIT expression (77%, p=.011) (Fig. 2A). However, the overall survival rate of PanNET patients with CK19 expression (5-year survival rate, 74%) was not significantly different from that of patients lacking CK19 expression (79%, p=.242) (Fig. 2B).

The relationships between the survival of PanNET patients and other clinicopathologic factors are summarized in Table 2. Of these clinicopathologic factors, increased age (p<.001), extrapancreatic extension (p=.003), increased pT classification (p=.009), lymph node metastasis (p=.026), distant metastasis (p=.003), and higher WHO grade (p<.001) were correlated with worse survival. In contrast, overall survival was not correlated with sex, functional status, or lymphovascular and perineural invasion.

Multivariate analysis was performed to assess which factors remained independent predictors of survival after adjusting for factors that were found to be significant by univariate analysis. Only WHO grade remained as an independent prognostic factor (p=.001) (Table 3). Conversely, KIT expression, pT classification, and lymph node and distant metastases were not found to be independent prognostic factors in the present model.

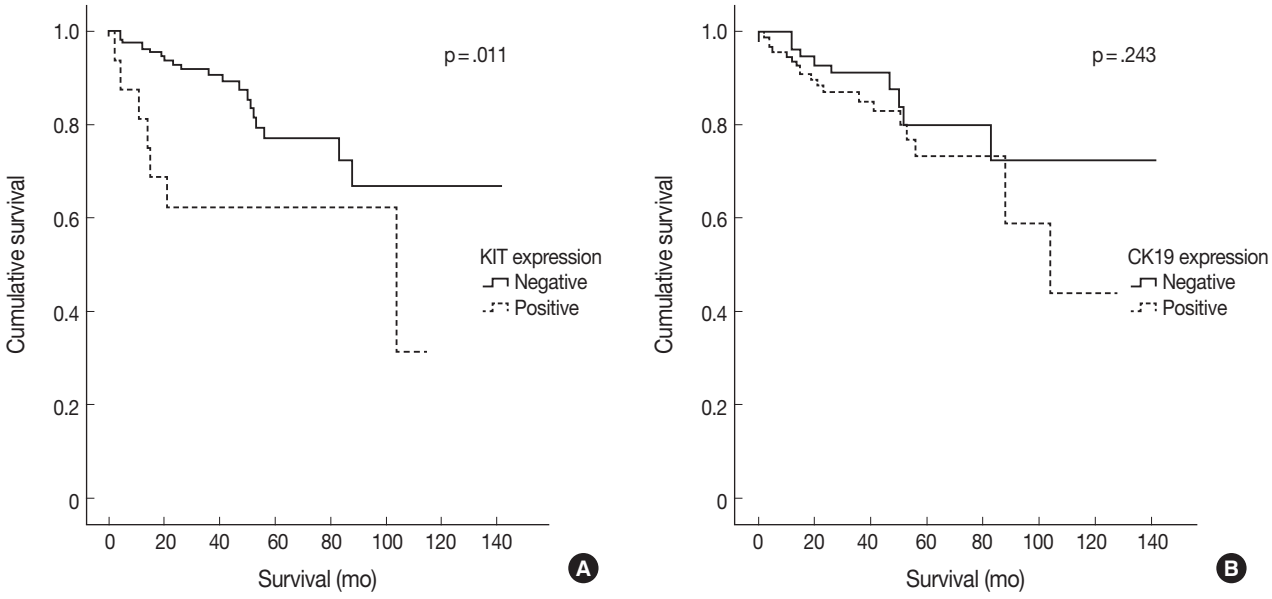

Fig. 2. Kaplan-Meier survival analysis of pancreatic neuroendocrine tumor patients according to KIT (A) and cytokeratin 19 (CK19) (B) expression status. (A) The overall 5-year survival rate for pancreatic neuroendocrine tumor (PanNET) patients with KIT expression is significantly lower (62%) than that of patients without KIT expression (77%, p=.011). (B) The overall 5-year survival rate for PanNET patients with CK19 expression (74%) is not significantly different from that of those without CK19 expression (79%, p=.243).

Table 2. Univariate analysis of overall survival by clinicopathologic features with PanNETs

Parameter		5-Year survival rate (%)	p-value
Sex	Male	82	.673
	Female	72	
Age (yr)	<60	87	<.001
	≥60	50	
Function status	Functioning tumors	91	.349
	Non-functioning	72	
Tumor size (cm)	≤2	85	.171
	>2	72	
Extrapancreatic extension	Absent	82	.003
	Present	66	
pT classification	pT1	88	.009
	pT2	78	
	pT3	65	
Lymph node metastasis	Absent	78	.026
	Present	56	
Distant metastasis	Absent	80	.003
	Present	63	
WHO grade	Grade 1	86	<.001
	Grade 2	62	
	Grade 3	0	
KIT expression	Negative	77	.011
	Positive	62	
CK19 expression	Negative	79	.243
	Positive	74	
Lymphovascular invasion	Absent	80	.071
	Present	68	
Perineural invasion	Absent	79	.152
	Present	63	

PanNET, pancreatic neuroendocrine tumor; WHO, World Health Organization; CK19, cytokertain 19.

Table 3. Multivariate analysis of overall survival by clinicopathologic features with pancreatic neuroendocrine tumors

Parameter		Hazard ratio	95% Confidence interval		p-value
			Low	Upper	
KIT expression		2.09	0.69	6.33	.195
pT classification	T1	1	-	-	.786
	T2	1.73	0.31	9.51	.529
	T3	1.84	0.31	11.01	.503
Lymph node metastasis		1.53	0.51	4.60	.446
Distant metastasis		0.5	0.17	1.46	.204
WHO Grade	1	1	-	-	.001
	2	2.41	0.84	6.89	.102
	3	18.27	4.12	80.99	<.001

WHO, World Health Organization.

DISCUSSION

KIT is a cytoplasmic membrane-bound receptor tyrosine kinase and a stem cell marker. Activation of KIT signaling has been found to mediate cell survival, migration, and proliferation.[14] Signaling from KIT is crucial for normal hematopoiesis, pigmentation, fertility, and gut movement. Deregulated KIT kinase activity has been observed in a number of pathological conditions, including small cell lung cancer, breast cancer, colon cancer, melanoma, gastrointestinal stromal tumors, and allergy.[14] KIT is involved in β-cell development and survival and in regulation of glucose metabolism of the endocrine pancreas

http://dx.doi.org/10.4132/jptm.2014.10.23

via receptor phosphorylation.[15-19] Normally, KIT expression in the endocrine pancreas is present during the embryonic and early fetal periods; however, it is not expressed in the adult pancreas.[15,19] Thus, KIT expression in the endocrine pancreas is considered to be a stem cell feature. Several pancreatic neoplasms with KIT expression have been reported, including ductal adenocarcinomas, intraductal papillary mucinous neoplasms, mucinous cystic neoplasms, serous cyst adenomas, and neuroendocrine tumors, although the proportion of pancreatic neoplasms expressing KIT was small.[20,21]

Several previous studies have reported KIT expression in PanNETs, with 22% to 46% of PanNETs expressing KIT.[2,13,22] In the present study, we observed KIT expression in 8.8% (16/182) of PanNET cases. This is a significantly lower percentage than reported in previous studies and might be related to ethnicity, as all previous studies were performed with Caucasians while all the cases included in the present study were Koreans. KIT expression is generally associated with worse prognosis in cancers of other organs, including colorectal, stomach, bile duct, and endometrial cancers, and malignant melanomas of the vulva.[23-27] In contrast, KIT expression in patients with neuroblastomas and hepatocellular carcinomas is an indicator of good survival.[28,29] There have been controversies with respect to the prognostic significance of KIT expression in PanNETs.[2,13] Zhang *et al.*[13] reported that KIT expression was an independent worse prognostic factor for PanNETs, while Han *et al.*[2] observed no significant survival differences based on KIT expression. PanNETs with KIT expression resulted in significantly worse survival than those without KIT expression in the present study; a finding that concurs with those of the previous study of Zhang *et al.*[13] A plausible explanation for the worse prognosis in PanNET cases with KIT expression is that these PanNETs may possess stem cell features. The mechanisms of KIT expression in PanNETs are unknown. One previous study demonstrated no *KIT* mutations in exons 9 and 11 in any of the 21 examined PanNETs expressing KIT.[13] Plausible explanations for KIT overexpression without mutations in exons 9 and 11 include *KIT* mutations that occur in other exons.

CK19 is one of a 20-member cytokeratin family that encompasses the intermediate filaments of epithelial cells. In the early embryonic stage, endocrine cells in the pancreas strongly express CK19. This expression is gradually lost such that most islet cells no longer express CK19 by 41 gestational weeks, whereas all ductal and acinar cells maintain CK19 labeling.[30,31]

Previous studies have demonstrated CK19 expression in 49% to 70% of PanNETs.[2,9,12,13] In the present study, CK19 expression was found in 53.3% (97/182 cases) of PanNETs, which is concordant with the results of previous studies. In previous studies, CK19-expressing PanNETs were associated with aggressive pathologic features, including increased tumor size, mitoses, lymphovascular invasion, and necrosis.[9-12] In accordance with the results of these previous studies, we also observed that PanNETs expressing CK19 were associated with larger tumor size, higher WHO grade, higher TNM stage, and lymphovascular and perineural invasions. Several previous studies have demonstrated that PanNET patients with CK19 expression had decreased survival rates.[9-12] However, in contrast to the results of previous studies, we did not observe any prognostic significance of CK19 expression in PanNET patients, although CK19 expression was related with aggressive clinical behavior in PanNET patients.

In summary, we observed that 1) subsets of PanNETs express KIT or CK19, 2) KIT and CK19 expression was associated with aggressive behavior of PanNETs, and 3) KIT expression was correlated with decreased survival of PanNET patients but was not an independent prognostic factor.

Conflicts of Interest

No potential conflict of interest relevant to this article was reported.

REFERENCES

1. Yao JC, Eisner MP, Leary C, *et al.* Population-based study of islet cell carcinoma. Ann Surg Oncol 2007; 14: 3492-500.
2. Han X, Zhao J, Ji Y, Xu X, Lou W. Expression of CK19 and KIT in resectable pancreatic neuroendocrine tumors. Tumour Biol 2013; 34: 2881-9.
3. Reichert M, Rustgi AK. Pancreatic ductal cells in development, regeneration, and neoplasia. J Clin Invest 2011; 121: 4572-8.
4. Strosberg JR, Cheema A, Weber J, Han G, Coppola D, Kvols LK. Prognostic validity of a novel American Joint Committee on Cancer Staging Classification for pancreatic neuroendocrine tumors. J Clin Oncol 2011; 29: 3044-9.
5. Jiao Y, Shi C, Edil BH, *et al.* DAXX/ATRX, MEN1, and mTOR pathway genes are frequently altered in pancreatic neuroendocrine tumors. Science 2011; 331: 1199-203.
6. Krausch M, Raffel A, Anlauf M, *et al.* Loss of PTEN expression in neuroendocrine pancreatic tumors. Horm Metab Res 2011; 43: 865-71.
7. Marinoni I, Kurrer AS, Vassella E, *et al.* Loss of *DAXX* and *ATRX* are associated with chromosome instability and reduced survival

of patients with pancreatic neuroendocrine tumors. Gastroenterology 2014; 146: 453-60.
8. Bosnan FT, Carneiro F, Hruban RH, Theise ND. WHO classification of tumours of the digestive system. 4th ed. Lyon: IARC Press, 2010.
9. Ali A, Serra S, Asa SL, Chetty R. The predictive value of CK19 and CD99 in pancreatic endocrine tumors. Am J Surg Pathol 2006; 30: 1588-94.
10. Jonkers YM, Claessen SM, Perren A, *et al.* DNA copy number status is a powerful predictor of poor survival in endocrine pancreatic tumor patients. Endocr Relat Cancer 2007; 14: 769-79.
11. La Rosa S, Rigoli E, Uccella S, Novario R, Capella C. Prognostic and biological significance of cytokeratin 19 in pancreatic endocrine tumours. Histopathology 2007; 50: 597-606.
12. Schmitt AM, Anlauf M, Rousson V, *et al.* WHO 2004 criteria and CK19 are reliable prognostic markers in pancreatic endocrine tumors. Am J Surg Pathol 2007; 31: 1677-82.
13. Zhang L, Smyrk TC, Oliveira AM, *et al.* KIT is an independent prognostic marker for pancreatic endocrine tumors: a finding derived from analysis of islet cell differentiation markers. Am J Surg Pathol 2009; 33: 1562-9.
14. Lennartsson J, Rönnstrand L. Stem cell factor receptor/c-Kit: from basic science to clinical implications. Physiol Rev 2012; 92: 1619-49.
15. Li J, Quirt J, Do HQ, *et al.* Expression of c-Kit receptor tyrosine kinase and effect on beta-cell development in the human fetal pancreas. Am J Physiol Endocrinol Metab 2007; 293: E475-83.
16. Ashman LK. The biology of stem cell factor and its receptor C-kit. Int J Biochem Cell Biol 1999; 31: 1037-51.
17. Feng ZC, Li J, Turco BA, Riopel M, Yee SP, Wang R. Critical role of c-Kit in beta cell function: increased insulin secretion and protection against diabetes in a mouse model. Diabetologia 2012; 55: 2214-25.
18. Kaligin MS, Gumerova AA, Titova MA, Andreeva DI, Sharipova ÉI, Kiiasov AP. C-kit is a marker of human pancreatic endocrinocyte stem cells. Morfologiia 2011; 140: 32-7.
19. Liu W, Chen L, Zhu J, Rodgers GP. The glycoprotein hGC-1 binds to cadherin and lectins. Exp Cell Res 2006; 312: 1785-97.
20. Kimura W, Ma J, Takeshita A, *et al.* Analysis of c-kit protein expression in pancreatic neoplasms and its implication for prognosis. Hepatogastroenterology 2007; 54: 2203-8.
21. Ohike N, Sato M, Hisayuki T, *et al.* Immunohistochemical analysis of nestin and c-kit and their significance in pancreatic tumors. Pathol Int 2007; 57: 589-93.
22. Yasuda A, Sawai H, Takahashi H, *et al.* The stem cell factor/c-kit receptor pathway enhances proliferation and invasion of pancreatic cancer cells. Mol Cancer 2006; 5: 46.
23. Sammarco I, Capurso G, Coppola L, *et al.* Expression of the protooncogene c-KIT in normal and tumor tissues from colorectal carcinoma patients. Int J Colorectal Dis 2004; 19: 545-53.
24. Heinzelmann-Schwarz VA, Nixdorf S, Valadan M, *et al.* A clinicopathological review of 33 patients with vulvar melanoma identifies c-KIT as a prognostic marker. Int J Mol Med 2014; 33: 784-94.
25. Kurokawa Y, Matsuura N, Kawabata R, *et al.* Prognostic impact of major receptor tyrosine kinase expression in gastric cancer. Ann Surg Oncol 2014; 21 Suppl 4: S584-90.
26. Hong SM, Hwang I, Song DE, Choi J, Yu E. Clinical and prognostic significances of nuclear and cytoplasmic KIT expressions in extrahepatic bile duct carcinomas. Mod Pathol 2007; 20: 562-9.
27. Scobie JV, Acs G, Bandera CA, *et al.* C-kit immunoreactivity in endometrial adenocarcinomas and its clinicopathologic significance. Int J Gynecol Pathol 2003; 22: 149-55.
28. Chung CY, Yeh KT, Hsu NC, *et al.* Expression of c-kit protooncogene in human hepatocellular carcinoma. Cancer Lett 2005; 217: 231-6.
29. Krams M, Parwaresch R, Sipos B, Heidorn K, Harms D, Rudolph P. Expression of the c-kit receptor characterizes a subset of neuroblastomas with favorable prognosis. Oncogene 2004; 23: 588-95.
30. Piper K, Brickwood S, Turnpenny LW, *et al.* Beta cell differentiation during early human pancreas development. J Endocrinol 2004; 181: 11-23.
31. Bouwens L, Lu WG, De Krijger R. Proliferation and differentiation in the human fetal endocrine pancreas. Diabetologia 1997; 40: 398-404.

 http://dx.doi.org/10.4132/jptm.2014.10.23

Journal of Pathology and Translational Medicine 2015; 49: 37-43
http://dx.doi.org/10.4132/jptm.2014.10.25

■ ORIGINAL ARTICLE ■

Transglutaminase 2 Expression and Its Prognostic Significance in Clear Cell Renal Cell Carcinoma

Min Jee Park[1] · Hae Woon Baek[1]
Ye-Young Rhee[1] · Cheol Lee[1]
Jeong Whan Park[1] · Hwal Woong Kim[2]
Kyung Chul Moon[1,3]

[1]Department of Pathology, Seoul National University College of Medicine, Seoul; [2]Department of Pathology, Good Moonhwa Hospital, Busan; [3]Kidney Research Institute, Medical Research Center, Seoul National University College of Medicine, Seoul, Korea

Received: August 12, 2014
Revised: October 24, 2014
Accepted: October 24, 2014

Corresponding Author
Kyung Chul Moon, M.D.
Department of Pathology, Kidney Research Institute, Medical Research Center, Seoul National University College of Medicine, 103 Daehak-ro, Jongno-gu, Seoul 110-799, Korea
Tel: +82-2-2072-1767
Fax: +82-2-743-5530
E-mail: blue7270@snu.ac.kr

Background: A few recent studies have demonstrated a possible role of transglutaminase 2 (TG2) in tumorigenesis or progression of renal cell carcinoma (RCC). The aim of this study was to examine TG2 expression and its clinicopathologic significance in a large number of human clear cell RCCs (CCRCCs). **Methods:** We analyzed 638 CCRCC patients who underwent partial or radical nephrectomy between 1995 and 2005. The expression of TG2 was determined by immunohistochemistry and categorized into four groups, according to staining intensity: negative (0), mild (1+), moderate (2+), and strong (3+). **Results:** TG2 staining intensity was negative in 8.5% of CCRCC (n=54), 1+ in 32.6% (n=208), 2+ in 50.5% (n=322), and 3+ in 8.5% (n=54). Strong TG2 expression was correlated with high Fuhrman nuclear grade (p=.011), high T category (p=.049), metastasis (p=.043) and male sex (p<.001) but not with N category.The survival analysis showed a significant association between strong TG2 expression and worse overall and cancer-specific survival (p=.027 and p=.010, respectively). On multivariate analysis, strong TG2 expression was a marginally significant prognostic indicator for Fuhrman nuclear grade and TNM staging (p=.054). **Conclusions:** Our study is the first to demonstrate the clinicopathologic significance of TG2 expression in a large number of human CCRCC samples. Strong TG2 expression was associated with high nuclear grade and poor prognosis.

Key Words: Transglutaminases; Carcinoma, renal cell; Prognosis

Renal cell carcinoma (RCC) is the most common renal malignant tumor in adults, accounting for approximately 90% of renal malignancies.[1] RCC is classified into several subtypes such as clear cell, chromophobe, papillary, collecting duct, and other rare subtypes. These subtypes show distinct clinical, pathological and molecular characteristics. Clear cell RCC (CCRCC) is the most common RCC and has a worse prognosis compared with other common histologic subtypes, such as chromophobe and papillary RCC. Approximately 25%–30% of patients are diagnosed with metastatic RCC at initial presentation,[2] and the disease will progress during the follow-up period in up to 50% of patients treated for localized RCC.[3] Prognostic indicators in CCRCC include clinical parameters and pathological factors, and many molecular prognostic markers have been suggested.[4]

Transglutaminases are a family of enzymes, that exist as cross-linked protein polymers and are resistant to proteolytic degradation.[5,6] Transglutaminase 2 (TG2) is ubiquitously expressed, and is a multifunctional molecule, that catalyzes calcium-dependent acyl-transfer activities, resulting in the formation of stable multiprotein complexes that are resistant to proteolysis. In addition, TG2 can also act as a calcium-independent GTPase, a protein disulfide isomerase, and a kinase.[7] In addition, cell surface TG2 is involved in cell adhesion via its tight interaction with fibronectin.[8,9]

TG2 is up-regulated and activated in some pathological conditions, including cancer, tissue fibrosis, and celiac disease.[10,11] Many previous studies have demonstrated the relationship between TG2 expression and some cancers, including breast cancer,[12,13] ovarian cancer,[14] pancreatic cancer,[15,16] lung cancer,[17] and melanoma.[18] TG2 may be involved in cancer progression or metastasis via regulation of tumor cell growth, tumor survival, tumor cell–extracellular matrix (ECM) interaction, or epithelial-

pISSN 2383-7837
eISSN 2383-7845

mesenchymal transition.[19,20]

A few recent studies showed that TG2 expression was increased in RCC,[21] and up-regulation of TG2 was associated with a decrease in tumor necrosis in RCC samples.[22] Furthermore a few studies have shown a relationship between TG2 and von Hippel–Lindau (*VHL*) gene expression in RCC cell lines.[23,24] However, the prognostic significance of TG2 expression in CCRCC has not been reported.

In this study, we investigated the TG2 expression in 638 CCRCC samples using immunohistochemistry and evaluated the clinicopathologic prognostic significance of TG2 expression.

MATERIALS AND METHODS

Patients and tumor specimens

We analyzed samples from 638 CCRCC patients who had undergone partial or radical nephrectomy at Seoul National University Hospital in Seoul, Korea between 1995 and 2005. The Seoul National University Hospital Institutional Review Board approved this study. All the clinicopathologic data were obtained from medical records, pathology reports and the review of hematoxylin and eosin (H&E)–stained slides. H&E slides were reviewed for tumor staging and nuclear grade. The tumor stage was determined according to the pTNM staging guidline published by the 2010 American Joint Committee on Cancer (AJCC),[25] and nuclear grading was performed based on the Fuhrman nuclear grading scale.[26] The recurrence or metastasis of CCRCC was determined by the clinical, radiological and pathological parameters. Confirmation of patients' deaths was obtained from medical records or death certificates.

Tissue microarray and immunohistochemistry

Following a review of the tumor slides, a representative area from each tumor block was selected and utilized to construct tissue microarrays (TMA) using a trephine apparatus (Superbiochips Laboratories, Seoul, Korea).

Immunohistochemical staining was performed on 4-μm-thick sections taken from the TMA slides using the Bond-Max Autostainer (Leica Microsystems, Bannockburn, IL, USA). Polyclonal rabbit anti-TG2 antibody (Neomarkers, Fremont, CA, USA) was diluted 1:100. After heat-induced antigen retrieval, primary antibodies were incubated with the samples for 15 minutes. The binding of the primary antibody was detected using the Bond Polymer Refine Detection kit (Leica Microsystems) according to the manufacturer's instructions. TG2 immunoreactivity was classified into four categories according to staining intensity: negative (0), weak (1+), moderate (2+), and strong (3+) expression. Constant TG2 staining on endothelial cells was regarded as an internal positive control.

Statistical analysis

SPSS ver. 21 (IBM Co., Armonk, NY, USA) was used for statistical analysis. The association between clinicopathologic findings and TG expression was analyzed using the linear by linear association. Overall survival and cancer-specific survival were analyzed using the Kaplan-Meier method supported by the log-rank test. The overall survival was defined as the time interval from primary radical or partial nephrectomy to last follow-up or patients' death. The cancer-specific survival was defined as the time interval from primary radical or partial nephrectomy to last follow-up or cancer-related death and was recorded at final follow-up visit as alive or dead from an unrelated cause. The Cox regression model was used for multivariate analysis. All statistical analyses were 2-tailed, and a $p < .05$ was regarded as statistically significant.

RESULTS

Clinicopathologic characteristics

The study population included 473 men and 165 women. The ages of the patient population ranged from 24 to 84 years with a mean age of 56.0 years (mean±SD, 56.02±11.53 years). The measured tumors ranged in size from 0.8 to 22 cm with a mean size of 5.6 cm (mean±SD, 5.63±3.40 cm). Patient follow-up times ranged from 2 to 223 months with an average follow-up period of 85.7 months (mean±SD, 85.71±48.46 months). At the time of surgery, lymph node metastases were found in 18 cases (2.8%), and distant metastases were found in 53 cases (8.3%). Four hundred and eight cases were classified as pTNM stage I (63.6%), 82 as stage II (12.8%), 91 as stage III (14.2%), and 57 as stage IV (8.9%). According to Fuhrman nuclear grade, 49 cases were classified as grade 1 (7.7%), 291 as grade 2 (45.6%), 235 as grade 3 (36.8%), and 63 as grade 4 (9.9%).

TG2 expression in CCRCC

In the non-neoplastic renal parenchyme, TG2 was faintly expressed, only focally. In CCRCC, TG2 was diffusely expressed in the cytoplasm of tumor cells in most cases (positive in 584 CCRCCs, 91.5%), but the staining intensity was variable. TG2 expression showed a cytoplasmic or membranous pattern. The evaluation of the staining intensity revealed that 54 (8.5%) were negative, 208 showed weak TG2 expression (32.6%), 322

http://dx.doi.org/10.4132/jptm.2014.10.25

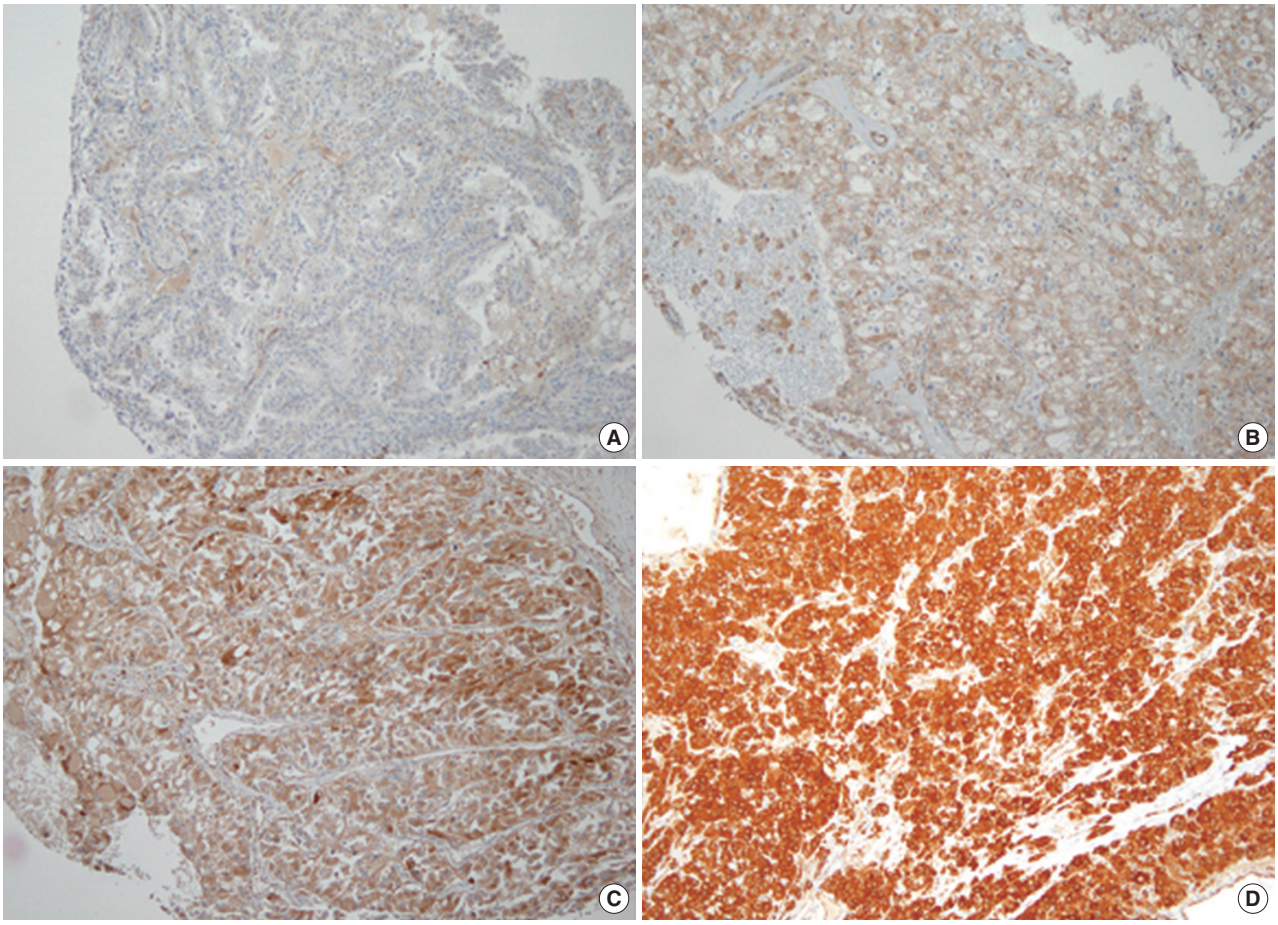

Fig. 1. Immunohistochemical analysis of the intensity of transglutaminase 2 expression in clear cell renal cell carcinoma showing 0 (A), 1+ (B), 2+ (C), and 3+ (D).

showed moderate TG2 expression (50.5%), and 54 (8.5%) showed strong TG2 expression (Fig. 1).

The relationship between TG2 expression and pathologic parameters is shown in Table 1. Strong TG2 expression was correlated with high Fuhrman nuclear grade ($p = .011$), high T category ($p = .049$), metastasis ($p = .043$) and male sex ($p < .001$) but not with N category.

TG2 expression and survival analysis

Overall and cancer-specific survival times were not significantly different between groups showing TG2 staining intensities of 0, 1+, and 2+ ($p = .872$ and $p = .816$, respectively). In contrast, the strong (3+) TG2 expression grouphad significantly shorter overall and cancer specific survival periods compared with groups showing staining intensities 0, 1+, or 2+ ($p = .027$ and $p = .010$, respectively) (Table 2, Fig. 2). Upon multivariate analysis, strong TG2 expression was shown to be a marginal independent prognostic indicator of cancer-specific survival for Fuhrman nuclear grade and TNM staging ($p = .054$). However, these analyses were not statistically significant for overall survival ($p = .154$) (Table 3).

DISCUSSION

In this study, we investigated the expression level and clinicopathologic significance of TG2 in CCRCC. TG2 was diffusely expressed in most CCRCCs (584/638, 91.5%). Strong TG2 expression in CCRCC was associated with high Fuhrman nuclear grade, but was not associated with TNM stage. In addition, strong expression of TG2 was associated with significantly worse cancer-specific survival in univariate analysis. A multivariate analysis also showed a marginally significant decrease in cancer-specific survival. To our knowledge, this is the first study to elucidate the prognostic significance of TG2 expression in CCRCC.

Previous studies using cancer cell lines or nude mice have

Table 1. Clinicopathological characteristics of patients with CCRCC and the associations with TG2 expression

Characteristic	Cases (n=638)	TG2 expression				p-value
		0 (n=54, 8.5%)	1+ (n=208, 32.6%)	2+ (n=322, 50.5%)	3+ (n=54, 8.5%)	
Sex						
Male	473	33	137	258	45	<.001
Female	165	21	71	64	9	
Age (yr)						
≤55	238	17	76	134	11	.779
>55	276	28	92	128	28	
Furman grade						
1, 2	340	32	118	172	18	.011
3, 4	298	22	90	150	36	
T category						
1, 2	511	47	172	251	41	.049
3, 4	127	7	36	71	13	
N category						
0 or x	620	53	201	316	50	.453
1	18	1	7	6	4	
M category						
0	585	53	194	289	49	.043
1	53	1	14	33	5	
Stage						
I, II	148	45	163	242	40	.147
III, IV		9	45	80	14	
Lung metastasis						
Absent	518	47	172	262	37	.031
Present	120	7	36	60	17	
Bone metastasis						
Absent	588	51	190	298	49	.767
present	50	3	18	24	5	

CCRCC, clear cell renal cell carcinoma; TG2, transglutaminase 2.

Table 2. A univariate analysis of overall survival and cancer-specific survival in CCRCC patients (log-rank test)

Prognostic factor	Overall survival		Cancer-specific survival	
	Survival time (mean±SE, mo)	p-value	Survival time (mean±SE, mo)	p-value
TG2 expression				
0, 1, 2	171.4±4.2	.027	184.7±4.0	.010
3	143.1±12.5		153.3±12.1	
Nuclear grade				
1, 2	193.7±4.1	<.001	209.0±3.2	<.001
3, 4	139.2±5.2		149.2±5.0	
TNM stage				
I, II	186.5±3.8	<.001	201.2±3.3	<.001
III, IV	105.1±8.7		111.6±8.9	

CCRCC, clear cell renal cell carcinoma; SE: standard error, TG2, transglutaminase 2.

shown the role of TG2 in cancer cell growth, survival and metastasis.[13,16,18] In addition, there have been a few studies showing the clinicopathologic significance of TG2 expression in human cancer tissues. Overexpression of TG2 was associated with poor prognosis in ovarian cancer,[14] and high TG2 expression was associated with nodal metastasis and lymphovascular invasion in pancreatic ductal adenocarcinoma.[15] It has also been suggested that TG2 contributes to cancer progression and metastasis by regulating cancer cell migration into the ECM, adhesion to endothelium, invasion, and angiogenesis.[20]

A few previous studies have described the relationship between TG2 and the *VHL* gene, a well-known gene altered in most CCRCCs.[27] Wykoff *et al*.[23] showed that TG2 is a novel target gene of *VHL* in RCC cell lines. Another study demonstrated that TG2 is a critical regulator of VHL.[24] These studies suggest a close relationship between TG2 and CCRCC. In addition to VHL, p53 was also depleted by TG2 in many RCC cell lines.[28] A recent study examining microRNA expression in RCC demonstrated that miR-1285, one of the microRNAs that are reduced in RCC specimens and cell lines, inhibited cancer cell

 http://dx.doi.org/10.4132/jptm.2014.10.25

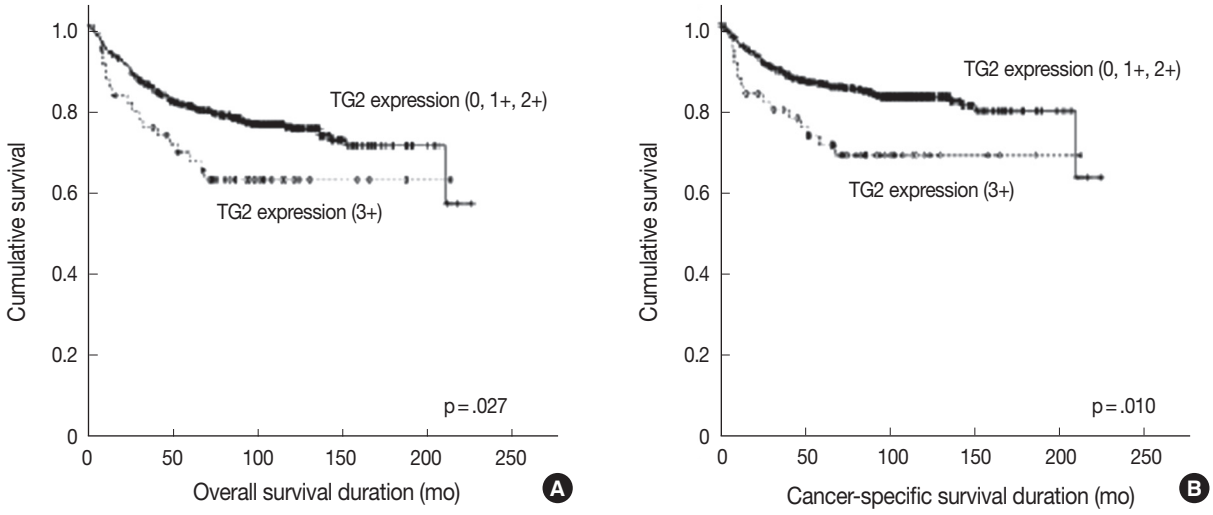

Fig. 2. Kaplan-Meier curves of overall survival (A) and cancer-specific survival (B) in 638 patients with clear cell renal cell carcinoma depending on the level of transglutaminase 2 (TG2) expression.

Table 3. A multivariate analysis of overall survival and cancer-specific survival in CCRCC patients (Cox proportional hazard model)

Prognostic factor		Overall survival		Cancer specific survival	
		HR (95% CI)	p-value	HR (95% CI)	p-value
TG2 expression	3 vs 0,1,2	0.665 (0.409–1.081)	.100	0.598 (0.350–1.020)	.059
Histologic grade	3,4 vs 1,2	0.472 (0.327–0.680)	<.001	0.295 (0.177–0.490)	<.001
TNM stage	III, IV vs I, II	0.190 (0.136–0.265)	<.001	0.107 (0.069–1.165)	<.001

CCRCC, clear cell renal cell carcinoma; HR, hazard ratio; CI, confidence interval; TG2, transglutaminase 2.

proliferation, invasion and migration, as well as directly regulating TG2 expression.[21] Thus, previous studies indicate that TG2 may play a role in pathogenesis or progression of RCC. However, only few studies examined TG2 expression in human RCC samples. Erdem *et al*.[22] investigated TG2 mRNA expression in 95 primary RCC samples and found that TG2 expression alone was not associated with RCC subtype, nuclear grade, T classification or tumor size. Another study examined TG2 expression by immunohistochemistry in 70 RCC samples, finding an increased TG2 expression in RCC tissue compared to normal kidney tissue and a significant correlation between increased TG2 expression and high T classification.[21] Although these two previous studies showed the significance of TG2 expression in human RCC, in part, they also had some limitations such as relatively small sample sizes and no evaluation of the prognostic significance of TG2 expression.

We showed the clinicopathologic significance and prognostic implications of TG2 expression in a large number of CCRCCs. The majority of CCRCCs showed diffuse TG2 staining, but the staining intensity was variable. Only a small subset of CCRCCs showed strong TG2 expression (54/638, 6.5%) that correlated with significantly worse prognosis. The remaining cases showing negative to moderate TG2 expression revealed no significant association of TG2 staining intensity with prognosis.

Although the precise role of TG2 in the progression of CCRCC is not clear, previous studies have suggested some possible mechanisms. First, TG2 can regulate cell adhesion. Overexpression of TG2 in breast cancer cell lines has been reported to contribute to cancer cell invasion and metastasis through the interaction of TG2 with ECM components such as β integrins and fibronectin.[13,29]

In primary RCC samples, increased expression of TG2, along with β1 integrin and syndecan-4, was reported to be associated with metastasis.[22] Second, TG2 has been suggested to regulate apoptosis. Inhibition of TG2 was found to stabilize p53 expression, increasing apoptosis in RCC cell lines.[28] These results suggest that TG2 might enhance metastasis and tumor cell survival.

Our study also demonstrated that high TG2 expression is associated with tumor aggressiveness such as T category and metastasis. Our results are similar to those of previous studies showing an association between TG2 expression and metastasis or tumor stage of RCC.[21,22] However, there were some differences between these previous studies and our study. First, the study sample was

smaller than that of our study (70 and 95 in previous studies versus 638 in our study). Second, they did not separate the RCC subtypes, but we included CCRCC only.

In addition our study showed that strong TG2 expression was related to high nuclear grade of CCRCC. This result suggests that TG2 expression might be related to the differentiation of CCRCC.

In conclusion, our study is the first to demonstrate the clinicopathologic significance of TG2 expression in a large number of human CCRCC samples. Strong TG2 expression was related to tumor aggressiveness, high nuclear grade and poor prognosis.

Conflicts of Interest

No potential conflict of interest relevant to this article was reproted.

Acknowledgments

This research was supported by Basic Science Research Program through the National Research Foundation of Korea (NRF) funded by the Ministry of Education, Science and Technology (grant number: 2010-0004550).

REFERENCES

1. Ljungberg B, Campbell SC, Choi HY, *et al*. The epidemiology of renal cell carcinoma. Eur Urol 2011; 60: 615-21.
2. Ljungberg B, Hanbury DC, Kuczyk MA, *et al*. Renal cell carcinoma guideline. Eur Urol 2007; 51: 1502-10.
3. Lam JS, Leppert JT, Figlin RA, Belldegrun AS. Surveillance following radical or partial nephrectomy for renal cell carcinoma. Curr Urol Rep 2005; 6: 7-18.
4. Ljungberg B. Prognostic markers in renal cell carcinoma. Curr Opin Urol 2007; 17: 303-8.
5. Lorand L, Graham RM. Transglutaminases: crosslinking enzymes with pleiotropic functions. Nat Rev Mol Cell Biol 2003; 4: 140-56.
6. Greenberg CS, Birckbichler PJ, Rice RH. Transglutaminases: multifunctional cross-linking enzymes that stabilize tissues. FASEB J 1991; 5: 3071-7.
7. Collighan RJ, Griffin M. Transglutaminase 2 cross-linking of matrix proteins: biological significance and medical applications. Amino Acids 2009; 36: 659-70.
8. Gaudry CA, Verderio E, Aeschlimann D, Cox A, Smith C, Griffin M. Cell surface localization of tissue transglutaminase is dependent on a fibronectin-binding site in its N-terminal beta-sandwich domain. J Biol Chem 1999; 274: 30707-14.
9. Gaudry CA, Verderio E, Jones RA, Smith C, Griffin M. Tissue transglutaminase is an important player at the surface of human endothelial cells: evidence for its externalization and its colocalization with the beta(1) integrin. Exp Cell Res 1999; 252: 104-13.
10. Belkin AM. Extracellular TG2: emerging functions and regulation. Febs J 2011; 278: 4704-16.
11. Wang Z, Griffin M. TG2, a novel extracellular protein with multiple functions. Amino Acids 2012; 42: 939-49.
12. Mehta K, Fok J, Miller FR, Koul D, Sahin AA. Prognostic significance of tissue transglutaminase in drug resistant and metastatic breast cancer. Clin Cancer Res 2004; 10: 8068-76.
13. Mangala LS, Fok JY, Zorrilla-Calancha IR, Verma A, Mehta K. Tissue transglutaminase expression promotes cell attachment, invasion and survival in breast cancer cells. Oncogene 2007; 26: 2459-70.
14. Hwang JY, Mangala LS, Fok JY, *et al*. Clinical and biological significance of tissue transglutaminase in ovarian carcinoma. Cancer Res 2008; 68: 5849-58.
15. Verma A, Wang H, Manavathi B, *et al*. Increased expression of tissue transglutaminase in pancreatic ductal adenocarcinoma and its implications in drug resistance and metastasis. Cancer Res 2006; 66: 10525-33.
16. Verma A, Guha S, Diagaradjane P, *et al*. Therapeutic significance of elevated tissue transglutaminase expression in pancreatic cancer. Clin Cancer Res 2008; 14: 2476-83.
17. Park KS, Kim HK, Lee JH, *et al*. Transglutaminase 2 as a cisplatin resistance marker in non-small cell lung cancer. J Cancer Res Clin Oncol 2010; 136: 493-502.
18. Fok JY, Ekmekcioglu S, Mehta K. Implications of tissue transglutaminase expression in malignant melanoma. Mol Cancer Ther 2006; 5: 1493-503.
19. Kumar S, Mehta K. Tissue transglutaminase, inflammation, and cancer: how intimate is the relationship? Amino Acids 2013; 44: 81-8.
20. Lentini A, Abbruzzese A, Provenzano B, Tabolacci C, Beninati S. Transglutaminases: key regulators of cancer metastasis. Amino Acids 2013; 44: 25-32.
21. Hidaka H, Seki N, Yoshino H, *et al*. Tumor suppressive microRNA-1285 regulates novel molecular targets: aberrant expression and functional significance in renal cell carcinoma. Oncotarget 2012; 3: 44-57.
22. Erdem M, Erdem S, Sanli O, *et al*. Up-regulation of TGM2 with ITGB1 and SDC4 is important in the development and metastasis of renal cell carcinoma. Urol Oncol 2014; 32: 25.e13-20.
23. Wykoff CC, Pugh CW, Maxwell PH, Harris AL, Ratcliffe PJ. Identification of novel hypoxia dependent and independent target genes of the von Hippel-Lindau (VHL) tumour suppressor by mRNA differential expression profiling. Oncogene 2000; 19: 6297-305.
24. Kim DS, Choi YB, Han BG, *et al*. Cancer cells promote survival

 http://dx.doi.org/10.4132/jptm.2014.10.25

through depletion of the von Hippel-Lindau tumor suppressor by protein crosslinking. Oncogene 2011; 30: 4780-90.
25. Edge SB, Byrd DR, Compton CC, Fritz AG, Greene FL, Trotti A. AJCC cancer staging manual. 7th ed. New York: Springer, 2010.
26. Fuhrman SA, Lasky LC, Limas C. Prognostic significance of morphologic parameters in renal cell carcinoma. Am J Surg Pathol 1982; 6: 655-63.
27. Eble JN, Sauter G, Epstein JI, Sesterhenn IA. Pathology and genetics of tumours of the urinary system and male genital organs. Lyon: IARC Press, 2004.
28. Ku BM, Kim DS, Kim KH, *et al*. Transglutaminase 2 inhibition found to induce p53 mediated apoptosis in renal cell carcinoma. FASEB J 2013; 27: 3487-95.
29. Herman JF, Mangala LS, Mehta K. Implications of increased tissue transglutaminase (TG2) expression in drug-resistant breast cancer (MCF-7) cells. Oncogene 2006; 25: 3049-58.

Journal of Pathology and Translational Medicine 2015; 49: 44-51
http://dx.doi.org/10.4132/jptm.2014.10.13

■ ORIGINAL ARTICLE ■

Expression of c-MET in Invasive Meningioma

Sumi Yun · Jae Moon Koh
Kyu Sang Lee[1] · An Na Seo[2]
Kyung Han Nam[3] · Gheeyoung Choe[1]

Department of Pathology, Seoul National University Hospital, Seoul National University College of Medicine, Seoul; [1]Department of Pathology, Seoul National University Bundang Hospital, Seoul National University College of Medicine, Seongnam; [2]Department of Pathology, Kyungpook National University Hospital, Kyungpook National University School of Medicine, Daegu; [3]Department of Pathology, Haeundae Paik Hospital, Inje University, Busan, Korea

Received: August 29, 2014
Revised: October 7, 2014
Accepted: October 13, 2014

Corresponding Author
Gheeyoung Choe, M.D.
Department of Pathology, Seoul National University Bundang Hospital, Seoul National University College of Medicine, 82 Gumi-ro 173beon-gil, Bundang-gu, Seongnam 463-707, Korea
Tel: +82-31-787-7711
Fax: +82-31-787-4012
E-mail: gychoe@snu.ac.kr

Background: Meningiomas show high recurrence rates even after curative tumor removal. The invasiveness of meningiomas may contribute to their high recurrence rates. Recently, c-MET and hepatocyte growth factor (HGF) have been reported to be involved in cancer invasion. **Methods:** We examined the immunohistochemical expression of c-MET and HGF in 100 cases of patients with meningiomas who have undergone complete tumor removal. **Results:** c-MET^{High} and HGF^{High} were found in 17% and 13% of meningiomas, respectively. Brain invasion was observed in 17.6% of c-MET^{High} meningiomas, but in only 2.4% of c-MET^{Low} meningiomas ($p=.033$). Bone/soft tissue invasion was observed in 23.5% of c-MET^{High} meningiomas and in 9.6% of c-MET^{Low} meningiomas ($p=.119$). HGF^{High} did not show statistical association with brain invasion or bone/soft tissue invasion. c-MET^{High} demonstrated shorter recurrence-free survival (RFS, 93.5±8.2 months vs 96.1±1.9 months); however, this difference was not statistically significant ($p=.139$). There was no association of HGF^{High} with RFS. **Conclusions:** This study demonstrates that c-MET^{High} is associated with brain invasion of meningiomas, and that c-MET expression may be a useful predictive marker for meningioma recurrence. Patients with invasive meningiomas with high expressions of c-MET may be good candidates for targeted therapy using c-MET inhibitors.

Key Words: Meningioma; Proto-oncogene proteins c-MET; Hepatocyte growth factor; Neoplasm invasiveness; Immunohistochemistry

Meningioma is a common intracranial tumor arising from the meningothelial (arachnoid) cells. Meningiomas are divided into 15 histologic subtypes and three grades, including benign (grade I), atypical (grade II), and anaplastic (grade III).[1] Most meningiomas are benign, corresponding to World Health Organization (WHO) grade I, and they have a favorable outcome. Alternatively, grade II atypical meningiomas and grade III anaplastic meningiomas have less favorable outcomes.[2,3] Even in benign cases, meningiomas have high recurrence rates after curative surgical treatment. They have been estimated to recur in 7%–25%, 29%–52%, and 50%–94% of cases in grades I, II, and III, respectively.[4]

Several markers, such as the proliferation index, the vascular density marker, and the expression of sex hormone receptors, are suggested for predicting the recurrence rates of tumors. However, it is generally accepted that both histopathological features, including histologic subtypes and clinical data, have limitations in their use as reliable markers for predicting tumor recurrence due to low accuracy.[5-8] Previous studies report an association among meningiomas, brain or bone invasion, and higher tumor recurrence rates. However, the mechanism of invasion has not been well established.[9-12]

Also called a hepatocyte growth factor (HGF), c-MET is a receptor tyrosine kinase that, upon binding of its ligand, is phosphorylated. Subsequently, c-MET activates the signaling pathway of cell proliferation and migration. The c-MET/HGF signaling pathway was first described as an oncogene in the 1980s. Accordingly, it has been known to induce tumor cell proliferation, motility, and invasion, as well as to promote angiogenesis in several human cancers, such as breast, lung and hepatocellular

pISSN 2383-7837
eISSN 2383-7845

carcinomas.[13-16] In meningiomas, the expression of c-MET/HGF has been reported to have a diverse relationship with tumor recurrence, angiogenesis, histologic subtypes, and the invasiveness of the meningioma. Existing reports are based on a limited number of samples and different methods, such as enzyme-linked immunosorbent assay, immunohistochemistry or reverse transcription polymerase chain reaction (RT-PCR).[17-19] To date, little is known about their expression in invasive meningiomas. The aim of this study, therefore, is to elucidate whether the protein expressions of c-MET and HGF are associated with clinicopathologic variables, as well as brain and bone/soft tissue invasion of meningiomas, in large scale studies of meningioma.

MATERIALS AND METHODS

Meningioma cases

Formalin-fixed, paraffin-embedded archival tissue samples from 100 patients who underwent complete surgical resection (Simpson grade I) of meningiomas between August 2003 and December 2012 were collected from the databases of the Department of Pathology, Seoul National University Bundang Hospital in Korea. Clinical and pathological data were obtained by reviewing medical records and pathology reports. Two pathologists (G.C. and S.Y.) independently reviewed the hematoxylin and eosin–stained slides, confirmed the diagnosis according to the 2007 WHO classification system, and classified the histological subtypes and grading of the meningiomas. All the patients received regular follow-up after surgery, without postoperative chemoradiation therapy. The recurrence-free survival (RFS) was calculated from the time of surgery to the first suspected recurrence of meningioma. Evidence of tumor recurrence was provided by a computed tomography scan or a magnetic resonance image showing a meningioma in a location contiguous with the previous operation site.

Demographic data

The clinicopathologic features of patients are summarized in Table 1. The 100 patients consisted of 23 males (23%) and 77 females (77%), with median age of 60 years (range, 36 to 85 years). Of these, bone/soft tissue invasion was observed in 12 cases, brain invasion was observed in five cases, and both bone/soft tissue invasion and brain invasion were observed in one case. We defined "soft tissue invasion" as invasion of the meningioma to the scalp or paranasal sinus. According to the 2007 WHO classification, all were cases of benign meningiomas (grade I). Histologically, the 100 cases consisted of meningothelial types (n = 32), transitional types (n = 32), fibrous types (n = 16), angiomatous types (n = 13), psammomatous types (n = 2), microcystic types (n = 4), and one metaplastic type (n = 1) (Table 1).

Table 1. Clinicopathologic characteristics of meningioma cases

Characteristic	No.
Meadian age (range, yr)	60 (36–85)
Sex	
Male	23
Female	77
Histologic subtype	
Meningothelial	32
Transitional	32
Fibrous	16
Angiomatous	13
Psammomatous	2
Microcystic	4
Metaplastic	1

Construction of tissue microarray

We chose one representative tumor block in each case, and harvested cores with diameters of 3 mm from the most representative tumor areas of the donor blocks. The cores were precisely arranged into new recipient tissue microarray (TMA) blocks using a trephine apparatus according to previously described protocols.[20]

Immunohistochemistry staining and interpretation

Immunohistochemical staining was carried out using TMA according to a previously described method.[20] Briefly, sections of 4 μm were transferred to poly-L-lysine coated adhesive slides and dried, deparaffinized, and rehydrated. The slides were subsequently subjected to heat-induced antigen retrieval. The following antibodies were used according to manufacturer instruction: c-MET (pre-dilution, rabbit monoclonal antibody, Ventana Medical Systems, Inc., Tucson, AZ, USA) and HGFα (1:100, rabbit polyclonal antibody, Santa Cruz Biotechnology, Santa Cruz, CA, USA). The sections were incubated with appropriate reagents from the Dako REAL EnVision Detection System (DAKO, Glostrup, Denmark), and were counterstained with Mayer's hematoxylin. Evaluation of c-MET and HGF expression was assessed according to previous reports.[21] As a positive control for c-MET and HGF, tubular cells of a normal kidney and normal colonic mucosa were used, respectively. Immunostaining without the primary antibody was used as the negative control. Each case was categorized as positive when it showed moderate-to-strong cytoplasmic and/or membranous positivity in tumor cells. Accordingly, we scored expression as c-MET^{High} and HGF^{High} (> 25% positive cells) and c-MET^{Low} and HGF^{Low} (0%–25%

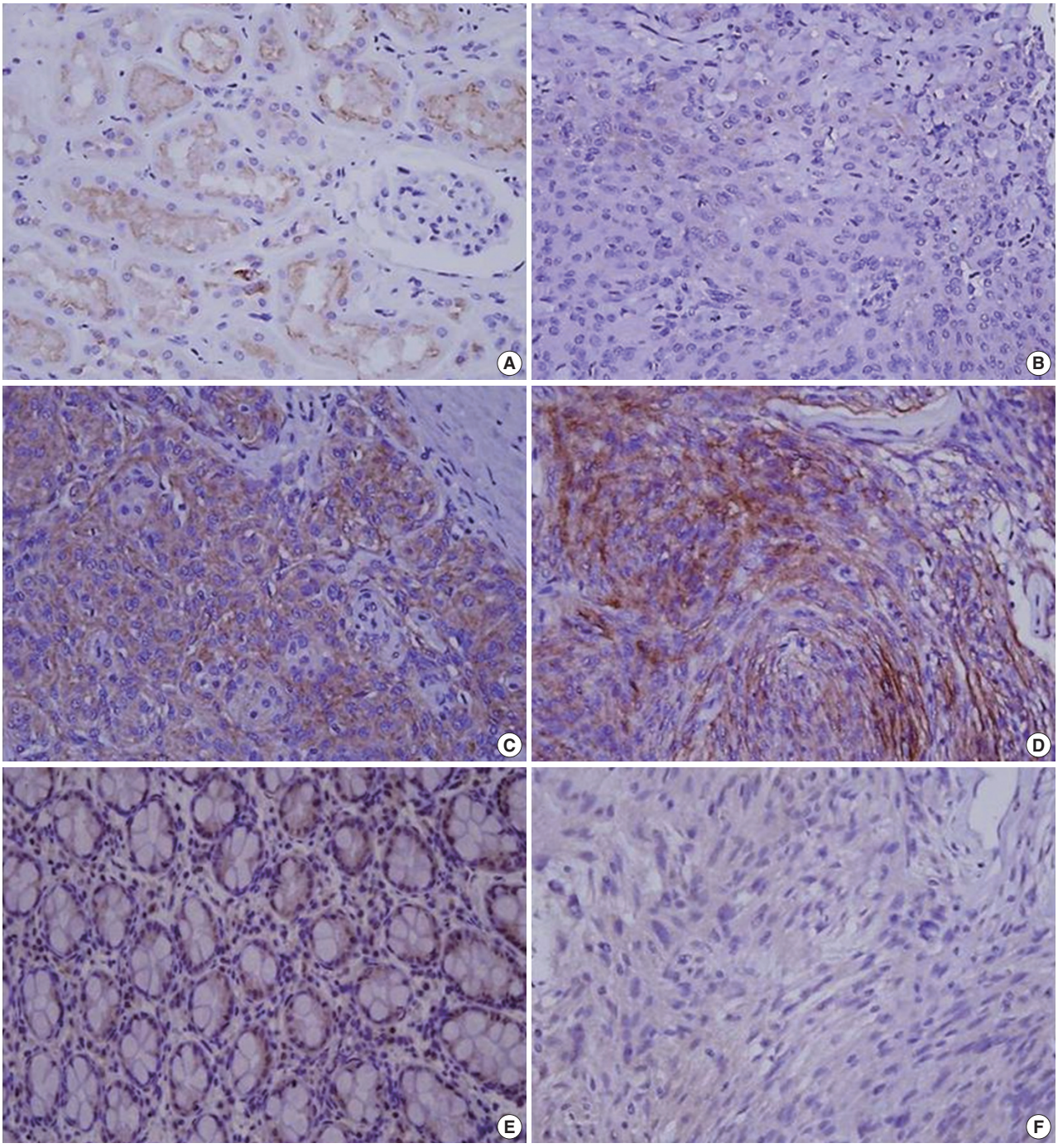

Fig. 1. Immunohistochemical staining in meningiomas. (A) c-MET staining in tubular cells in normal kidney. (B) c-MET weak staining in meningioma. (C) c-MET moderate staining in meningioma. (D) c-MET strong staining in meningioma. (E) Hepatocyte growth factor (HGF) staining in colonic mucosa. (F) HGF weak staining in meningioma.
(*Continued to the next page*)

tumor cells) (Fig. 1).[22]

Ethics statements

The study was conducted according to the ethics standards of the World Medical Association's Declaration of Helsinki.

Statistical analysis

All statistical analyses were conducted using the SPSS ver. 21.0 (IBM Co., Armonk, NY, USA). Associations between the protein expressions of each antibody and the categorical variables were assessed using chi-square tests or Fisher exact tests, if ap-

http://dx.doi.org/10.4132/jptm.2014.10.13

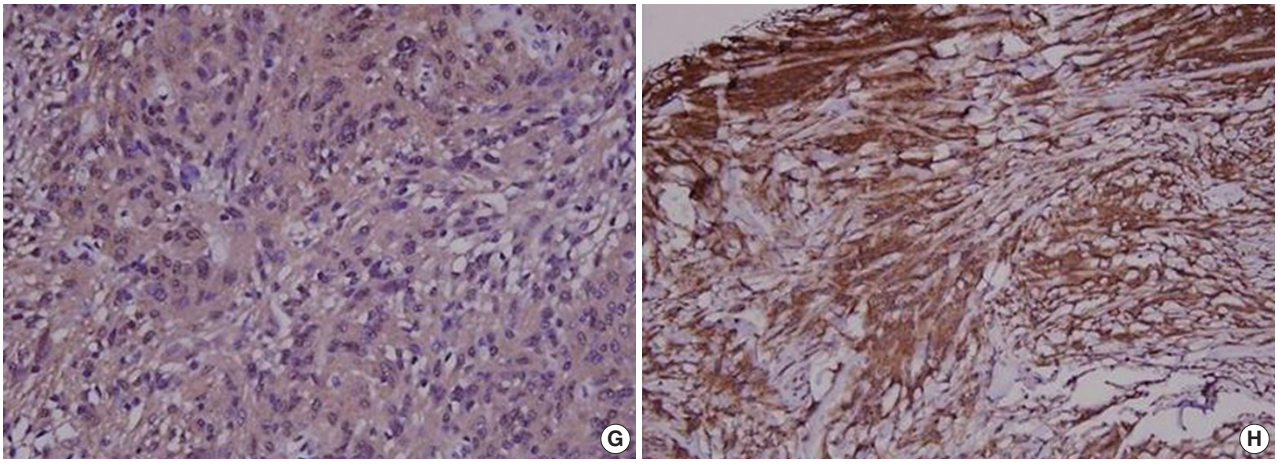

Fig. 1. (*Continued*) (G) HGF moderate staining in meningioma. (H) HGF strong staining in meningioma.

Table 2. Summary of brain and bone/soft tissue invasion in meningiomas

Characteristic	Brain invasion			Bone/soft tissue invasion		
	Yes (n=5)	No (n=95)	p-value	Yes (n=12)	No (n=88)	p-value
Age (yr)	73 (47–77)	60 (36–85)	-	58 (42–75)	60 (36–85)	-
Sex						
Male	3 (13.0)	20 (87.0)	.078	2 (8.7)	21 (91.3)	.728
Female	2 (2.6)	75 (97.4)		10 (13.0)	67 (87.0)	

Values are presented as median (range) or number (%).

propriate. Kaplan-Meier survival curves for RFS were plotted for each antibody, and the survival comparison was determined using log rank tests. All tests were two-tailed, and statistical significance was set as $p < .05$.

RESULTS

Clinical characteristics according to brain invasion and bone/soft tissue invasion

Among the 100 cases of meningiomas, brain invasion was observed in five cases (5%). The median age of cases with brain invasion was 73 years (range, 47 to 77 years). Additionally, 13% (3/23) of male patients presented with brain invasion, and 2.6% (2/77) of female patients presented with brain invasion. Therefore, brain invasion was found to be more common in male patients. Even in male patients, however, statistical significance was not reached ($p = .078$). Bone and/or soft tissue invasion was observed in 12 cases of meningiomas, consisting of two males (8.7%, 2/23) and 10 females (13%, 10/77). Therefore, there was no significant association between bone/soft tissue invasion and sex ($p = .728$). The median age of patients with bone/soft tissue invasion was 58 years (range, 42 to 75 years) (Table 2).

Expression of c-MET and HGF in meningiomas according to histologic subtypes

Of the cases, c-MET$^{\text{High}}$ and HGF$^{\text{High}}$ were found in 17% (17/100) and 13% (13/100) of meningiomas, respectively, and c-MET$^{\text{High}}$/HGF$^{\text{High}}$ co-expressions were observed in 1% (1/100) of meningiomas. c-MET$^{\text{High}}$ and HGF$^{\text{High}}$ showed no significant correlation with the histologic subtypes of meningiomas (Table 3).

Association of the expression of c-MET and HGF with brain invasion

Brain invasion was observed in 3/17 (17.6%) of c-MET$^{\text{High}}$ meningiomas and in 2/83 (2.4%) of c-MET$^{\text{Low}}$ meningiomas. Therefore, there was a statistically significant correlation between c-MET$^{\text{High}}$ and brain invasion ($p = .033$). Neither HGF$^{\text{High}}$ nor c-MET$^{\text{High}}$/HGF$^{\text{High}}$ co-expression showed statistical associations with brain invasion ($p = .375$ and $p = .562$, respectively) (Table 4).

Association of the expression of c-MET and HGF with bone/soft tissue invasion

Of the cases, bone/soft tissue invasion was observed in 4/17 (23.5%) of c-MET$^{\text{High}}$ meningiomas and in 8/83 (9.6%) of c-MET$^{\text{Low}}$ meningiomas. There was a tendency for c-MET$^{\text{High}}$

Table 3. Expression of c-MET and HGF in meningiomas according to histologic subtypes

Histologic subtype	c-MET^{High}	HGF^{High}	c-MET^{High}/HGF^{High}
Meningothelial (n=32)	10 (31.3)	6 (18.8)	4 (12.5)
Transitional (n=32)	1 (3.1)	3 (9.4)	0
Fibrous (n=16)	3 (18.8)	2 (12.5)	1 (6.3)
Angiomatous (n=13)	2 (15.4)	1 (7.7)	0
Psammomatous (n=1)	0	0	0
Microcystic (n=4)	1 (25.0)	1 (25.0)	1 (25.0)
Metaplastic (n=1)	0	0	0

Values are presented as number (%).
HGF, hepatocyte growth factor.

Table 4. Association of the expression of c-MET and HGF with brain invasion and bone/soft tissue invasion

	Brain invasion		p-value	Bone/soft tissue invasion		p-value
	Negative	Positive		Negative	Positive	
c-MET (n=100)						
c-MET^{Low}	81	2	.033	75	8	.119
c-MET^{High}	14	3		13	4	
HGF (n=100)						
HGF^{Low}	82	5	.375	77	10	.653
HGF^{High}	13	0		11	2	
c-MET^{High}/HGF^{High} (n=100)						
Negative	89	5	.562	84	10	.151
Positive	6	0		4	2	

HGF, hepatocyte growth factor.

meningiomas to show bone/soft tissue invasion more frequently than c-MET^{Low} meningiomas; however, statistical significance was not reached (p=.119). Additionally, bone/soft tissue invasion was found in 15.4% (2/13) of HGF^{High} meningioma and 33.3% (2/6) of c-MET^{High}/HGF^{High} meningioma. As a result, HGF^{High} and c-MET^{High}/HGF^{High} co-expressions did not show a significant association with bone/soft tissue invasion (p=.653 and p=.151, respectively).

Tumor RFS according to c-MET and HGF expressions

To identify whether the complete removal of meningiomas from patients differently impacts RFS periods depending on the status of c-MET and HGF expressions, we performed a univariate analysis of 100 cases of Simpson grade I meningiomas. In the current study, the median follow-up period was 26.7 months (range, 1.1 to 106.2 months). Four cases (4%) suffered tumor recurrence.

Among the 17 cases with c-MET^{High}, two cases (11.8%) experienced recurrence, whereas two of 83 cases (2.4%) with c-MET^{Low} suffered recurrence. Cases with c-MET^{High} showed shorter RFS periods (mean±standard deviation [SD], 93.5±8.2 months) than those of c-MET^{Low} (mean±SD, 96.1±1.9 months); however, statistical significance was not reached (p=.139). HGF^{High} and c-MET^{High}/HGF^{High} were not correlated with RFS according to our results (Fig. 2).

DISCUSSION

We set out to determinate whether the expression of c-MET and HGF is associated with the invasiveness of meningiomas and their clinical implications. In the present study, c-MET^{High} correlated with brain invasion and bone/soft tissue invasion. To the best of our knowledge, this is the first large scale report on meningiomas in East Asian patients.

The protein known as c-MET is a receptor tyrosine kinase (RTK), and is a well-known proto-oncogene that is expressed in many organs, including the liver, pancreas, and prostate. In development and wound tissue, c-MET regulates many cellular processes, including cell proliferation, motility and cell survival. HGF is the known ligand of the c-MET RTK.[13-15] Previous studies demonstrate that the c-MET/HGF signaling pathway, as well as c-MET overexpression, has a strong relationship with tumor cell proliferation, motility, invasion, tumor angiogenesis, and poor prognosis. A therapeutic agent targeting c-MET and HGF is currently receiving attention.[13,15] Meningiomas, as previously described, show high recurrence rates, even after curative resection of the tumors. The recurrence rate depends on several prognostic factors, including the invasiveness of the tu-

http://dx.doi.org/10.4132/jptm.2014.10.13

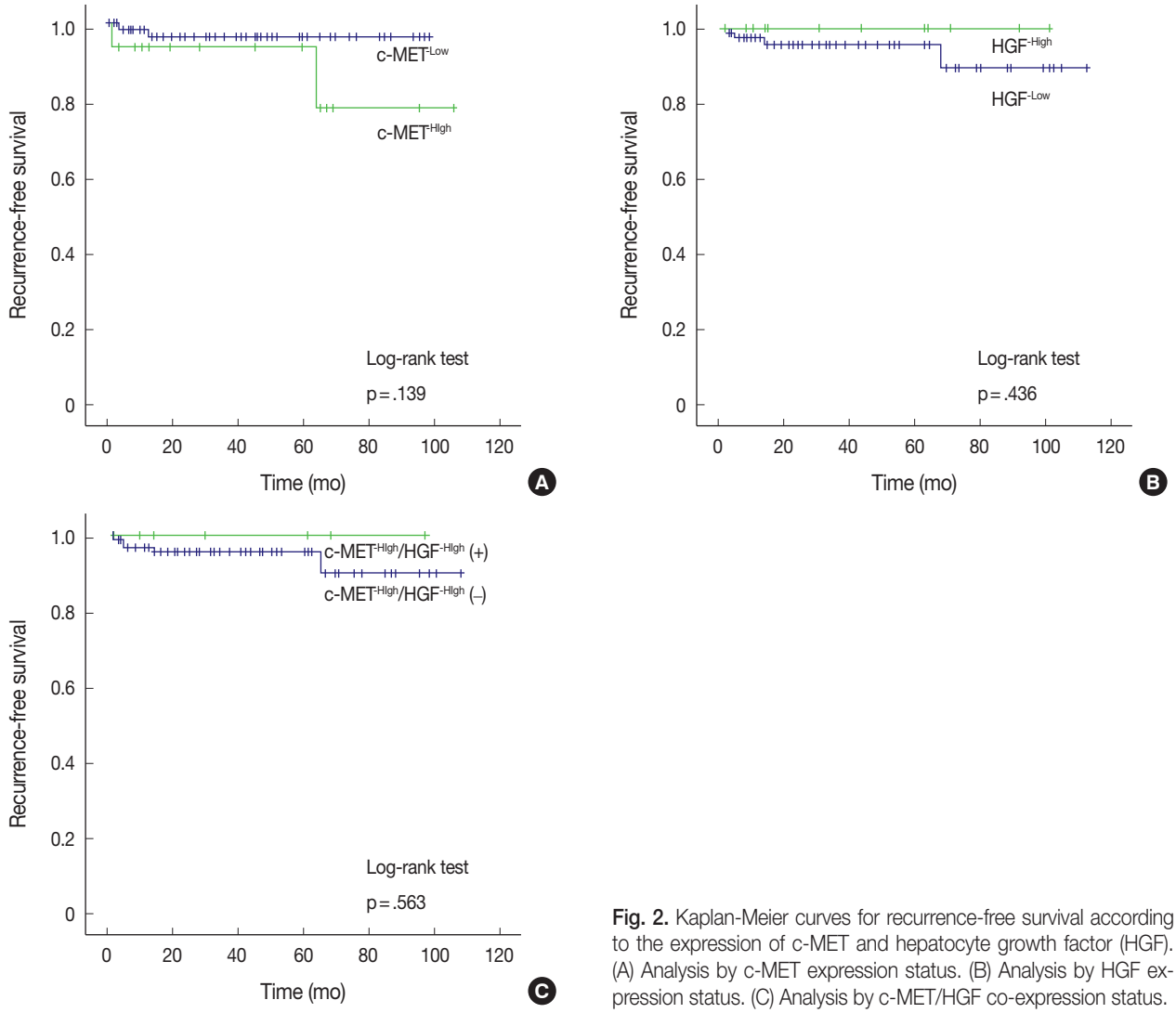

Fig. 2. Kaplan-Meier curves for recurrence-free survival according to the expression of c-MET and hepatocyte growth factor (HGF). (A) Analysis by c-MET expression status. (B) Analysis by HGF expression status. (C) Analysis by c-MET/HGF co-expression status.

mor. Because invasive meningiomas show poor prognosis, the identification of their mechanism may be useful in the management of meningiomas.[23,24] Several studies identify an association of c-MET/HGF expression and clinical significance, and most of these studies imply an association between c-MET/HGF expression and tumor recurrence in meningioma. In Martinez-Rumayor *et al*.'s study,[17] immunohistochemical co-expression of c-MET/HGF is related to cell proliferation and the recurrence of meningiomas. Kim *et al*.[19] also shows that the expression of HGF and the co-expression of c-MET/HGF are associated with the histologic grade of and recurrence of meningiomas by RT-PCR. In contrast, studies by Karja *et al*.[3] and Lamszus *et al*.[18] use enzyme-linked immunosorbent assay and immunohistochemistry to argue that HGF is not related to tumor recurrence in meningioma.[3,21] Few studies demonstrate an association of c-MET/HGF with brain and bone invasion of meningiomas. The present study provides data on the expression of c-MET and HGF in a large scale studies of meningiomas, as well as on the relationships of the meningiomas with brain and bone/soft tissue invasion in patients. In addition, the study shows that c-MET^{High} is significantly associated with meningioma brain invasion, and that there is a tendency for increased c-MET^{High} in meningiomas with bone/soft tissue invasion. However, HGF^{High} does not show any significant association with the invasiveness of meningiomas. Recent studies reveal that the c-MET signaling cascade facilitates the invasion of cancer. The downstream cascade signaling of activated c-MET, by either autocrine or paracrine interaction, leads to the dissociation of tumor cells from the surrounding stromal tissue, resulting in tumor cell invasion.[13,14,25] Our study supports these findings that c-MET is closely related to tumor invasion. One limitation of this study is that only a few cases of rare specific histologic subtypes

are included in the data. Nevertheless, the results suggest that c-MET may participate in tumor invasion.

We also evaluate a possible association between the c-MET and HGF expression and disease recurrence. In this study, the recurrence rate of meningiomas with complete tumor resection is 5%, a finding which is slightly lower than findings in previous reports.[26] Also, we demonstrate that c-MET^{High} only shows a tendency for association with shorter RFS periods. In general, the recurrence of meningiomas occurred within two years of surgical treatment, and up to 94% of patients with meningiomas experienced recurrence within five years.[27] However, the vast majority of meningiomas are slow-growing tumors, and benign meningiomas that have been completely removed from patients recur at a rate of 19% after 20 years of follow-up.[28] Thus our findings about recurrence rates are limited due to an insufficient follow-up period (median follow-up time in this study, 26.7 months). Several studies report an intratumoral heterogeneity of c-MET and HGF expression, revealing an increase in these factors at cancer-invading fronts in breast carcinoma and cholangiocarcinoma.[29,30] Accordingly, further studies are needed to elucidate intratumoral heterogeneity in meningiomas, and the association between c-MET overexpression and RFS.

In summary, our results demonstrate that c-MET is associated with the brain invasion of meningiomas, and that c-MET expression may be useful predictive markers for meningioma recurrence.

Many previous studies reveal that c-MET signaling is involved in the progression and spread of several cancers.[16-19,25,28] The collective understanding of c-MET's role in cancers has evoked considerable interest in c-MET and HGF as major targets in the development of cancer drugs. This has led to the development of a variety of c-MET pathway antagonists with potential clinical applications. Several c-MET antagonists are now under clinical investigation.[13,14,25] We conclude that c-MET expression may be a useful predictive marker for meningioma recurrence, and that invasive meningiomas with high expression of c-MET may be good candidates for targeted therapy using selective c-MET inhibitors.

Conflicts of Interest

No potential conflict of interest relevant to this article was reported.

REFERENCES

1. Louis DN, Ohgaki H, Wiestler OD, Cavenee WK. WHO classification of tumours of the central nervous system. Lyon: IARC Press, 2007.
2. Choy W, Kim W, Nagasawa D, *et al*. The molecular genetics and tumor pathogenesis of meningiomas and the future directions of meningioma treatments. Neurosurg Focus 2011; 30: E6.
3. Karja V, Sandell PJ, Kauppinen T, Alafuzoff I. Does protein expression predict recurrence of benign World Health Organization grade I meningioma? Hum Pathol 2010; 41: 199-207.
4. Perry A, Stafford SL, Scheithauer BW, Suman VJ, Lohse CM. Meningioma grading: an analysis of histologic parameters. Am J Surg Pathol 1997; 21: 1455-65.
5. Ildan F, Erman T, Göçer AI, *et al*. Predicting the probability of meningioma recurrence in the preoperative and early postoperative period: a multivariate analysis in the midterm follow-up. Skull Base 2007; 17: 157-71.
6. Durand A, Labrousse F, Jouvet A, *et al*. WHO grade II and III meningiomas: a study of prognostic factors. J Neurooncol 2009; 95: 367-75.
7. Caltabiano R, Barbagallo GM, Castaing M, *et al*. Prognostic value of EGFR expression in *de novo* and progressed atypical and anaplastic meningiomas: an immunohistochemical and fluorescence *in situ* hybridization pilot study. J Neurosurg Sci 2013; 57: 139-51.
8. Barresi V, Vitarelli E, Tuccari G, Barresi G. MMP-9 expression in meningiomas: a prognostic marker for recurrence risk? J Neurooncol 2011; 102: 189-96.
9. Fathi AR, Roelcke U. Meningioma. Curr Neurol Neurosci Rep 2013; 13: 337.
10. Alahmadi H, Croul SE. Pathology and genetics of meningiomas. Semin Diagn Pathol 2011; 28: 314-24.
11. Terzi A, Saglam EA, Barak A, Soylemezoglu F. The significance of immunohistochemical expression of Ki-67, p53, p21, and p16 in meningiomas tissue arrays. Pathol Res Pract 2008; 204: 305-14.
12. Kliese N, Gobrecht P, Pachow D, *et al*. miRNA-145 is downregulated in atypical and anaplastic meningiomas and negatively regulates motility and proliferation of meningioma cells. Oncogene 2013; 32: 4712-20.
13. Liu X, Newton RC, Scherle PA. Developing c-MET pathway inhibitors for cancer therapy: progress and challenges. Trends Mol Med 2010; 16: 37-45.
14. Guessous F, Zhang Y, diPierro C, *et al*. An orally bioavailable c-Met kinase inhibitor potently inhibits brain tumor malignancy and growth. Anticancer Agents Med Chem 2010; 10: 28-35.
15. Organ SL, Tsao MS. An overview of the c-MET signaling pathway. Ther Adv Med Oncol 2011; 3(1 Suppl): S7-19.
16. Feng Y, Thiagarajan PS, Ma PC. MET signaling: novel targeted inhibition and its clinical development in lung cancer. J Thorac Oncol

2012; 7: 459-67.
17. Martínez-Rumayor A, Arrieta O, Guevara P, *et al*. Coexpression of hepatocyte growth factor/scatter factor (HGF/SF) and its receptor cMET predict recurrence of meningiomas. Cancer Lett 2004; 213: 117-24.
18. Lamszus K, Lengler U, Schmidt NO, Stavrou D, Ergün S, Westphal M. Vascular endothelial growth factor, hepatocyte growth factor/scatter factor, basic fibroblast growth factor, and placenta growth factor in human meningiomas and their relation to angiogenesis and malignancy. Neurosurgery 2000; 46: 938-47.
19. Kim NR, Chae YS, Lim WJ, Cho SJ. Expression of hepatocyte growth factor/c-met by RT-PCR in meningiomas. Korean J Pathol 2011; 45: 463-8.
20. Suh JH, Park JW, Lee C, Moon KC. ERG immunohistochemistry and clinicopathologic characteristics in Korean prostate adenocarcinoma patients. Korean J Pathol 2012; 46: 423-8.
21. Bozkaya G, Korhan P, Cokakli M, *et al*. Cooperative interaction of MUC1 with the HGF/c-Met pathway during hepatocarcinogenesis. Mol Cancer 2012; 11: 64.
22. Kong DS, Song SY, Kim DH, *et al*. Prognostic significance of c-Met expression in glioblastomas. Cancer 2009; 115: 140-8.
23. Palma L, Celli P, Franco C, Cervoni L, Cantore G. Long-term prognosis for atypical and malignant meningiomas: a study of 71 surgical cases. J Neurosurg 1997; 86: 793-800.
24. Gabeau-Lacet D, Aghi M, Betensky RA, Barker FG, Loeffler JS, Louis DN. Bone involvement predicts poor outcome in atypical meningioma. J Neurosurg 2009; 111: 464-71.
25. Eder JP, Vande Woude GF, Boerner SA, LoRusso PM. Novel therapeutic inhibitors of the c-Met signaling pathway in cancer. Clin Cancer Res 2009; 15: 2207-14.
26. Yamasaki F, Yoshioka H, Hama S, Sugiyama K, Arita K, Kurisu K. Recurrence of meningiomas. Cancer 2000; 89: 1102-10.
27. Violaris K, Katsarides V, Sakellariou P. The recurrence rate in meningiomas: analysis of tumor location, histological grading, and extent of resection. Open J Mod Neurosurg 2011; 2: 6-10.
28. Jääskeläinen J. Seemingly complete removal of histologically benign intracranial meningioma: late recurrence rate and factors predicting recurrence in 657 patients: a multivariate analysis. Surg Neurol 1986; 26: 461-9.
29. Edakuni G, Sasatomi E, Satoh T, Tokunaga O, Miyazaki K. Expression of the hepatocyte growth factor/c-Met pathway is increased at the cancer front in breast carcinoma. Pathol Int 2001; 51: 172-8.
30. Terada T, Nakanuma Y, Sirica AE. Immunohistochemical demonstration of MET overexpression in human intrahepatic cholangiocarcinoma and in hepatolithiasis. Hum Pathol 1998; 29: 175-80.

Journal of Pathology and Translational Medicine 2015; 49: 52-60
http://dx.doi.org/10.4132/jptm.2014.10.26

■ ORIGINAL ARTICLE ■

Diagnostic Accuracy of Endoscopic Ultrasound-Guided Fine Needle Aspiration Cytology of Pancreatic Lesions

Hae Woon Baek · Min Jee Park
Ye-Young Rhee · Kyoung Bun Lee
Min A Kim · In Ae Park

Department of Pathology, Seoul National University College of Medicine, Seoul, Korea

Received: September 5, 2014
Revised: October 24, 2014
Accepted: October 24, 2014

Corresponding Author
In Ae Park, M.D.
Department of Pathology, Seoul National University College of Medicine, 103 Daehak-ro, Jongno-gu, Seoul 110-799, Korea
Tel: +82-2-2072-3312
Fax: +82-2-743-5530
E-mail: iapark@snu.ac.kr

Background: Endoscopic ultrasound–guided fine needle aspiration cytology (EUS-FNAC) is currently the most commonly used procedure for obtaining cytologic specimens of the pancreas. It is accurate, minimally invasive, safe and cost-effective. However, there is discrepancy between cytological and surgical diagnoses. This study was aimed at evaluating the diagnostic accuracy of EUS-FNAC of the pancreas. **Methods:** We performed a retrospective review of 191 cases of pancreatic lesions initially diagnosed by EUS-FNAC with subsequent histological diagnosis between 2010 and 2012 in the Department of Pathology, Seoul National University Hospital. Cytologic and surgical diagnoses were categorized into five groups: negative, benign, atypical, malignant, and insufficient for diagnosis. Subsequently, 167 cases with satisfactory yield in both surgical and cytology specimens were statistically analyzed to determine correlations with diagnosis. **Results:** In comparison to surgical diagnoses, cytologic diagnoses were true-positive in 103 cases (61.7%), true-negative in 28 cases (16.8%), false-positive in 9 cases (5.4%), and false-negative in 27 cases (16.1%). The diagnostic accuracy was 78.4%, sensitivity was 79.2%, and specificity was 75.7%. The positive predictive value was 92.0%, and negative predictive value was 50.9%. **Conclusions:** EUS-FNAC has high accuracy, sensitivity, specificity and positive predictive value. Overcoming the limitations of EUS-FNAC will make it a useful and reliable diagnostic tool for accurate evaluation of pancreatic lesions.

Key Words: Pancreas; Endoscopic ultrasound-guided fine needle aspiration cytology; Accuracy; Diagnosis

Pancreatic cancer is notorious for its poor prognosis, with a low overall 5-year survival rate of merely 8.7%. It is the fifth leading cause of cancer-related mortality in South Korea[1] because of the delayed detection of tumors, typical presentation at an advanced stage, and its aggressive disease behavior. Only 20% of tumors are surgically resectable when detected. Remaining 80% of patients cannot help undergoing palliative therapy, the only treatment practical for those with unresectable tumor. In addition, pancreatic cancer has a poor response to chemotherapy and radiation therapy, increasing the complexity of patient management. Therefore, early detection is key in order to increase the survival rate of pancreatic cancer patients and to improve overall patient care.

Early detection, though it is crucial, is challenging since pancreatic cancer is usually asymptomatic in the initial stage and anatomically less accessible due to surrounding organs in the retroperitoneum. To overcome these limitations, imaging modalities such as abdominal ultrasound, computed tomography, magnetic resonance imaging, endoscopic retrograde cholangiopancreatography, endoscopic ultrasonography (EUS), and positron emission tomography have been used to localize the lesions.

For the detection of pancreato-biliary diseases, EUS is currently widely accepted. This technique enables precise visualization of the lesion and the ability to proficiently determine the depth of gastrointestinal malignancies.[2] By combining the advantages of EUS with fine-needle aspiration cytology (FNAC) for the retrieval of specimens for pathologic diagnosis, EUS-FNAC has improved diagnostic capabilities. With EUS-FNAC, distinguishing pancreatic cancer from chronic pancreatitis, detection of tumor smaller than 2 cm and staging of the cancer are superior to those with the other modalities. EUS-FNAC has become the most popular technique with which to obtain cytology specimens and diagnose patients suspected to have pancreatic malignancy.

EUS-FNAC has been shown to be diagnostically useful, obviating unwarranted procedures and reducing costs.[3] It is also

pISSN 2383-7837
eISSN 2383-7845

minimally invasive and comparatively safe. The conclusion from a recently published meta-analysis stated that EUS-FNAC should be included in algorithms for the management of patients with solid pancreatic tumor due to its high accuracy as a diagnostic test.[4]

Although EUS-FNAC for diagnosis of solid pancreatic masses is recognized as 'a nearly perfect procedure,'[5] there are still several flaws that need to be ameliorated. Problematic issues may arise due to limited skills of the endoscopy operator in terms of insufficient yield and targeting-error, misinterpretation and misdiagnosis by pathologists and absence of on-site cytopathologists for adequacy assessment.

This study was aimed to evaluate the diagnostic accuracy of EUS-FNAC of the pancreas and to further investigate the reason for incorrect diagnosis by comparison with confirmed histological diagnosis. The reason which we focused on the discrepancy between cytological and surgical specimen diagnosis was to identify the pitfalls that pathologists may face during diagnosis. In some patients, the initial diagnostic cytology specimen may be the only material that has viable tumor cells for diagnosis if the tumor is unresectable or they receive neoadjuvant therapy prior to resection. This situation emphasizes the importance of the accuracy of cytopathologic diagnosis. Furthermore, on-site cytopathologic assessment for adequacy is usually not performed in South Korea for financial reasons,[6] making it even more challenging for pathologists in Korea to diagnose cytological specimens.

Retrospective examination was performed in this study, correlating cytology-histology diagnosis of pancreatic lesions obtained by EUS-FNAC with several clinicopathologic variables. In doing so, we hope to optimize the accuracy of cytological diagnosis in an effort to improve the care of pancreatic cancer patients.

MATERIALS AND METHODS

A retrospective study was carried out to review 191 cases of EUS-FNAC of pancreatic lesions between January 2010 and December 2012 in Seoul National University Hospital. This study was approved by the Seoul National University Hospital Institutional Review Board (IRB Study No. H-1408-022-601).

Case selection

The data from 579 patients who underwent pancreatic FNAC over a 36-month period (January 2010 to December 2012) were obtained by computerized search of PathPACS (Humintec, Suwon, Korea), a database used at the Department of Pathology of Seoul National University Hospital. Cases with no follow-up biopsy or surgical resection were excluded from this study, leaving 207 cases. Among those cases, 191 patients underwent EUS-FNAC. Specimens from 8 patients were retrieved by intraoperative brush cytology, 4 from ultrasound-guided gun biopsy, and 4 were unclear with no specific record of the procedure. In this study, only patients who underwent EUS-FNAC were included. For statistical analysis, patients surgically diagnosed as 'atypical' or 'insufficient for diagnosis (IFD)' were further excluded since those diagnoses were not as satisfactory as confirmation of cytologic diagnosis. The remaining 167 cases were analyzed to assess the diagnostic accuracy of EUS-FNAC.

Procedure: EUS-guided fine-needle aspiration and specimen preparation

Radial and linear endoscopic ultrasonographies were used for EUS-FNAC. Fine-needle aspiration was performed by gastroenterologists of Seoul National University Hospital. For cytopathologic analysis, the aspirated specimen was smeared onto glass slides and fixed in 95% ethanol, followed by Papanicolaou staining and Diff-Quick staining. A cell block was prepared in 2 cases using a standard protocol.

Cytologic diagnosis

Diagnoses were made by several pathologists at Seoul National University Hospital. The specimen was initially rated either as adequate or inadequate. Suboptimal specimens with less than minimal pancreatic tissue needed for diagnosis were rated inadequate. Adequate samples were then categorized into four groups: negative for malignancy, benign lesion, atypical, and malignant neoplasm. Altogether there were five groups, including inadequate samples grouped as 'IFD.' Diagnosis of EUS-FNAC was then compared with subsequent corresponding histologic diagnosis.

Retrospective review of cases with discrepancy

Of the 167 included cases, 36 showed major discrepancy between cytological diagnosis and surgical diagnosis. Retrospective review of those slides was conducted by three pathologists: the corresponding author (I.A.P.) and K.B.L, who are experienced pathologists, and the first author (H.W.B.). For non-biased review results, final histological diagnosis was blinded.

Statistical analysis

The data on patient sex, age, type of procedure, diagnosis for cytology and surgical specimen, and site of aspiration were ana-

lyzed using Microsoft Excel 2007 calculation sheets. For patients with several cytological specimens obtained from the same site on the same day, that with the most corresponding result with final surgical diagnosis was included in the data analysis. The diagnostic accuracy, sensitivity, specificity, positive and negative predictive values, false-positive rate, false-negative rate, and false-discovery rate of EUS-FNAC results were calculated. For the statistical analysis, cytology and surgical diagnosis of 'benign lesion' were categorized as a negative result, meaning 'negative for tumor,' while 'atypical' and 'suspicious for malignancy' (the *gray-zone*) were considered and categorized as 'positive for tumor.' Although surgical diagnoses of 'atypical' and 'IFD' were excluded from statistical analysis, we included 'atypical' and 'IFD' diagnoses of cytology specimens for broader evaluation.

RESULTS

Patient characteristics

Among 191 patients who underwent EUS-FNAC, the male to female ratio was 0.95, with 93 males and 98 females. The median age of the patients was 60.25 years, ranging from 20 to

Table 1. Correlation of EUS-FNAC diagnosis and corresponding final histological diagnosis

Cytology diagnosis	Surgical diagnosis		No. of cases	Category
Negative	Non-neoplastic lesion		15	True-negative
(35 cases, 18.3%)	Benign lesion		2	True-negative
	Atypical (undetermined)		2	Excluded
	Malignant neoplasm (n=15)	Ductal adenocarcinoma	13	False-negative
		Neuroendocrine tumor	1	
		IPMN	1	
Benign lesion	TIFD		1	Excluded
(5 cases, 2.6%)	Non-neoplastic lesion		0	True-negative
	Benign lesion		5	True-negative
	Atypical (undetermined)		0	Excluded
	Malignant neoplasm		0	False-negative
Atypical (undetermined)	TIFD		0	Excluded
(37 cases, 19.4%)	Non-neoplastic lesion		4	False-positive
	Benign lesion		1	False-positive
	Atypical (undetermined)		5	Excluded
	Malignant neoplasm (n=24)	Ductal adenocarcinoma	18	True positive
		Neuroendocrine tumor	2	
		IPMN	2	
		Malignant tumor, unspecified	2	
Malignant neoplasm	TIFD		3	Excluded
(94 cases, 49.2%)	Non-neoplastic lesion		4	False-positive
	Benign lesion		0	False-positive
	Atypical (undetermined)		9	Excluded
	Malignant neoplasm (n=79)	Ductal adenocarcinoma	57	True-positive
		Neuroendocrine tumor	10	
		Carcinoma	4	
		IPMN	3	
		Solid-pseudopapillary neoplasm	2	
		Mucinous neoplasm	1	
		Malignant mesenchymal tumor	1	
		Metastatic leiomyosarcoma	1	
Insufficient for diagnosis	TIFD		2	Excluded
(20 cases, 10.5%)	Non-neoplastic lesion		5	True-negative
	Benign lesion		1	True-negative
	Atypical (undetermined)		1	Excluded
	Malignant neoplasm (n=12)	Ductal adenocarcinoma	10	False-negative
		IPMN	1	
		Malignant tumor, unspecified	1	
	TIFD		1	Excluded
Total			191	

TIFD, tissue insufficient for diagnosis; IPMN, intraductal papillary mucinous neoplasm.

http://dx.doi.org/10.4132/jptm.2014.10.26

82 years.

Cytologic results consisted of 35 cases (18.3%) of 'negative for tumor,' 5 cases (2.6%) of 'benign lesion,' 37 cases (19.4%) of 'atypical,' 94 cases (49.2%) of 'malignant neoplasm,' and 20 cases (10.5%) of 'IFD' (Table 1). Specific diagnoses of cytologically 'malignant neoplasm' included 53 cases of ductal adenocarcinoma, 28 cases of 'malignant tumor, unspecified,' 10 cases of neuroendocrine neoplasm, 2 cases of mucinous neoplasm, and 1 case of squamous cell carcinoma (Table 2).

Histological results consisted of 28 cases (14.7%) of 'negative for tumor,' 9 cases (4.7%) of 'benign lesion,' 17 cases (8.9%) of 'atypical,' 130 cases (68.1%) of 'malignant neoplasm,' and 7 cases (3.6%) of 'tissue insufficient for diagnosis (TIFD)' (Table 1).

Comparison between cytological and surgical diagnoses

In a comparison of cytology-surgical diagnoses (Table 1), 35 cases of negative cytology diagnosis were surgically diagnosed as 'non-neoplastic lesion' in 15 cases and 'benign lesion' in 2 cases. Those cases were classified as true-negative results. On the contrary, there were 15 false-negative cases showing major discrepancy, which were initially diagnosed negative on cytology but malignant on surgical specimen. Two cases with surgical diagnosis of 'atypical (undetermined)' and 1 case of 'TIFD' were excluded from the statistical analysis due to unsatisfactory results of confirmation. Five cases were cytologically diagnosed as 'benign lesion' and were also diagnosed as 'benign lesion' on surgical diagnosis. These cases were classified as true-negative.

There were 37 cytologically 'atypical (undetermined)' cases. Surgical diagnosis of these cases was true-positive ('malignant neoplasm') in 24 cases and false-positive in 5 cases (4 'benign lesion' and one 'non-neoplastic lesion'). Eight cases that were surgically diagnosed 'TIFD' (3 cases) and 'atypical' (5 cases) were likewise excluded. As for cytological specimens diagnosed 'malignant neoplasm', 79 of 94 cases were true-positive with surgical diagnosis of 'malignant neoplasm.' There were 4 false-positive results for specimens surgically diagnosed as 'non-neoplastic lesion.' In the same manner as the other categories, 9 cases of surgically 'atypical' and 2 cases of surgically 'TIFD' were excluded.

Table 2. Specific diagnoses of cytologically 'malignant neoplasm'

Cytology diagnosis	Total
Ductal adenocarcinoma	53
Malignant tumor, unspecified	28
Neuroendocrine neoplasm	10
Mucinous neoplasm	2
Squamous cell carcinoma	1
Total	94

Among 20 cases of cytologically 'IFD' cases, 6 were true-negative (five surgically 'non-neoplastic lesion' and one 'benign lesion'), while 12 cases were false-negative with a surgical diagnosis of 'malignant neoplasm.' Cases with surgical diagnosis of 'IFD' (1 case) and 'atypical' (1 case) were excluded. Last of all, there was a case that was cytologically diagnosed as 'suspicious for neuroendocrine tumor' but surgically diagnosed as solid pseudopapillary neoplasm, which are distinctive in diagnosis. Despite the discrepancy, this case was classified as true-positive in order to acknowledge the cytological diagnosis for recognizing a malignancy.

Statistical results

According to the data, the 167 cases remaining after applying exclusion criteria were true-positive in 103 cases (61.7%), true-negative in 28 cases (16.8%), false-positive in 9 cases (5.4%), and false-negative in 27 cases (16.1%). The diagnostic accuracy was 78.4%, sensitivity was 79.2%, and specificity was 75.7%. The positive predictive value was 92.0%, and negative predictive value was 50.9%. The false-positive rate was 24.3%, false-negative rate was 11.6%, and false discovery rate was 8.0% (Table 3).

Analysis of discrepant cases: false-positives and false-negatives

Thirty-five cases showed discrepancy in cytological-surgical correlation, and 9 cases among them were false-positive (Table 4). Cytologically diagnosed 'atypical' specimens were surgically diagnosed negative in 2 cases and lymphoplasmacytic sclerosing pancreatitis in 2 cases. Two cytologic diagnoses of 'suspected carcinoma,' one 'carcinoma,' and one 'adenocarcinoma' were also false-positive, later surgically diagnosed as 'negative for tumor.'

Table 3. Statistical analysis of 167 cases[a]

Category	Percentage	Equation
TP (103 cases)	61.7	N/A
TN (28 cases)	16.8	N/A
FP (9 cases)	5.4	N/A
FN (27 cases)	16.1	N/A
Diagnostic accuracy	78.4	(TP+TN)/(TP+TN+FP+FN) × 100
Sensitivity	79.2	TP/(TP+FN) × 100
Specificity	75.7	TN/(TN+FP) × 100
Positive predictive value	92.0	TP/(TP+FP)
Negative predictive value	50.9	TN/(TN+FN)
FP rate	24.3	FP/(FP+TN)
FN rate	11.6	FN/(TP+FN)

TP, true positive; TN, true negative; FP, false positive; FN, false negative; N/A, not applicable.
[a]Surgically 'atypical' (17 cases) and 'tissue insufficient for diagnosis' (7 cases) cases are excluded.

Table 4. Discrepant cases with a false-positive or false-negative cytology diagnosis

Category[a]		Case No.	Sex	Age (yr)	Location	Cytology diagnosis	Surgical diagnosis
1	False-negative	1	F	70	Neck	IFD	Ductal adenocarcinoma
		2	F	53	Uncinate	IFD	Ductal adenocarcinoma
		3	M	69	Tail	IFD	Ductal adenocarcinoma
		4	F	65	Body	IFD	Ductal adenocarcinoma
		5	M	76	Body	IFD	Ductal adenocarcinoma
		6	M	58	Head	IFD	Ductal adenocarcinoma
		7	M	77	Body	IFD	Ductal adenocarcinoma
		8	M	76	Body	IFD	Ductal adenocarcinoma
		9	F	69	Neck	IFD	Ductal adenocarcinoma
		10	M	71	Body	IFD	IPMN
		11	F	70	Main p-duct	IFD	Malignancy, unspecified
		12	F	50	Body	IFD	Neuroendocrine tumor
2	False-positive	13	M	75	Body	Suspected carcinoma	Negative for tumor
		14	M	75	Body	Suspected carcinoma	Negative for tumor
		15	M	60	Neck	Carcinoma	Negative for tumor
		16	F	58	Body	Adenocarcinoma	Negative for tumor
		17	F	82	Head	Atypical	Negative for tumor
		18	F	38	Body	Atypical	Negative for tumor
	False-negative	19	M	57	Tail	Negative for tumor	Ductal adenocarcinoma
		20	F	61	Uncinate	Negative for tumor	Ductal adenocarcinoma
		21	F	51	Tail	Negative for tumor	Ductal adenocarcinoma
		22	F	41	Head	Negative for tumor	Ductal adenocarcinoma
		23	M	77	Body	Negative for tumor	Ductal adenocarcinoma
		24	F	67	Head	Negative for tumor	Ductal adenocarcinoma
		25	F	72	Head	Negative for tumor	Ductal adenocarcinoma
		26	M	57	Tail	Negative for tumor	Ductal adenocarcinoma
		27	F	73	Uncinate	Negative for tumor	Ductal adenocarcinoma
		28	M	64	Body	Negative for tumor	Ductal adenocarcinoma
3	False-positive	29	M	50	Body	Atypical	Lymphoplasmocytic sclerosing pancreatitis
		30	F	60	Distal part	Atypical	Lymphoplasmocytic sclerosing pancreatitis
	False-negative	31	M	76	Body	Negative for tumor	Ductal adenocarcinoma
		32	M	56	Head	Negative for tumor	Ductal adenocarcinoma
		33	M	61	Tail	Negative for tumor	Ductal adenocarcinoma
		34	F	58	Tail	Negative for tumor	Ductal adenocarcinoma
		35	F	70	Uncinate	Negative for tumor	IPMN

F, female; IFD, insufficient for diagnosis; M, male; IPMN, intraductal papillary mucinous neoplasm.
[a]Discrepancy category: 1) Insufficient for diagnosis (cytology specimen of too few cells), 2) Technical targeting error (normal parenchyma or other non-lesion area aspirated), and 3) Misdiagnosis by pathologists.

There were 27 cases that resulted in false-negative results (Table 4). Cytologically diagnosed 'negative for tumor' or 'IFD' were surgically diagnosed ductal adenocarcinoma in 23 cases, intraductal papillary mucinous neoplasm in 2 cases, neuroendocrine tumor in 1 case, and 'malignancy, unspecified' in 1 case.

We reviewed the cytology slides for discrepant cases in order to analyze reasons for such results and assigned cases to the following three main categories: 1) IFD (cytologic specimen with too few cells), 2) technical targeting error (aspiration of normal parenchyma or other non-lesion area), and 3) misdiagnosis by pathologists. The number of cases that fall into these categories is 12 (7.2%), 16 (9.6%), and 7 (4.2%), respectively (Table 4).

Through a group review by 3 pathologists, the reasons for the discrepancy in each case in category 3 were analyzed. In 3 cases that were histologically adenocarcinoma but cytologically diagnosed negative, obvious malignant cell clusters that resembled adenocarcinoma were observed (cases Nos. 31–34) (Table 4, Fig. 1A). These cases were analyzed as misdiagnosis due to omission of tumor cells by inattentive screening. Another case diagnosed 'histologically adenocarcinoma but cytologically negative' (case No. 32) (Table 4, Fig. 1B, C) showed some malignant cell clusters that were intermixed with and camouflaged by a massive amount of benign parenchymal cells. This case was analyzed as a misdiagnosis due to misinterpretation of the pathologist.

Intraductal papillary mucinous neoplasm was diagnosed as negative in one case (case No. 35) (Table 4, Fig. 1D). Some mucin-producing epithelial cells with suspicious atypism were observed from the slide review, leading us to also analyze this case

 http://dx.doi.org/10.4132/jptm.2014.10.26

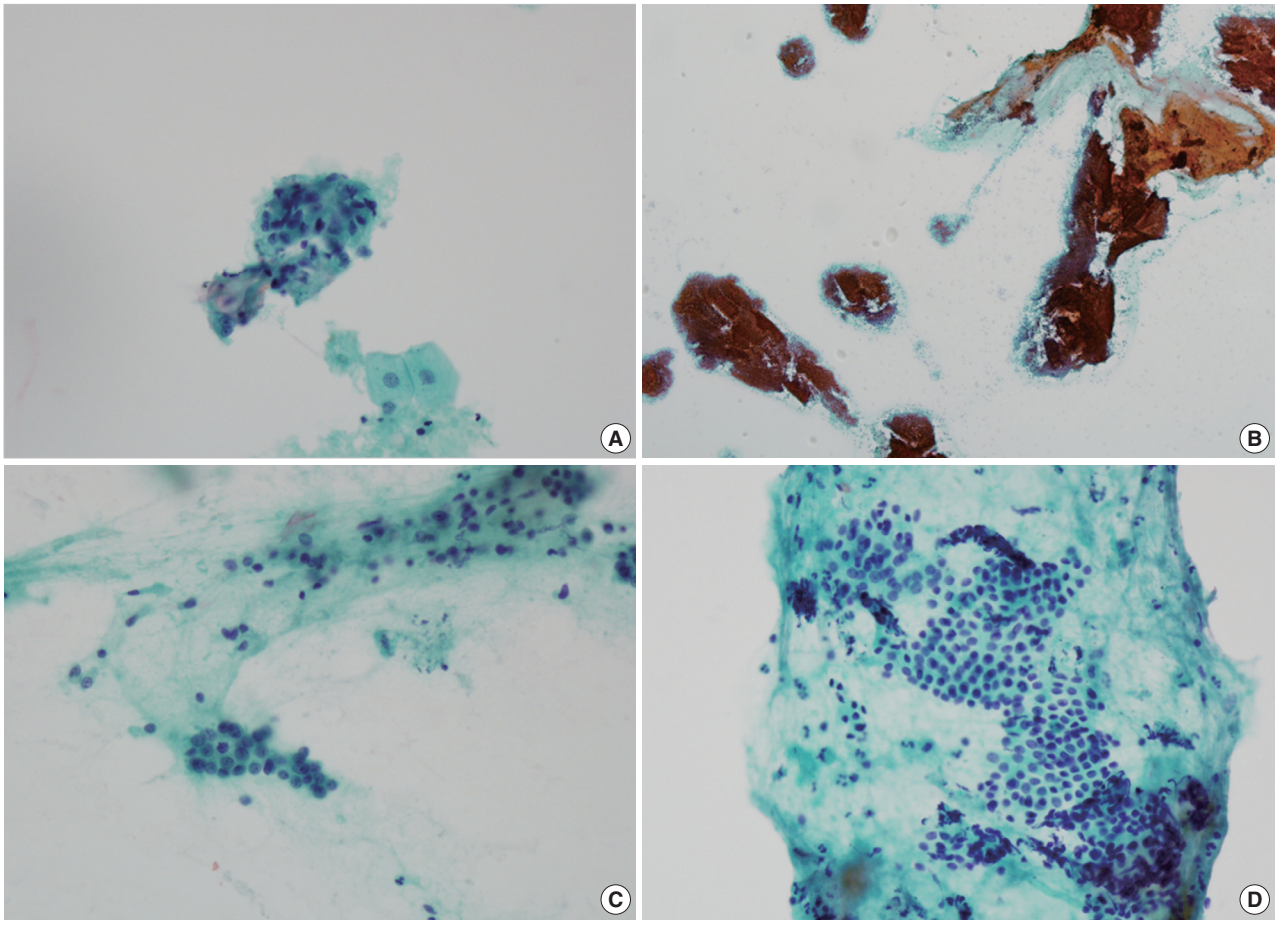

Fig. 1. Cytologic specimens with false-negative discrepant results (Table 4). (A) Case No. 31 with histological diagnosis of ductal adenocarinoma. Obvious malignant cell clusters that resemble adenocarcinoma. (B, C) Case No. 32 with histological diagnosis of ductal adenocarinoma. Malignant cell clusters are intermixed with and camouflaged by a massive amount of benign parenchymal cells. (D) Case No. 35 with histological diagnosis of intraductal papillary mucinous neoplasm. Some mucin-producing epithelial cells with suspicious atypism are observed.

as a misinterpretation by the pathologist.

Three cases were surgically diagnosed as 'consistent with lymphoplasmacytic sclerosing pancreatitis.' Among them, 2 cases were cytologically misdiagnosed as 'atypical,' resulting in discrepancy (cases Nos. 29 and 30) (Table 4). The remaining case was cytologically diagnosed 'negative for tumor,' which was categorized as a true-negative result in this study. In cytology specimens, inflammatory infiltrate consisted mainly of lymphocytes and plasma cells were observed.

A cytology specimen that was diagnosed as 'a few atypical cells' and histologically diagnosed schwannoma (Fig. 2) was also reviewed. This case was not included in category 3 since it is not a serious misdiagnosis. Cytopathologic features presented mostly in tissue fragments or in fascicles, with cells fusiform and an elongated shape with poorly defined cell borders. Cytology showed low nuclear-cytoplasmic ratio with long and wavy nuclei. Nucleoli were inconspicuous, and cytoplasm was pale.

The anatomical site of aspiration in category 1 was the body in 6 cases, neck in 2 cases, uncinate process in 1 case, head in 1 case, tail in 1 case, and 'main p-duct' in 1 case. For category 2, aspirations were conducted in the body in 5 cases, neck in 4 cases, tail in 3 cases, uncinate process in 2 cases, and neck in 1 case. Category 3 cases were collected from the body in 3 cases, tail in 2 cases, neck in 1 case, uncinate process in 1 case, and distal part in 1 case (Table 4).

DISCUSSION

EUS-FNAC for pancreatic solid tumor is widely performed and has been shown to be useful.[3,5,7,8] As EUS-FNAC has gained acknowledgement as the gold standard for obtaining patient specimens, the importance and demand for optimization of EUS-

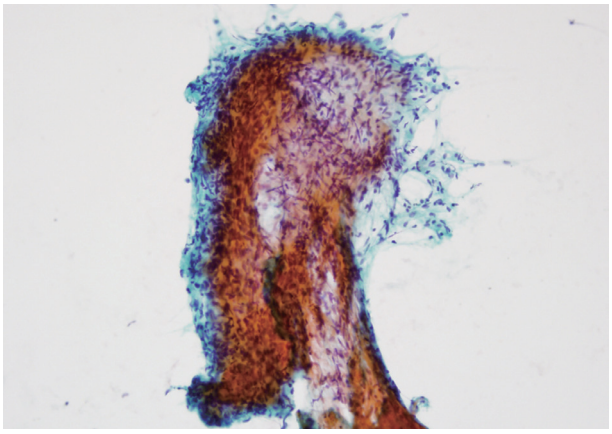

Fig. 2. Cytologic specimen with corresponding histological diagnosis of schwannoma. Cytopathologic features present mostly in tissue fragments or in fascicles, with cells fusiform and elongated with poorly defined cell borders, a low nuclear-cytoplasmic ratio with long and wavy nuclei, inconspicuous nucleoli and pale cytoplasm.

FNAC increase. We, given the relatively large number of cases of pancreatic FNAC in South Korea, have recognized that follow up and review are needed of past EUS-FNAC results in order to determine the validity of the examination process. The aim of the current study was to contribute to the advancement of management for pancreatic cancer patients by improving the detection and diagnosis results.

To analyze the accuracy, we investigated the diagnosis of EUS-FNAC by comparing with final diagnoses confirmed by histological examination of biopsy or surgically resected specimens. During evaluation of the diagnoses made by EUS-FNAC, we emphasized the agreement with the final diagnoses.

In our data, 61.7% of cases were true-positive and 16.8% of cases were true-negative, with false-negative and false-positive cases comprising only 21.6%, which is acceptably low considering that most were due to adequacy problems with the EUS-FNAC specimen. As a result, diagnostic accuracy, sensitivity, and specificity were 78.4%, 79.2%, and 75.7% respectively. The positive predictive value was 92.0%, and negative predictive value was 50.9%. The false-positive rate was 24.3%, false-negative rate was 11.6%, and false discovery rate was 8.0%. According to Yoshinaga *et al*.,[5] a medical literature review to evaluate the role of EUS-FNAC for diagnosis of solid pancreatic masses showed 78%–95% sensitivity, 75%–100% specificity, 98%–100% positive predictive value, 46%–80% negative predictive value, and 78%–95% accuracy. In comparison of this data with data from several other studies,[9-12] our study showed lower but within the range values of diagnostic accuracy, sensitivity and specificity. The positive predictive value was 12% higher than the upper margin, but the negative predictive value was lower than the mean. Our overall results were affirmative and supportive of the continued use of EUS-FNAC for pancreatic lesion, but it is apparently lower than other institutes. This encourages us to look for an explanation and identify mechanisms for improvement. Such relatively poor result may be due to the way of manipulating raw data during patient selection and categorization of diagnoses. By adjusting our methods to be more identical to those of other studies, we may have gained more satisfying results, similar to those of other institutes.

After confirming that the overall results were comparatively favorable in our study, we focused on the cases that showed discrepancy in order to identify the pitfalls of diagnosis and further improve the cytologic diagnosis. We reviewed the slides and analyzed the diagnoses of 35 cases in which the cytologic diagnosis did not concur with the surgical diagnosis. Among those cases, 12 were due to insufficient aspiration of cells for diagnosis (category 1), and 16 were due to targeting error (category 2), containing only benign parenchyma instead of tumor. The remaining 7 discrepant cases (category 3) were due to misinterpretation and misdiagnosis by pathologists.

Categories 1 and 2 results indicate aspiration failures caused by technical variables, such as operator skills/experiences, tumor type and location. With regard to location, cases were aspirated most often from the body (11 cases), followed by head (5 cases) and tail (4 cases). The interpretation is that the aspirations from these regions have a tendency to be insufficient due to poor accessibility and technical difficulty. However, it could just be a matter of fraction, representing the most common location of the suspected tumor in this study population. The most common cytologic diagnosis for categories 1 and 2 was 'adenocarcinoma' (19 cases), followed by 'negative for tumor' (5 cases), neuroendocrine tumor (1 case), intraductal papillary neoplasm (1 case), and 1 case of 'malignancy, unspecified.' Considering that adenocarcinoma was the most common diagnosis overall (adequate/inadequate, discrepant/non-discrepant), tumor type may have less impact on aspiration failure. In addition, we took into consideration that cases of intraductal papillary mucinous neoplasm may have been underdiagnosed as 'benign lesion' in this study. Therefore, we concluded that the relativity of tumor type and diagnostic accuracy is still ambiguous. Also, we assumed that there are significant influences from variability in operator skills and tumor size on EUS-FNAC results. However, we could not analyze such data because the electric medical records did not document the specific operator's name and tumor

 http://dx.doi.org/10.4132/jptm.2014.10.26

size in all cases.

For category 3, the misdiagnosed cases, we reviewed the slides to identify the factor that led to such discrepancy. Of 7 cases, four were histologically adenocarcinoma but cytologically diagnosed negative. Meticulous observation led to identification of some obviously malignant cells that resemble adenocarcinoma in 3 cases (cases Nos. 31–34) (Table 4, Fig. 1A). In these cases, we think the misdiagnosis was due to screening failure and simple exclusion of the applicable areas on the slide. On the other hand, one histologically adenocarcinoma but cytologically diagnosed 'negative' case was actually challenging (case No. 32) (Table 4, Fig. 1B, C). As reviewers retrospectively observing the collection of 'discrepant' cases only, it was not difficult to interpret this case as malignant since we knew that something must be wrong. However, tumor cells in this case were intermixed with and camouflaged by a massive amount of benign parenchymal cells, making the malignancy ambiguous. In a situation like this, a pathologist may be discouraged and hesitant to conclude a diagnosis of definite cancer.

Intraductal papillary mucinous neoplasm was misdiagnosed as negative in 1 case (case No. 35) (Table 4, Fig. 1D). From review of the slide, we recognized some mucin-producing epithelial cells with suspicious atypism. We assumed that the discrepancy in this case was due to diagnosis by a relatively inexperienced pathologist, leading to misinterpretation.

There were 3 cases surgically diagnosed as 'consistent with lymphoplasmacytic sclerosing pancreatitis.' Among them, 2 cases were cytologically misdiagnosed as 'atypical,' resulting in discrepancy (cases Nos. 29 and 30) (Table 4). The remaining case was cytologically diagnosed 'negative for tumor' and was categorized as a true negative result. Lymphoplasmacytic sclerosing pancreatitis, a form of chronic pancreatitis with mixed inflammatory infiltrate, clinically mimics pancreatic cancer. Preoperative detection is important because lymphoplasmacytic sclerosing pancreatitis patients usually respond to steroid therapy with reversible improvement in pancreatic morphology and function.[13] In our cases, inflammatory infiltrate consisting mainly of lymphocytes and plasma cells was observed. According to Abraham *et al*.,[14] this infiltrate may also contain some macrophages and occasionally neutrophilic and eosinophilic granulocytes. Although the role of FNAC is mainly to distinguish malignant from benign cells, it is worth considering the possibility of lymphoplasmacytic sclerosing pancreatitis when investigators recognize such microscopic features because patients will benefit from earlier initiation of therapy.

We also reviewed a case of schwannoma that was cytologically diagnosed as 'a few atypical cells' (Fig. 2). Cytopathologic features presented mostly in tissue fragments or in fascicles, with cells fusiform and elongated with poorly defined cell borders. The cells showed a low nuclear-cytoplasmic ratio with long and wavy nuclei. Nucleoli were inconspicuous, and cytoplasm was pale. Pancreatic schwannoma is an extremely rare neoplasm, with only 47 cases reported in the English literature in the last three decades.[15] Therefore, it is not routine for pathologists to suspect such schwannoma when screening. However, the possibility that cells are mesenchymal should be considered, which may suggest the diagnosis.

Navina *et al*.[16] and Kim *et al*.[6] reported that absence of an immediate on-site cytopathologist is not critical, and they found no association with on-site evaluation and specimen cellularity. However, many groups, for example, Fisher *et al*.[8], have reported that on-site evaluation was relatively accurate (77.5%) and highly specific for malignancy (100%), significantly contributing to the efficiency and accuracy of the procedures. With respect to our lower diagnostic accuracy in comparison to those of other institutes, absence of on-site evaluation may be the cause because 28 of 35 discrepant cases in our study were due to unsatisfactory specimens. We presume that we could have benefited from on-site evaluation to improve diagnostic results and reduce the number of discrepant cases. In our opinion, having immediate on-site evaluation would be beneficial and valuable, if circumstances allowed.

The design of this study was limited by the fact that it was a single-center retrospective review of a relatively small number of consecutive cases over a 36-month period. Thorough adequacy assessment of pancreatic EUS-FNAC was impossible since only one representative specimen of patients with multiple aspirations was analyzed. Had we not excluded numerous 'IFD' cases, there would have been a greater amount of useful data, which would have reduced the impact of incorrect results caused by technical difficulty. Also, data identifying the operator and pathologist should have been retrieved to analyze artificial error that depends on skill and experience. Further study on cases with discrepancy aimed to identify the pitfalls of diagnosis should involve more cases of misdiagnosis, increasing the power of the analysis. Awareness of such pitfalls is important because it increases diagnostic confidence, resulting in improved accuracy.

In summary, the diagnostic accuracy of EUS-FNAC for obtaining pancreatic specimens suspicious of malignancy was confirmed to be high in this study. Diagnostic accuracy, sensitivity, and specificity were 78.4%, 79.2%, and 75.7% respectively. Although 35 of 191 cases showed discrepancy in cytology-his-

tology diagnosis, most were due to insufficient aspiration or mistargeted aspiration of cells, both of which preclude proper examination. Therefore, we conclude that EUS-FNAC is reliable and accurate. Based on these results, pathologists can be assured of their diagnosis, as EUS-FNAC provides a desirable representation of the specimen. However, particular attention to adequacy assessment and meticulous observation of samples are critical in order to reduce the discrepancy between cytology-histological diagnoses. Though the percentage of correct diagnoses in EUS-FNAC results is relatively inferior compared to that from histological diagnosis, statistical results, such as diagnostic accuracy, were satisfactory in several studies including ours. Therefore, EUS-FNAC can be encouraged as a first-line pathologic examination for pancreatic lesion with high clinical suspicion of malignancy when patient safety and financial benefits are the priority.

Conflicts of Interest

No potential conflict of interest relevant to this article was reported.

Acknowledgments

This paper was supported by Seoul National University College of Medicine in 2014.

REFERENCES

1. Jung KW, Won YJ, Kong HJ, Oh CM, Lee DH, Lee JS. Cancer statistics in Korea: incidence, mortality, survival, and prevalence in 2011. Cancer Res Treat 2014; 46: 109-23.
2. Matsumoto K, Takeda Y, Harada K, Horie Y, Yashima K, Murawaki Y. Effect of pancreatic juice cytology and/or endoscopic ultrasound-guided fine-needle aspiration biopsy for pancreatic tumor. J Gastroenterol Hepatol 2014; 29: 223-7.
3. Bluen BE, Lachter J, Khamaysi I, *et al*. Accuracy and quality assessment of EUS-FNA: a single-center large cohort of biopsies. Diagn Ther Endosc 2012; 2012: 139563.
4. Hewitt MJ, McPhail MJ, Possamai L, Dhar A, Vlavianos P, Monahan KJ. EUS-guided FNA for diagnosis of solid pancreatic neoplasms: a meta-analysis. Gastrointest Endosc 2012; 75: 319-31.
5. Yoshinaga S, Suzuki H, Oda I, Saito Y. Role of endoscopic ultrasound-guided fine needle aspiration (EUS-FNA) for diagnosis of solid pancreatic masses. Dig Endosc 2011; 23 Suppl 1: 29-33.
6. Kim TH, Choi KH, Song HS, Kim JW, Jeon BJ. Histology combined with cytology by endoscopic ultrasound-guided fine needle aspiration for the diagnosis of solid pancreatic mass and intra-abdominal lymphadenopathy. Gut Liver 2013; 7: 605-10.
7. Matsuyama M, Ishii H, Kuraoka K, *et al*. Ultrasound-guided vs endoscopic ultrasound-guided fine-needle aspiration for pancreatic cancer diagnosis. World J Gastroenterol 2013; 19: 2368-73.
8. Fisher L, Segarajasingam DS, Stewart C, Deboer WB, Yusoff IF. Endoscopic ultrasound guided fine needle aspiration of solid pancreatic lesions: performance and outcomes. J Gastroenterol Hepatol 2009; 24: 90-6.
9. Ardengh JC, Lopes CV, de Lima LF, *et al*. Diagnosis of pancreatic tumors by endoscopic ultrasound-guided fine-needle aspiration. World J Gastroenterol 2007; 13: 3112-6.
10. Varadarajulu S, Tamhane A, Eloubeidi MA. Yield of EUS-guided FNA of pancreatic masses in the presence or the absence of chronic pancreatitis. Gastrointest Endosc 2005; 62: 728-36.
11. Mitsuhashi T, Ghafari S, Chang CY, Gu M. Endoscopic ultrasound-guided fine needle aspiration of the pancreas: cytomorphological evaluation with emphasis on adequacy assessment, diagnostic criteria and contamination from the gastrointestinal tract. Cytopathology 2006; 17: 34-41.
12. Erickson RA, Sayage-Rabie L, Beissner RS. Factors predicting the number of EUS-guided fine-needle passes for diagnosis of pancreatic malignancies. Gastrointest Endosc 2000; 51: 184-90.
13. Kawamoto S, Siegelman SS, Hruban RH, Fishman EK. Lymphoplasmacytic sclerosing pancreatitis (autoimmune pancreatitis): evaluation with multidetector CT. Radiographics 2008; 28: 157-70.
14. Abraham SC, Leach S, Yeo CJ, *et al*. Eosinophilic pancreatitis and increased eosinophils in the pancreas. Am J Surg Pathol 2003; 27: 334-42.
15. Moriya T, Kimura W, Hirai I, *et al*. Pancreatic schwannoma: Case report and an updated 30-year review of the literature yielding 47 cases. World J Gastroenterol 2012; 18: 1538-44.
16. Navina S, McGrath K, Chennat J, *et al*. Adequacy assessment of endoscopic ultrasound-guided, fine-needle aspirations of pancreatic masses for theranostic studies: optimization of current practices is warranted. Arch Pathol Lab Med 2014; 138: 923-8.

 http://dx.doi.org/10.4132/jptm.2014.10.26

Journal of Pathology and Translational Medicine 2015; 49: 61-65
http://dx.doi.org/10.4132/jptm.2014.09.17

■ BRIEF CASE REPORT ■

Mixed Carcinoid–Mucinous Adenocarcinoma Arising in Mature Teratoma of Mesentery

Su-Jin Shin · Eun-Mi Son · Chang Ohk Sung · Kyu-Rae Kim

Department of Pathology, Asan Medical Center, University of Ulsan College of Medicine, Seoul, Korea

Malignant transformation of mature cystic teratoma is uncommon, and occurs in approximately 2%–4% of cases.[1] The most common tumor is squamous cell carcinoma, followed by mucinous carcinoma, carcinoid tumor, thyroid carcinoma, etc.; however, any of the tissues in mature teratoma may undergo malignant transformation.[1]

Goblet cell carcinoid (mucinous carcinoid) is a distinctive neoplasm with features of both carcinoid tumor and adenocarcinoma. Most cases described in the literature have occurred in the appendix and rarely, in the ovary. Although mature cystic teratomas occur in many extragonadal areas including the mesentery[2] and greater omentum, occurrence of goblet cell carcinoid arising in extragonadal teratoma has been rarely described, with only a single case in mediastinum being reported in the English literature.[3] Moreover, a combination of mucinous adenocarcinoma, goblet cell carcinoid, carcinoid tumor, and mature teratoma in an extragenital organ has not been reported.

Herein, we present a rare case of combined mucinous adenocarcinoma and goblet cell and typical carcinoid tumor arising in mature cystic teratoma of the mesentery in a 48-year-old woman.

CASE REPORT

A 48-year-old woman presented with a palpable abdominal mass in the periumbilical area with a vague abdominal pain of one month duration. Past medical history was unremarkable. She had no symptoms of carcinoid syndrome. On physical examination, the abdomen was markedly distended due to a solid movable mass. Abdominal and pelvic computed tomography scans revealed a huge heterogeneously enhanced mass in the abdominal cavity, which was associated with multiple smaller nodules throughout the entire abdominal and pelvic cavities and the right lobe of the liver. Bilateral ovaries were diffusely enlarged to form a semisolid mass. Laboratory findings demonstrated increased serum levels of carcinoembryonic antigen (264 ng/mL; normal < 6 ng/mL) and carbohydrate antigen 125 (294 U/mL, normal < 35 U/ml). Alpha-fetoprotein, beta-subunit of human chorionic gonadotropin and carcinohydrate antigen-19-9 were within normal range.

Exploratory laparotomy revealed a huge mass in the mesentery of the small intestine (Fig. 1A), measuring 20×18×11 cm, with coexisting multiple outbulging hepatic masses, bilateral ovarian masses, and diffusely seeding nodules on the peritoneal surface and omentum. On cut section, the mesenteric mass had solid and cystic portions. The cystic portion, occupying approximately 60% of the tumor, was filled with yellow-tan sebum-like materials, hair, mucoid and gelatinous substances, while the solid portion (40%) was composed of loose myxoid tissue (Fig. 1B). Bilateral ovaries were enlarged, measuring 12.5×8×6 cm in the right ovary and 10×6×3 cm in the left ovary, and multiple gelatinous tumor nodules were observed on both ovarian surfaces and parenchyma (Fig. 1C). The cut surface of the ovarian masses was greyish white and gelatinous. The seeding nodules of the peritoneal surface and omentum had myxoid and gelatinous appearances. Excision of the mesenteric mass, bilateral salpingo-oophorectomy, total omentectomy and appendectomy were undertaken. Intraoperative frozen sections were per-

Corresponding Author
Kyu-Rae Kim, M.D.
Department of Pathology, Asan Medical Center, University of Ulsan College of Medicine, 88 Olympic-ro 43-gil, Songpa-gu, Seoul 138-736, Korea
Tel: +82-2-3010-4514, Fax: +82-2-472-7898, E-mail: krkim@amc.seoul.kr

Received: June 30, 2014 **Revised:** September 3, 2014
Accepted: September 17, 2014

pISSN 2383-7837
eISSN 2383-7845

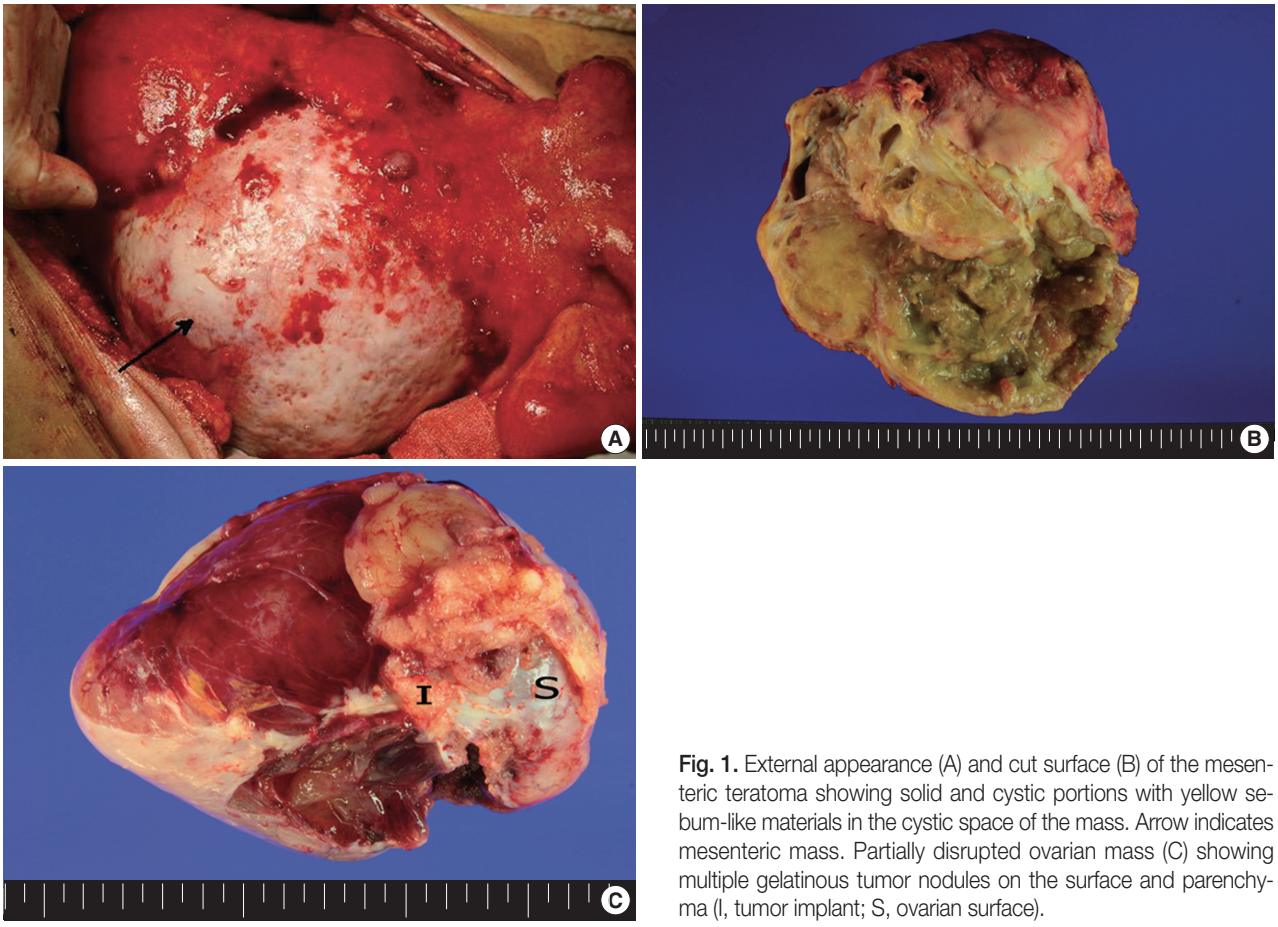

Fig. 1. External appearance (A) and cut surface (B) of the mesenteric teratoma showing solid and cystic portions with yellow sebum-like materials in the cystic space of the mass. Arrow indicates mesenteric mass. Partially disrupted ovarian mass (C) showing multiple gelatinous tumor nodules on the surface and parenchyma (I, tumor implant; S, ovarian surface).

formed for the ovarian mass, and the diagnosis was mucinous adenocarcinoma.

On microscopic examinations, the mesenteric tumor was encapsulated by thick fibrous tissue. The cystic portion of the mesenteric mass showed characteristic histologic features of mature teratoma containing various mature tissues derived from all three germ layers, including skin and its appendages, salivary glands, cartilage, adipose tissue, and smooth muscle bundles (Fig. 2A). The adjacent solid portion showed various histologic features of carcinoid tumors; a 1.5-cm sized well-circumscribed nodule showing insular, small glandular, rosettoid, and solid tubular patterns similar to those of midgut (insular) carcinoid tumors, thin cord-like or anastomosing trabecular patterns resembling hindgut (trabecular) carcinoid tumors, and dissecting mucin pools containing floating tumor cells (Fig. 2A, B), suggesting goblet cell carcinoid tumor. The insular and trabecular carcinoid tumor cells were composed of uniformly small and round nuclei with finely stippled chromatin, and abundant cytoplasm with eosinophilic granules. Mitotic figures were rare in insular and trabecular carcinoid areas (Ki-67 labeling index was less than 2%). The tumor cells within mucin pools were individually scattered or formed small nests having signet ring cell-like or goblet cell appearances, abundant foamy cytoplasm, low nuclear cytoplasmic ratio, and flattened nuclei pushed to the periphery (Fig. 2B). There was mild variation in nuclear sizes, mitotic figures were rarely identified, and Ki-67 labeling index was low (less than 2%) (Fig. 2B). On immunohistochemical stains, the trabecular and insular carcinoid tumor components showed strong and diffuse immunoreactivity for synaptophysin (Fig. 2C) and focal immunoreactivity for chromogranin. The tumor cells within mucin pools showed multifocal immunopositivity for synaptophysin (Fig. 2B inset).

In the vicinity of the carcinoid tumors, there were mucin pools containing signet ring cell-like or goblet cells showing significantly enlarged nuclei with high nuclear cytoplasmic ratio, marked nuclear pleomorphism, prominent nucleoli, and frequent mitotic figures (Fig. 2D). Immunohistochemical stain for synaptophysin was completely lost in the malignant signet ring cell-like tumor cells, and proliferating cells defined by Ki-67 immunohistochemical stains were significantly increased, up to 20%,

http://dx.doi.org/10.4132/jptm.2014.09.17

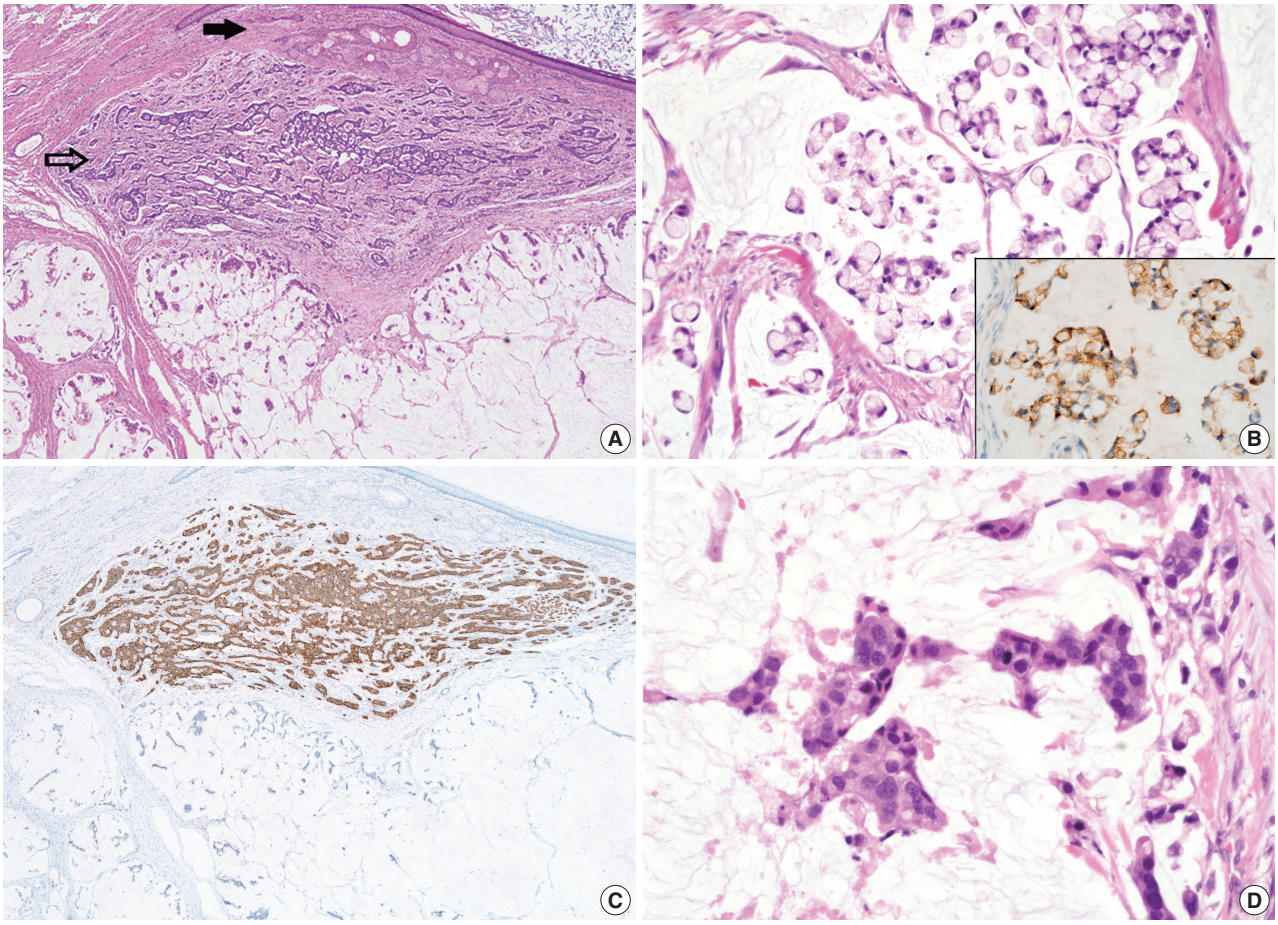

Fig. 2. Histopathologic findings of mesenteric mass showing mature cystic teratoma containing a mature teratomatous component (A, closed arrow), an area of trabecular carcinoid (A, open arrow), goblet cell carcinoid (B) showing immunopositivities for synaptophysin (B inset and C), and mucinous adenocarcinoma with signet ring cells within dissecting mucin pools (D). Note a high nuclear cytoplasmic ratio and significant nuclear pleomorphism in the mucinous adenocarcinoma component (D) in contrast to low nuclear cytoplasmic ratio and flattened nuclei in goblet cell carcinoid (B).

in those malignant cells. The two areas containing the signet ring cell-like appearance with and without nuclear pleomorphism were intermingled with each other and the border could not be clearly delineated.

Both ovaries were mostly replaced by tumor tissue with a multinodular appearance. Each nodule was well-circumscribed and was composed of a mucin pool containing signet ring cells identical to those in the mesenteric mass (Fig. 3A). Extraovarian mucin pools were also noted in the omentum and serosal surfaces of the pelvic organs, forming pseudomyxoma peritonei (Fig. 3B). There were no insular or trabecular carcinoid areas in either ovarian tumor.

The patient received five cycles of adjuvant chemotherapy with paclitaxel and cisplatin, but she died of multiorgan metastasis eight months postoperatively.

DISCUSSION

Historically, a tumor describing mixed glandular and neuroendocrine neoplasm has had many synonyms, including goblet cell carcinoid, mucinous carcinoid, adenocarcinoid, microglandular carcinoma, intermediate cell carcinoid, amphicrine neoplasia, and composite tumor. There remains confusion and debate regarding the terminologies amongst pathologists and clinicians. In the appendix and ovaries, intimately admixed glandular and neuroendocrine neoplasm composed of goblet cells, neuroendocrine cells, or hybrid cells containing both mucin and neuroendocrine granules floating in pools of mucin are designated as goblet cell carcinoid. Goblet cell carcinoid tumors in the appendix present in four types: 1) pure and uniform tubules composed entirely of goblet cells; 2) goblet cell carcinoid with

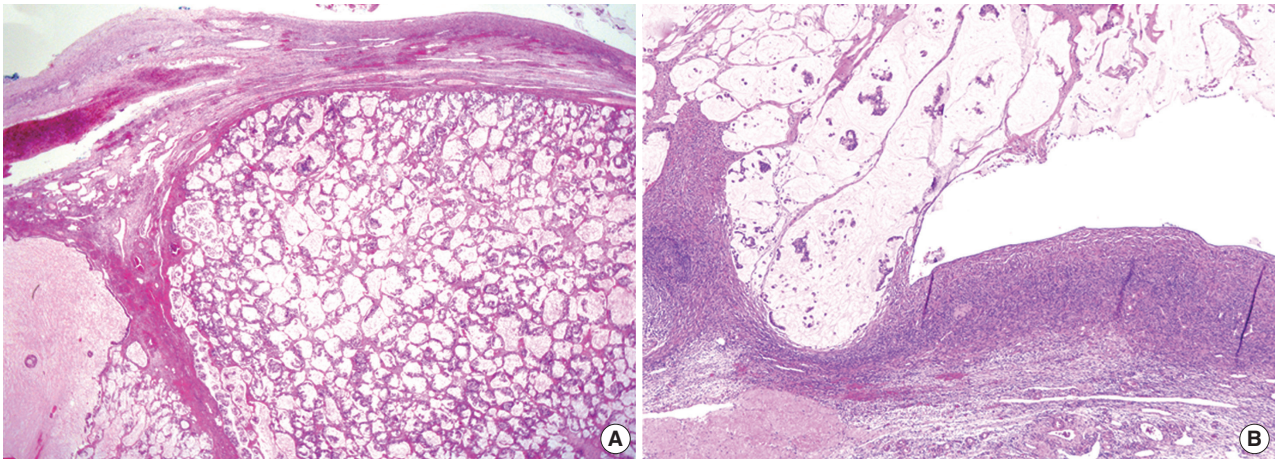

Fig. 3. Histopathologic findings of ovarian mass. The tumor tissue shows a multinodular appearance with well-circumscribed margins. Each nodule is composed of a mucin pool containing malignant tumor cells identical to those in the mesenteric mass (A). The tumor tissue in the ovarian surface and superficial cortex formed pseudomyxoma peritonei composed of mucin pools with floating signet ring cells, which are connected to the extraovarian mucin pools in the pelvic cavity (B).

adenocarcinomatous area (adenocarcinoma ex goblet cell carcinoid); 3) goblet cell carcinoid with mucinous cystadenoma; and 4) the combined classical carcinoid with goblet cell carcinoid tumor.[4] In our case, goblet cell carcinoid was combined with mucinous adenocarcinoma and additional typical insular and trabecular carcinoid tumor. Histologically, it is not easy to distinguish the pure goblet cell carcinoid from mucinous adenocarcinoma arising in goblet cell carcinoid tumors because of the same goblet cell morphology in mucin pools in both tumors and intimately admixed tumor components in most cases. Goblet cell carcinoid tumors have more aggressive clinical behaviors, showing metastasis in 20% of cases,[5] compared to the classic type of carcinoid tumor, but the tumors have relatively favorable prognosis compared to the mucinous adenocarcinoma ex goblet cell carcinoid.[6] Pools of mucin are usually small in goblet cell carcinoid and they usually lie within the glands or in the periglandular stroma. The nuclear atypia is not significant in goblet cell carcinoid; however, mucinous adenocarcinoma ex goblet cell carcinoid has greater nuclear pleomorphism, higher mitotic rate, and Ki-67 proliferating activity, which can lead to a diagnosis of mucinous adenocarcinoma ex goblet cell carcinoid.

Histogenetically, two neoplasms in adjacent but separate areas are designated as a collision tumor of a biclonal derivation, while composite tumors having intimate admixture of the two components are believed to result from bidirectional differentiation of a single neoplasm. A molecular study suggested that goblet cell carcinoid has similar expression patterns of genes for secretory and Paneth cell differentiation to those of mucinous cystadenomas and colonic adenocarcinomas; thus, goblet cell carcinoids are closer to colonic adenocarcinomas than to classical carcinoids,[7] implicating that the goblet cell carcinoid probably arises in progenitor cells of the epithelial crypt.

Rarely, mature cystic teratomas have been described in the mesentery and greater omentum.[2] The pathogenetic origin is explained as primitive germ cells entrapped during embryonic development, a supernumerary (ectopic) ovary located in the omentum,[8] or secondary implantation of a teratomatous component to the omentum following the torsion and rupture of ovarian teratoma.[9]

The diagnosis of extra-appendiceal and extraovarian goblet cell carcinoid should be determined after thorough examination of the two organs and exclusion of appendiceal or ovarian origins. The patient in our case received an appendectomy at the same time, which was thoroughly examined, but only serosal tumor implants were identified. Mucinous adenocarcinoma involved bilateral ovaries in our case; however, the ovaries were thought to be metastatic sites because of their bilateral multinodular appearance, and involvement of the ovarian surface and superficial cortex of the ovary only. A significant amount of mucin pools dissecting the ovarian stroma and signet ring cell-like morphology are extremely rare in primary mucinous adenocarcinoma of the ovary.[10] Moreover, the existence of mesenteric mature teratoma and significantly larger extraovarian mucin pools forming pseudomyxoma peritonei are supporting features of extraovarian origin.

This case had combined features of several rare findings: primary mesenteric mature teratoma associated with carcinoid tu-

 http://dx.doi.org/10.4132/jptm.2014.09.17

mor, coexistence of all three types of carcinoid tumors including insular, trabecular and goblet cell carcinoid, overgrown mucinous adenocarcinoma of goblet cell morphology in the background of goblet cell carcinoid, metastasis of extragonadal goblet cell carcinoid to the ovaries, and formation of pseudomyxoma peritonei from extra-appendiceal neoplasm, but the clinical course followed those of mucinous adenocarcinoma and high grade pseudomyxoma peritonei. Recognition of mucinous adenocarcinoma components seems to be closely correlated with the patient's prognosis. Thus, careful histological observation is required to make a clinically relevant diagnosis.

Conflicts of Interest

No potential conflict of interest relevant to this article was reported.

REFERENCES

1. Kurman RJ, Ellenson LH, Ronnett BM. Blaustein's pathology of the female genital tract. 6th ed. New York: Springer, 2011; 877.
2. Papakonstantinou E, Iavazzo C, Hasiakos D, Kleanthis CK, Fotiou S, Kondi-Pafiti A. Extraovarian mature cystic teratoma of the mesentery: a case report and literature review. Clin Exp Obstet Gynecol 2011; 38: 291-3.
3. Lancaster KJ, Liang CY, Myers JC, McCabe KM. Goblet cell carcinoid arising in a mature teratoma of the mediastinum. Am J Surg Pathol 1997; 21: 109-13.
4. Chetty R, Klimstra DS, Henson DE, Albores-Saavedra J. Combined classical carcinoid and goblet cell carcinoid tumor: a new morphologic variant of carcinoid tumor of the appendix. Am J Surg Pathol 2010; 34: 1163-7.
5. Toumpanakis C, Standish RA, Baishnab E, Winslet MC, Caplin ME. Goblet cell carcinoid tumors (adenocarcinoid) of the appendix. Dis Colon Rectum 2007; 50: 315-22.
6. Turaga KK, Pappas SG, Gamblin T. Importance of histologic subtype in the staging of appendiceal tumors. Ann Surg Oncol 2012; 19: 1379-85.
7. van Eeden S, Offerhaus GJ, Hart AA, *et al.* Goblet cell carcinoid of the appendix: a specific type of carcinoma. Histopathology 2007; 51: 763-73.
8. Abrego D, Ibrahim AA. Mesenteric supernumerary ovary. Obstet Gynecol 1975; 45: 352-3.
9. Kearney MS. Synchronous benign teratomas of the greater omentum and ovary: case report. Br J Obstet Gynaecol 1983; 90: 676-9.
10. Lee KR, Young RH. The distinction between primary and metastatic mucinous carcinomas of the ovary: gross and histologic findings in 50 cases. Am J Surg Pathol 2003; 27: 281-92.

Journal of Pathology and Translational Medicine 2015; 49: 66-70
http://dx.doi.org/10.4132/jptm.2014.10.14

■ BRIEF CASE REPORT ■

Ewing's Sarcoma/Primitive Neuroectodermal Tumor of the Uterine Corpus

Eung-Seok Lee · Won Hwangbo[1] · Insun Kim[1]

Department of Pathology, Korea University Ansan Hospital, Ansan; [1]Department of Pathology, Korea University Anam Hospital, Seoul, Korea

Ewing's sarcoma (ES)/primitive neuroectodermal tumor (PNET) is defined as a round cell sarcoma that shows varying degrees of neuroectodermal differentiation. The term PNET was first introduced by Hart and Earle in 1973.[1] Cases of ES/PNET in the female genital tract are rare. Now we report a case of ES/PNET arising in the uterine body which was confirmed by all studies performed, including morphologic, immunohistochemical, ultrastructural, and cytogenetic examinations.

CASE REPORT

A 23-year-old Korean woman presented with irregular vaginal bleeding and low abdominal pain. Ultrasonography and magnetic resonance imaging of the pelvis revealed a huge intramural mass of the uterus, measuring 8.4 cm in diameter. Bilateral adnexal abnormality or significant lymphadenopathy was not identified. Total abdominal hysterectomy, bilateral salpingo-oophorectomy, and lymph node dissections were done.

Grossly, the uterus was slightly enlarged, measuring 6×13×8 cm. On opening the uterus, there was a mass arising from the anterior wall of the uterus, bulging out into the endometrial cavity with an area of ulceration on the endometrium. The cut surface of the uterus showed an unencapsulated but relatively well-circumscribed intramural tumor, measuring 9×7.5 cm (Fig. 1). The tumor showed a homogeneous gray-tan, solid, and fish-fleshy appearing cut surface with no conspicuous necrosis or hemorrhage. The tumor abutted the endometrium and serosal surface of the uterus. Both ovaries and salpinges were grossly unremarkable without any enlargement or tumor identified.

Microscopically, the tumor was composed of relatively uniform small round-to-oval neoplastic cells arranged in a diffuse sheet or solid nesting pattern of growth with intervening fibrous septa throughout the myometrium. The tumor invaded the endometrium focally but did not involve the serosal surface of the uterus. There were numerous areas of lymphatic tumor invasion and a metastatic tumor implant on the surface of the left ovary, but there was no evidence of metastatic tumor in the pelvic lymph nodes. The tumor cells had scanty cytoplasm with indistinct cytoplasmic border, round-to-oval nuclei of stippled chromatin pattern, and inconspicuous nucleoli (Fig. 2). Mitoses, apoptotic bodies, and focal areas of necrosis were frequently found (22/10 high power fields of mean mitotic count). Pseudorosettes were also frequently present but no malignant glandular areas were identified within or adjacent to the tumor.

On immunohistochemical examination the tumor cells showed diffuse strong positivity for cluster of differentiation 99 antigen (CD99) and neuron-specific enolase (NSE) in a membranous pattern and Friend leukemia virus integration 1 (FLI-1) in a nuclear pattern. The tumor cells were focally positive for vimentin but negative for c-kit, WT-1, CAM5.2, chromogranin, synaptophysin, CD56, CD10, CD3, CD20, leukocyte common antigen, desmin, and myogenin (Fig. 3). Electromicroscopic study showed a variable number of glycogen particles in a dispersed pattern and there were primitive intercellular and synaptic-like junctions. We also performed dual-color fluorescence *in situ* hybridization (FISH) analysis with a break-apart rearrangement probe. In normal cells, a combined two-signal pattern is seen, reflecting intact regions; we found separated single green

Corresponding Author
Eung-Seok Lee, M.D.
Department of Pathology, Korea University Ansan Hospital, 123 Jeokgeum-ro, Danwon-gu, Ansan 425-707, Korea
Tel: +82-31-412-5323, Fax: +82-31-412-5324, E-mail: a9604@chollian.net

Received: July 16, 2014 **Revised:** September 21, 2014
Accepted: October 13, 2014

pISSN 2383-7837
eISSN 2383-7845

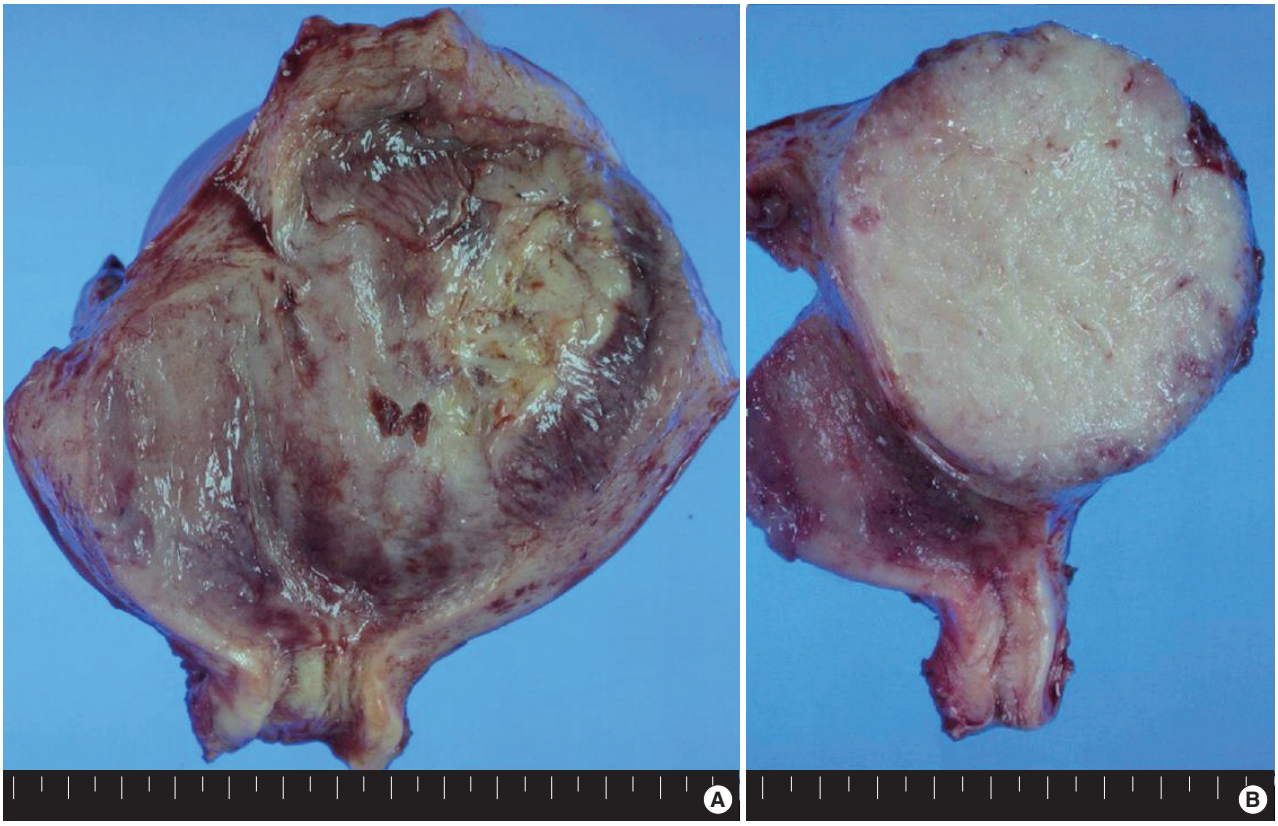

Fig. 1. (A) The uterus is slightly enlarged, measuring 6×13×8 cm. On opening the uterus, there is a mass arising from the anterior wall of the uterus, bulging out into the endometrial cavity with an area of ulceration on the endometrium. (B) The cut surface of the uterus shows an unencapsulated but relatively well-circumscribed intramural tumor, measuring 9×7.5 cm. The tumor shows a homogeneous gray-tan, solid, and fish-fleshy appearing cut surface with no conspicuous necrosis or hemorrhage. The tumor abuts the endometrium and serosal surface of the uterus.

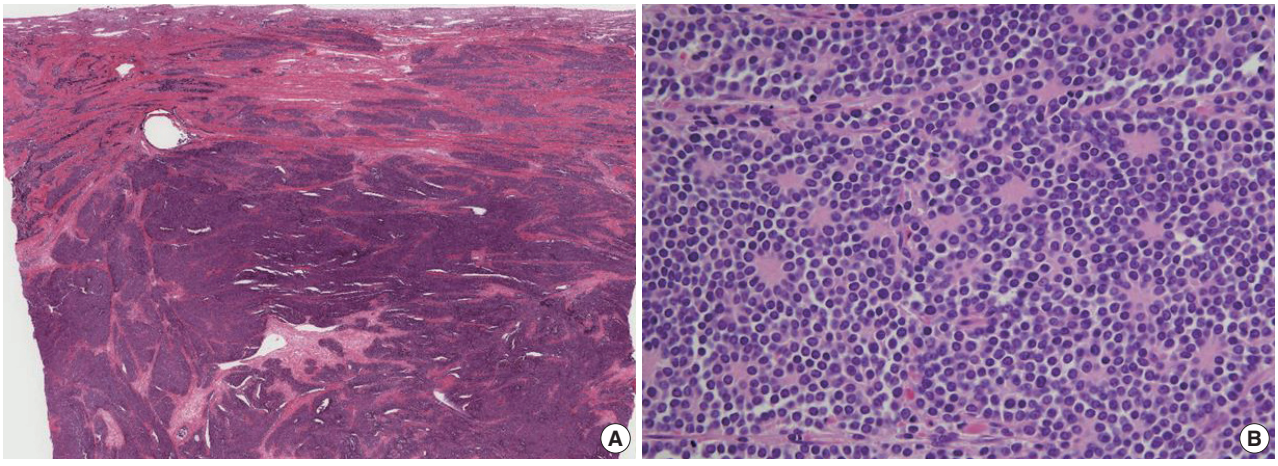

Fig. 2. (A) The tumor is composed of relatively uniform small round-to-oval neoplastic cells and arranged in a diffuse sheet or solid nesting pattern of growth with intervening fibrous septa throughout the myometrium. The tumor invades the endometrium focally but does not involve the serosal surface of the uterus. (B) The tumor cells have scant cytoplasm with an indistinct cytoplasmic border, round-to-oval nuclei of stippled chromatin pattern, and inconspicuous nucleoli. Pseudorosettes are also frequently present but no malignant glandular areas are identified within or adjacent to the tumor.

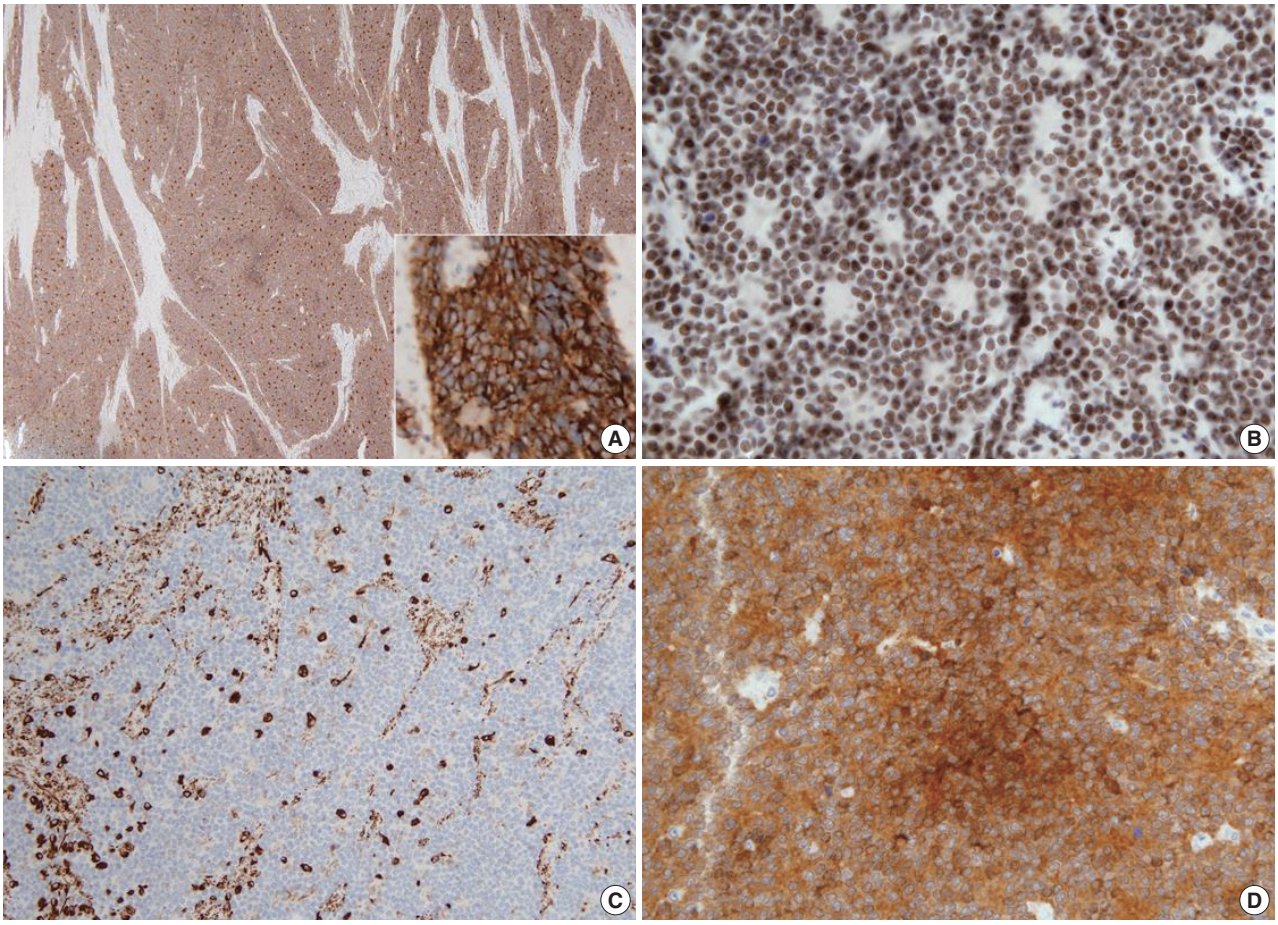

Fig. 3. The tumor cells show diffuse strong positivity for CD99 (A) and neuron-specific enolase (D) in a membrane pattern and FLI-1 (B) in a nuclear pattern. The tumor cells are focally positive for vimentin (C).

and single orange signal patterns and identified rearrangement in the tumor. On the basis of the FISH results, we performed reverse transcription polymerase chain reaction (RT-PCR) and confirmed the products of *EWS-FLI1* fusion transcript with 330 bp.

DISCUSSION

ES/PNET is defined as a round cell sarcoma that shows varying degrees of neuroectodermal differentiation. The term PNET was first introduced by Hart and Earle in 1973 to describe a group of small round cell tumors that appeared to be derived from fetal neuroectodermal cells with variable degrees of neuroectodermal differentiation.[1] ES and PNET are regarded as two extremes of a morphologic spectrum of the same tumor entity. Their classification depends on the degree of differentiation of their neuroectodermal components. ES with no evidence of neuroectodermal differentiation lies at one end of the spectrum and PNET with clear evidence of neuroectodermal differentiation at the other. ES/PNET shows characteristic signature translocations involving the ES gene (*EWSR1*, Ewing sarcoma breakpoint region 1) at 22q12.2 and various erythroblastic transformation specific (ETS)-family transcription factor genes, the most common of which is *FLI1* at 11q24.1–q24.3.[2] *EWSR1* is a ubiquitously expressed gene encoding a multifunctional protein that regulates multiple cellular processes, while FLI-1 is a transcription factor that plays a role during vascular development and in lymphoid function.[3] The resulting fusion genes act as an oncogenic transcription factor. Cases of ES/PNET in the female genital tract are rare. Such tumors are found in the ovary,[4] vulva,[5] vagina,[6] cervix,[7] and uterine corpus.[8]

On the basis of microscopic examination the differential diagnosis of ES/PNET of the uterine corpus includes poorly differentiated endometrioid carcinoma, stromal sarcoma, small cell neuroendocrine carcinoma, and lymphoma, which are composed of sheets of cytologically malignant small cells with little or no

 http://dx.doi.org/10.4132/jptm.2014.10.14

evidence of glandular or squamous differentiation. Small cell neuroendocrine carcinomas and lymphomas make developing a differential diagnosis difficult because they show immunohistochemical overlap as well as morphologic similarities with ES/PNET. Histologically, small cell neuroendocrine carcinomas tend to grow in sheets of small cells having nuclei with stippled "salt and pepper" chromatin, absence of nucleoli, and nuclear molding of adjacent cells. Although rosettes and pseudorosettes, positive staining for chromogranin, synaptophysin, and NSE, and ultrastructural dense-core granules may be observed in both small cell carcinomas and ES/PNET, the former is usually immunohistochemically negative for MIC-2 and FLI-1, which are relatively specific markers for ES/PNET. The absence of lymphoid markers virtually excludes a diagnosis of lymphoma. Ultrastructural investigation may be helpful, since lymphoma shares no features with ES/PNET, which usually demonstrates neural differentiation, dense-core granules, and glycogen accumulation. Endometrioid carcinomas virtually always contain focal areas of glandular differentiation with positivity for epithelial markers. Stromal sarcomas are composed of cells that closely resemble non-neoplastic endometrial stroma and have a prominent vascular pattern of spiral arteriole-like spaces and mild nuclear atypia with low mitotic index. Stromal sarcoma can be excluded by areas of marked nuclear atypia with frequent mitotic figures and the absence of the typical vascular pattern in ES/PNET. The absence of CD10 and estrogen and progesterone receptors also helps to make a diagnosis of ES/PNET.

MIC-2 and FLI-1 are very useful markers for the diagnosis of ES/PNET, as they are expressed in nearly all ES/PNET.[8] In addition, ES/PNET tumor cells are positive for vimentin and may focally express NSE, chromogranin, synaptophysin, and S-100. In our case, the tumor cells were diffusely strongly positive for MIC-2 and FLI-1, and focally positive for vimentin. Ultrastructural features are helpful in making the diagnosis of ES/PNET. Ultrastructurally, neural differentiation, including neurosecretory granules and neurite-like cytoplasmic processes, can be recognized in ES/PNET.[8] Glycogen accumulation in the cytoplasm also can be seen in ES/PNET. All ultrastructural features of the above were present in our case. ES/PNET is also characterized by balanced chromosomal translocation of t(11;22)(q24;q12), resulting in the production of the *EWS-FLI1* fusion gene in approximately 85% of cases. Other translocations leading to the fusion of the EWS gene with one of several members of the ETS family of transcription factors have subsequently been identified, including t(21,22)(q22;q21) in 10%–15% of cases and t(7;22), t(17; 22) and t(2;22) in less than 1% of cases. Thus genetic analysis would be helpful when histologic and immunohistochemical examinations are not conclusive.[8] Numerous molecular techniques such as DNA- and RNA-based polymerase chain reaction, Southern blotting, and FISH have been used for detection of the *EWS* translocations associated with ES/PNET. Ideally, cytogenetic investigation for the assessment of such translocations on paraffin sections should include FISH and RT-PCR.[2] RT-PCR is unique in its ability to identify both genes involved in the most common translocations encountered in ES/PNET. A variety of RT-PCR assays have been developed for the detection of *EWS* translocation products.[2] Recently, *EWSR1* (22q12), a dual-color, break-apart rearrangement probe using FISH analysis (Abbott Laboratories, Abbott Park, IL, USA), has been commercially available, and its diagnostic value in ES/PNET is well-established.[9] However, due to the presence of the t(11;22) translocation in other tumor types such as desmoplastic small round cell tumor,[10] FISH results should be interpreted in light of the morphology and immunohistochemical profile.

At initial diagnosis, the tumor is often already at an advanced stage in most patients. In addition, there is no uniformity in the treatment of ES/PNET in the uterus. Total hysterectomy with bilateral salpingo-oophorectomy, with or without chemotherapy and/or radiotherapy, is the usual course of treatment provided. In this case, the patient underwent surgical resection and six courses of chemotherapy. The patient is still alive with no evidence of recurrence or metastasis after operation in December 2012, and chemotherapy with ifosfamide.

Conflicts of Interest

No potential conflict of interest relevant to this article was reported.

REFERENCES

1. Hart MN, Earle KM. Primitive neuroectodermal tumors of the brain in children. Cancer 1973; 32: 890-7.
2. Masoura S, Kourtis A, Kalogiannidis I, *et al*. Primary primitive neuroectodermal tumor of the cervix confirmed with molecular analysis in a 23-year-old woman: a case report. Pathol Res Pract 2012; 208: 245-9.
3. Truong AH, Ben-David Y. The role of Fli-1 in normal cell function and malignant transformation. Oncogene 2000; 19: 6482-9.
4. Kleinman GM, Young RH, Scully RE. Primary neuroectodermal tumors of the ovary: a report of 25 cases. Am J Surg Pathol 1993; 17: 764-78.

5. Vang R, Taubenberger JK, Mannion CM, *et al*. Primary vulvar and vaginal extraosseous Ewing's sarcoma/peripheral neuroectodermal tumor: diagnostic confirmation with CD99 immunostaining and reverse transcriptase-polymerase chain reaction. Int J Gynecol Pathol 2000; 19: 103-9.
6. Liao X, Xin X, Lü X. Primary Ewing's sarcoma-primitive neuroectodermal tumor of the vagina. Gynecol Oncol 2004; 92: 684-8.
7. Tsao AS, Roth LM, Sandler A, Hurteau JA. Cervical primitive neuroectodermal tumor. Gynecol Oncol 2001; 83: 138-42.
8. Ren YL, Tang XY, Li T. Ewing sarcoma-primitive neuroectodermal tumor of the uterus: a clinicopathologic, immunohistochemical and ultrastructural study of one case. Arch Gynecol Obstet 2011; 283: 1139-43.
9. Mhawech-Fauceglia P, Herrmann F, Penetrante R, *et al*. Diagnostic utility of FLI-1 monoclonal antibody and dual-colour, break-apart probe fluorescence *in situ* (FISH) analysis in Ewing's sarcoma/primitive neuroectodermal tumour (EWS/PNET): a comparative study with CD99 and FLI-1 polyclonal antibodies. Histopathology 2006; 49: 569-75.
10. Sandberg AA, Bridge JA. Updates on the cytogenetics and molecular genetics of bone and soft tissue tumors: desmoplastic small round-cell tumors. Cancer Genet Cytogenet 2002; 138: 1-10.

http://dx.doi.org/10.4132/jptm.2014.10.14

Journal of Pathology and Translational Medicine 2015; 49: 71-74
http://dx.doi.org/10.4132/jptm.2014.12.14

■ BRIEF CASE REPORT ■

Placental Mesenchymal Dysplasia with Fetal Gastroschisis

Binnari Kim · Jiyeon Hyeon · Minju Lee · Hyewon Hwang · Yooju Shin · Suk-Joo Choi[1] · Jung-Sun Kim

Departments of Pathology and Translational Genomics, [1]Obstetrics and Gynecology, Samsung Medical Center, Sungkyunkwan University School of Medicine, Seoul, Korea

Placental mesenchymal dysplasia (PMD) is a rare, benign condition characterized by placentomegaly and abnormal chorionic villi with vesicle formation, fibroblastic hyperplasia, and vascular abnormalities. This condition can be misdiagnosed as molar pregnancy due to similar ultrasonographic findings;[1] however, unlike molar pregnancy, a fetus is usually present and there is no risk of trophoblastic proliferative disease in PMD. The authors report a case of placental mesenchymal dysplasia at 15 weeks of gestation associated with fetal gastroschisis and high serum beta human chorionic gonadotropin (β-hCG) that mimicked molar pregnancy.

CASE REPORT

A 29-year-old female with abnormal ultrasonographic findings was transferred to our institution. The patient had a normal sequential screening with the exception of an elevated serum β-hCG of 165,870 mIU/mL. Serum α-fetoprotein was not evaluated. Transabdominal ultrasound at 14^{+0} weeks of gestation revealed a thick globular placenta measuring 6.5×4.5 cm with multiple small, hypoechoic areas. Subsequent ultrasound at 14^{+5} weeks of gestation demonstrated a large multicystic honeycomb-like placenta measuring 8.8×5.7 cm with no sign of blood flow within the lesion (Fig. 1A). A fetus was identified with a crown-rump length of 9.6 cm (Fig. 1B). Based on the clinical setting, partial hydatidiform mole was suspected. Therapeutic termination was performed at 15^{+0} weeks of gestation.

Corresponding Author
Jung-Sun Kim, M.D.
Department of Pathology and Translational Genomics, Samsung Medical Center, Sungkyunkwan University School of Medicine, 81 Irwon-ro, Gangnam-gu, Seoul 135-710, Korea
Tel: +82-2-3410-2767, Fax: +82-2-3410-0025, E-mail: jsunkim@skku.edu

Received: October 6, 2014 **Revised:** December 8, 2014
Accepted: December 14, 2014

Grossly, the placenta was markedly enlarged with a diameter of 10 cm and the placental disc had multiple cystic vesicles; enlarged chorionic vessels were not found (Fig. 1C). A nonviable male fetus with a body weight of 73.57 g and with a crown-rump length of 9.8 cm, which were appropriate for gestational age, was delivered. However, he had a left lateral abdominal wall defect from which the liver and bowels protruded (Fig. 1D).

Microscopic examination of the placenta revealed several enlarged villi with cistern formation and abnormally thick vessels scattered among normal-sized terminal villi without abnormal trophoblast proliferation. Some chorionic villi showed proliferation of primitive stromal cells (Fig. 2A-C). Cytotrophoblasts were diffusely positive for p57KIP2 on immunohistochemical staining (Fig. 2D). Macroscopic and microscopic morphology confirmed a diagnosis of PMD accompanied by gastroschisis of the fetus.

DISCUSSION

PMD was first described as a rare, benign condition associated with an enlarged placenta in 1991 by Moscoso *et al.*[2] The true incidence of PMD remains unclear, but it was reported to account for about 0.02% (7/30,758) of placentas examined at a Japanese hospital.[3] Most cases are asymptomatic and are diagnosed postpartum upon delivery of an abnormally large placenta. The typical sonographic feature of PMD is a thickened placenta with hypoechoic cystic spaces, which overlaps with that of molar pregnancy.[4] Thus, the differentiation of the two conditions may be difficult without placental pathology. One of the common laboratory abnormalities observed in PMD is increased maternal serum alpha fetoprotein, which is thought to originate from the fetus.[2] Serum β-hCG is typically normal to slightly elevated; the serum β-hCG level in this case was higher than that of normal pregnancy, which was unusual.

pISSN 2383-7837
eISSN 2383-7845

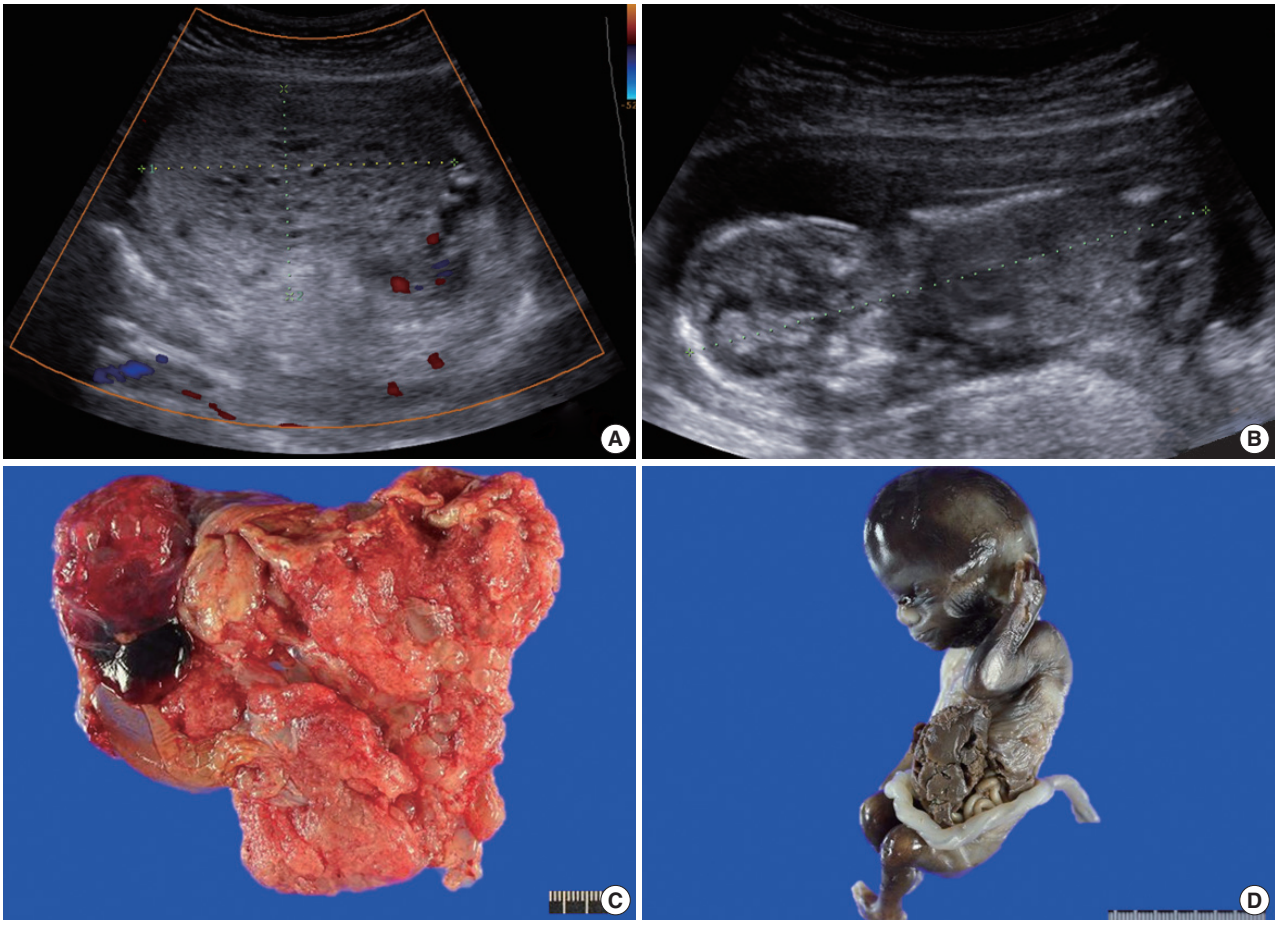

Fig. 1. Radiologic and gross findings. (A) Transabdominal ultrasound at 14^{+5} weeks of gestation shows a large multicystic honeycomb-like placenta measuring 8.8×5.7 cm with no sign of blood flow within the lesion. (B) The fetus has a crown-rump length of 9.6 cm. (C) The placenta is markedly enlarged with multiple vesicles. (D) The fetus exhibits gastroschisis.

Grossly, the placenta is markedly enlarged for gestational age and the placental disc has multiple grape-like vesicles from 0.3 to 2.5 cm in size, which resemble those of molar pregnancy. Enlarged chorionic vessels are usually found in third-trimester PMD placentas, not seen in hydatidiform mole. However, prominent chorionic vessels may not be identified grossly during the early stages, as in this case. Histologically, enlarged villi with cistern formation and abnormally thick vessels are scattered among normal-sized terminal villi. Some chorionic villi show mesenchymal cell hyperplasia. Neither abnormal trophoblast proliferation nor scalloping of the villous surface, common histologic findings of hydatidiform mole, is present. p57KIP2 immunopositivity of the cytotrophoblasts in our case was helpful for excluding the possibility of complete hydatidiform mole.[4]

The precise etiology of PMD has not been established. One theory is that it results from a congenital malformation of the mesoderm. Hypoxia and hypoperfusion of unknown origin may be responsible for the pathologic placental changes. More recently, androgenetic/biparental mosaicism has been suggested to be the underlying cause of PMD.[4]

Unlike molar pregnancy, PMD is not associated with gestational trophoblastic diseases, but does increase the risk of intrauterine fetal growth restriction and intrauterine fetal death. Approximately 15% to 25% of PMD cases are associated with Beckwith-Wiedemann syndrome.[5-7] PMD and Beckwith-Wiedemann syndrome represent a broad spectrum of phenotypes with common etiology.[4,8] In our case, PMD was associated with fetal gastroschisis, which has not been reported previously.[6] A recently-favored hypothesis for the pathogenesis of gastroschisis is folding failure of the embryonic lateral body due to defective mesoderm.[9] Mesodermal abnormality is suggested to be the cause of the association between PMD and gastroschisis in this case.

In summary, PMD is a rare but clinically important placental abnormality that can be confused with partial hydatidiform mole

 http://dx.doi.org/10.4132/jptm.2014.12.14

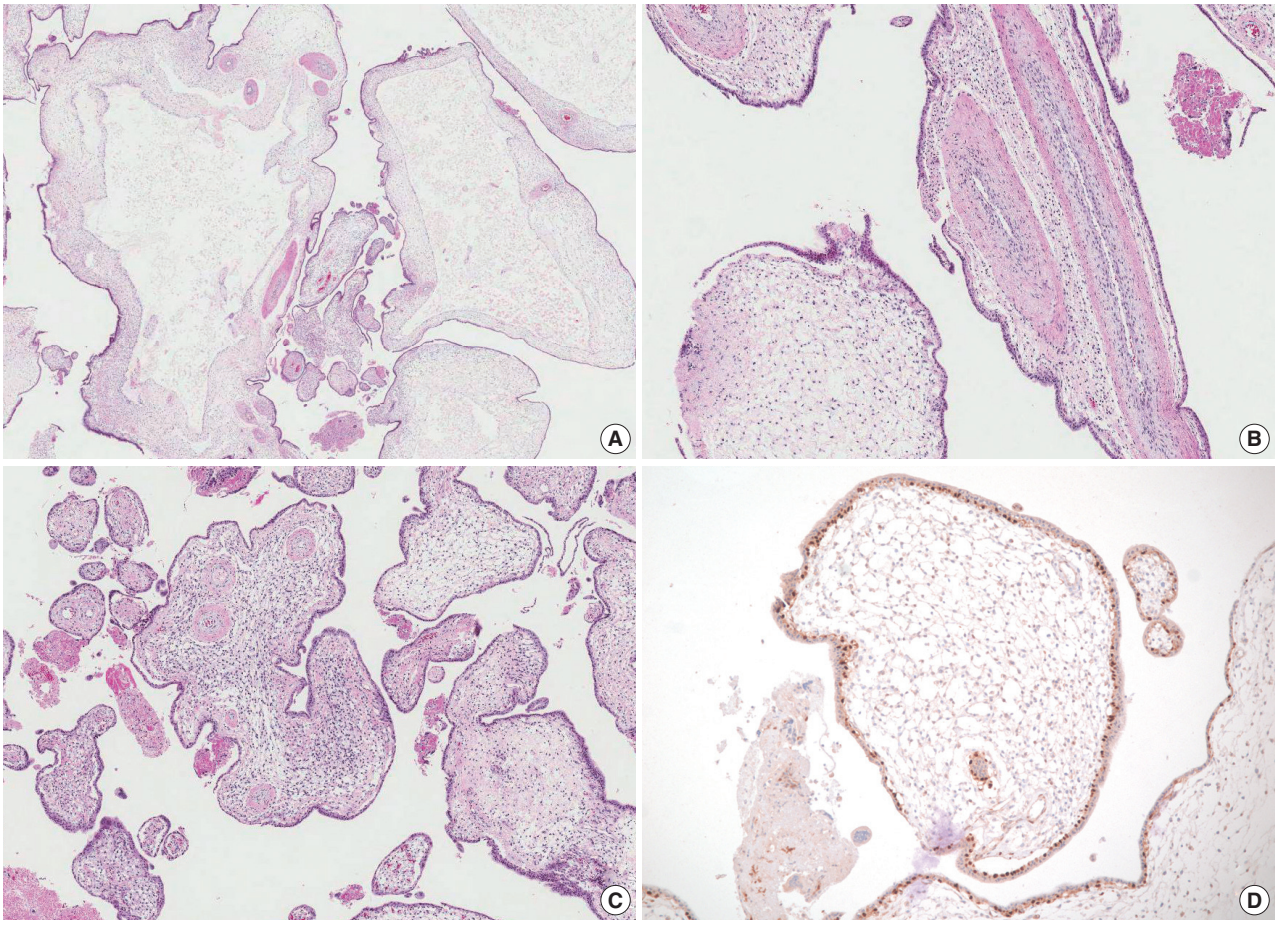

Fig. 2. Microscopic findings of the placenta. (A) Cystic vesicles are surrounded by stromal tissue and trophoblasts, indicating cysts in enlarged stem villi. No abnormal trophoblast proliferation is observed. (B) The majority of the enlarged stem villi have abnormal vessels with thickened muscular walls. (C) Some of the villi show mesenchymal cell proliferation. (D) Cytotrophoblasts are diffusely immunopositive for p57KIP2.

and can be associated with abnormal fetal conditions. Therefore, PMD should be considered in the differential diagnosis of multicystic placenta. Awareness of this entity based on its sonographic similarity to molar pregnancy, unique pathologic features, and association with fetal complications needs to be emphasized in prenatal monitoring for the avoidance of unnecessary terminations.

Conflicts of Interest

No potential conflict of interest relevant to this article was reported.

REFERENCES

1. Vaisbuch E, Romero R, Kusanovic JP, *et al*. Three-dimensional sonography of placental mesenchymal dysplasia and its differential diagnosis. J Ultrasound Med 2009; 28: 359-68.
2. Moscoso G, Jauniaux E, Hustin J. Placental vascular anomaly with diffuse mesenchymal stem villous hyperplasia: a new clinico-pathological entity? Pathol Res Pract 1991; 187: 324-8.
3. Arizawa M, Nakayama M. Suspected involvement of the X chromosome in placental mesenchymal dysplasia. Congenit Anom (Kyoto) 2002; 42: 309-17.
4. Parveen Z, Tongson-Ignacio JE, Fraser CR, Killeen JL, Thompson KS. Placental mesenchymal dysplasia. Arch Pathol Lab Med 2007; 131: 131-7.
5. Pham T, Steele J, Stayboldt C, Chan L, Benirschke K. Placental mesenchymal dysplasia is associated with high rates of intrauterine growth restriction and fetal demise: a report of 11 new cases and a review of the literature. Am J Clin Pathol 2006; 126: 67-78.
6. Heazell AE, Sahasrabudhe N, Grossmith AK, Martindale EA, Bhatia K. A case of intrauterine growth restriction in association with placental mesenchymal dysplasia with abnormal placental lymphatic development. Placenta 2009; 30: 654-7.

7. Woo GW, Rocha FG, Gaspar-Oishi M, Bartholomew ML, Thompson KS. Placental mesenchymal dysplasia. Am J Obstet Gynecol 2011; 205: e3-5.
8. Ulker V, Aslan H, Gedikbasi A, Yararbas K, Yildirim G, Yavuz E. Placental mesenchymal dysplasia: a rare clinicopathologic entity confused with molar pregnancy. J Obstet Gynaecol 2013; 33: 246-9.
9. Feldkamp ML, Carey JC, Sadler TW. Development of gastroschisis: review of hypotheses, a novel hypothesis, and implications for research. Am J Med Genet A 2007; 143A: 639-52.

http://dx.doi.org/10.4132/jptm.2014.12.14

Journal of Pathology and Translational Medicine 2015; 49: 75-77
http://dx.doi.org/10.4132/jptm.2014.10.27

■ BRIEF CASE REPORT ■

A Rare Case of Mixed Type A Thymoma and Micronodular Thymoma with Lymphoid Stroma

Yoon Jin Cha · Joungho Han · Jimin Kim · Kyung Soo Lee[1] · Young Mog Shim[2]

Departments of Pathology, [1]Radiology, and [2]Thoracic Surgery, Samsung Medical Center, Sungkyunkwan University School of Medicine, Seoul, Korea

Micronodular thymoma with lymphoid stroma (MNTLS) is a rare subtype of thymoma and accounts for only 1%–5% of all thymoma.[1] Histologically, MNTLS shows characteristic segregating epithelial components in rich lymphoid stroma. Though the histogenesis of MNTLS is not yet elucidated, it is postulated that type A thymoma and MNTLS are common in origin. Here we report a case of mixed thymoma composed of type A thymoma and MNTLS.

CASE REPORT

A 63-year-old man presented with a mediastinal mass incidentally found on routine chest radiograph during a regular health check-up. He had a history of hypertension and diabetes treated with medication. There was no evidence of myasthenia gravis. On further evaluation by chest computed tomography (CT), a 7.3-cm mediastinal mass was identified in the right anterior mediastinum (Fig. 1A). The mass had a lobulated contour, and intratumoral septation suggested a thymic epithelial tumor. No enlargement of mediastinal lymph nodes or pleural seeding was found on CT. He received extended thymectomy via median sternotomy. During the operation, there was no pleural adhesion or invasion into surrounding structures.

On cut sections, the tumor measured 7×6 cm and was enclosed by a thin fibrous capsule. Vague, tan-colored nodules averaging 1.5 cm in size were identified. These were partly separated by thin fibrous septa and areas of numerous tiny cobblestone-like micronodules (Fig. 1B). On histological examination, two different types of thymoma were noted, showing partly infiltrative growth into adjacent fat tissue (Fig. 1C). Large nodules seen were composed of epithelial cells with sparse lymphocytes. Spindled tumor cells formed an organoid pattern, arranged in short fascicles and a solid sheet. The tumor cells had elongated, bland nuclei with fine chromatin and inconspicuous small nucleoli. These characteristics, together with positivity for cytokeratin (CK) and Bcl-2, were compatible with World Health Organization (WHO) type A thymoma. The type A area was ill-defined, showing gradual transition into the rest of the tumor, which harbored a mixture of epithelial and lymphoid components (Fig. 1D). Multiple small epithelial nodules were embedded in the lymphoid stroma. The tumor cells from the smaller nodules were spindled, bland-looking and formed pseudorosettes that had elongated nuclei with fine chromatin and inconspicuous nucleoli, similar to type A thymoma. Epithelial tumor nodules were segregated by lymphoid stroma that occasionally harbored germinal centers (Fig. 1E). Tumor cells were strongly positive for CK and moderately positive for Bcl-2 (Fig. 1F, G). Lymphoid stroma was positive for CD5 (Fig. 1G). Bcl-2 was diffusely positive throughout the lymphoid stroma (Fig. 1H) but was negative in germinal centers. Additional CD20 and CD3 immunohistochemical staining showed reactive B- and T-cells in the lymphoid stroma. The patient was diagnosed ultimately with mixed type A thymoma and MNTLS.

DISCUSSION

MNTLS, first coined by Suster and Moran,[1] is a rare subtype of thymoma. A micronodular pattern of epithelial components

Corresponding Author
Joungho Han, M.D.
Department of Pathology, Samsung Medical Center, Sungkyunkwan University School of Medicine, 81 Irwon-ro, Gangnam-gu, Seoul 135-710, Korea
Tel: +82-2-3410-2800, Fax: +82-2-3410-0025, E-mail: hanjho@skku.edu

Received: September 2, 2014 **Accepted:** October 24, 2014

pISSN 2383-7837
eISSN 2383-7845

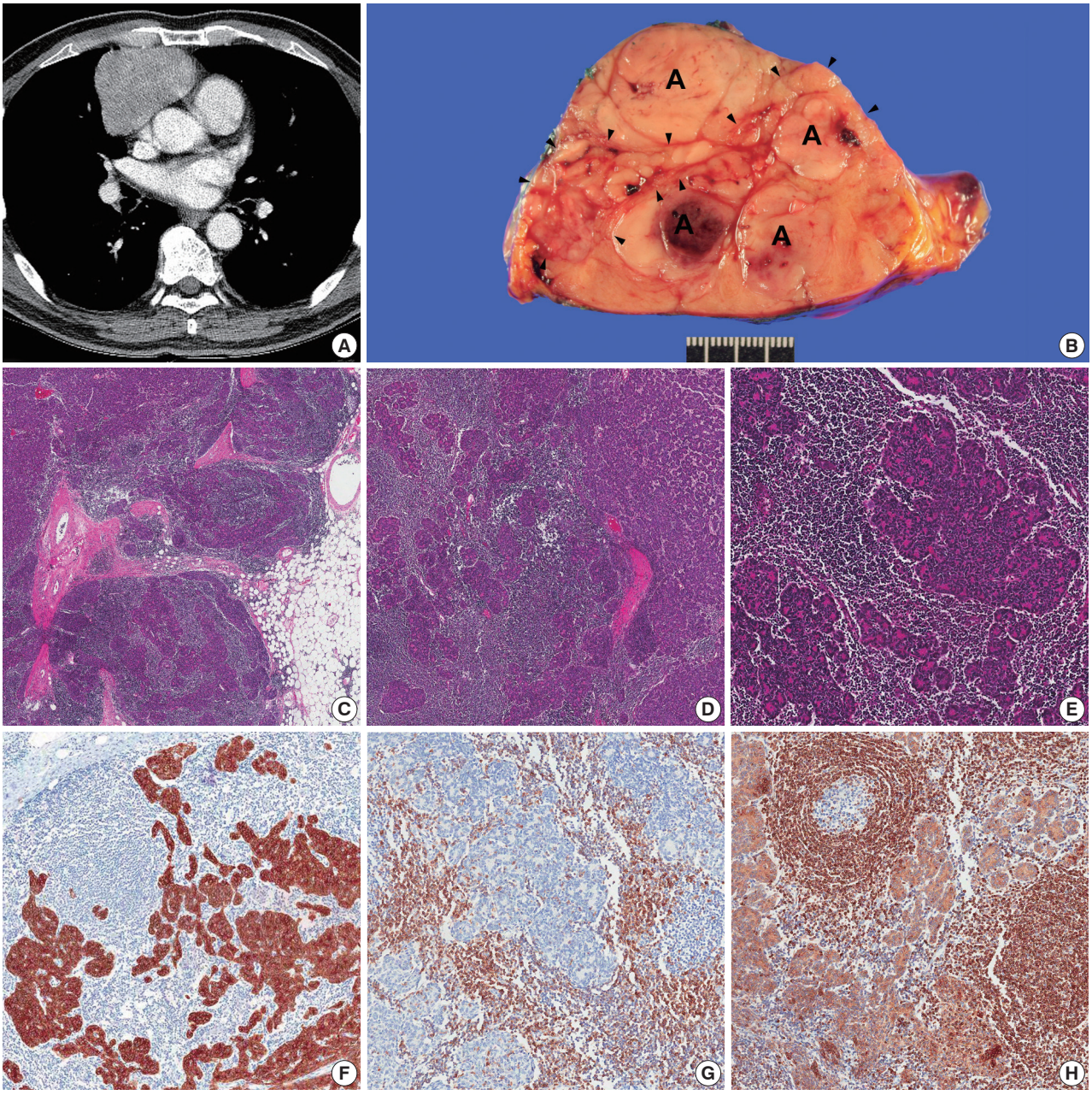

Fig. 1. Mixed Type A Thymoma and Micronodular Thymoma with Lymphoid Stroma. (A) Chest computed tomography imaging demonstrates a lobulated mass in the right anterior mediastinum. (B) Grossly, the tumor is encapsulated with a thin fibrous capsule, and is composed of vague nodules with tiny internodular micronodules, which matched with both type A thymoma (capital A on figure) and micronodular thymoma (arrowheads). (C) A microscopic area of infiltrative growth into fat tissue is noted. (D) A gradual transition is found between type A thymoma and micronodular thymoma with lymphoid stroma (MNTLS). (E) The MNTLS tissue has epithelial micronodules arranged in pseudorosettes that are separated by lymphoid stroma. (F) The tumor cells are strongly positive for cytokeratin, whereas lymphoid stroma lacks any epithelial component. (G) Lymphoid stroma is diffusely positive for CD5. (H) Together with type A thymoma, the epithelial component of MNTLS is positive for Bcl-2. Lymphoid stroma, except for within germinal centers, also is positive for Bcl-2.

is found in approximately 10% of type A and type AB thymoma.[2] Cases accompanied by thymic cyst,[3] heart myxoma,[4] and ectopic lesions arising in the salivary gland[5] have been reported. Characteristically, MNTLS demonstrates small nodules of epithelial components resembling those of type A thymoma within lymphoid stroma that is predominantly composed of B-cells with occasional germinal centers. Being devoid of epithelial components is helpful in excluding type AB thymoma, which also

http://dx.doi.org/10.4132/jptm.2014.10.27

contains epithelial components and lymphoid follicles. With its rich B-cells, occasional germinal centers, and nodules of epithelial cells, MNTLS could be misdiagnosed as metastatic carcinoma in a small biopsy specimen.[4] Although the histogenesis of MNTLS is not yet clarified, its medullary epithelial cells suggest MNTLS may be a variant of type A thymoma in the setting of thymic B-cell hyperplasia.[1] Bcl-2, a B-cell marker, is expressed in type A thymoma and thymic carcinoma.[6] We observed Bcl-2 expression in both type A thymoma and MNTLS. These findings support the hypothesis that MNTLS originates from type A thymoma. Stobel *et al.*[7] found that 33% of MNTLS had lymphoid stroma of a monoclonal B-cell population whereas thymic lymphoid hyperplasia or other types of thymoma had a polyclonal population of lymphocytes. Because of the monoclonal lymphoid stroma, they suggested that MNTLS might be a precursor lesion of mediastinal lymphoma.[7] In the present case, the lymphoid stroma was positive for both CD20 and CD3, reflecting a polyclonal lymphocyte nature. Although patient outcomes of MNTLS have not been established because of its rarity, MNTLS has reported cases that have shown excellent prognosis so far.[1,8] Ishikawa *et al.*[9] explained that an immune response induced by intratumoral MNTLS Langerhans cells would contribute to improved patient outcomes.

We report a case of mixed thymoma containing type A thymoma and MNTLS. In the present case, epithelial components of type A thymoma and MNTLS showed similar histologic and immunohistochemical profiles with areas of gradual transition, suggesting type A thymoma and MNTLS share a common histogenesis. Although this tumor showed focal infiltrative growth of MNTLS, it was postulated that this tumor would have a good clinical course.

Conflicts of Interest

No potential conflict of interest relevant to this article was reported.

REFERENCES

1. Suster S, Moran CA. Micronodular thymoma with lymphoid B-cell hyperplasia: clinicopathologic and immunohistochemical study of eighteen cases of a distinctive morphologic variant of thymic epithelial neoplasm. Am J Surg Pathol 1999; 23: 955-62.
2. Pan CC, Chen WY, Chiang H. Spindle cell and mixed spindle/lymphocytic thymomas: an integrated clinicopathologic and immunohistochemical study of 81 cases. Am J Surg Pathol 2001; 25: 111-20.
3. Kim NR, Lee JI, Ha SY. Micronodular thymoma with lymphoid stroma in a multilocular thymic cyst: a case study. Korean J Pathol 2013; 47: 392-4.
4. Song HJ, Han J, Kim TS. Micronodular thymoma with lymphoid stroma: a case report. J Lung Cancer 2011; 10: 56-8.
5. Mende S, Moschopulos M, Marx A, Laeng RH. Ectopic micronodular thymoma with lymphoid stroma. Virchows Arch 2004; 444: 397-9.
6. Hiroshima K, Iyoda A, Toyozaki T, *et al*. Proliferative activity and apoptosis in thymic epithelial neoplasms. Mod Pathol 2002; 15: 1326-32.
7. Strobel P, Marino M, Feuchtenberger M, *et al*. Micronodular thymoma: an epithelial tumour with abnormal chemokine expression setting the stage for lymphoma development. J Pathol 2005; 207: 72-82.
8. Tateyama H, Saito Y, Fujii Y, *et al*. The spectrum of micronodular thymic epithelial tumours with lymphoid B-cell hyperplasia. Histopathology 2001; 38: 519-27.
9. Ishikawa Y, Tateyama H, Yoshida M, *et al*. Micronodular thymoma with lymphoid stroma: an immunohistochemical study of the distribution of Langerhans cells and mature dendritic cells in six patients. Histopathology 2014 Apr 4 [Epub]. http://dx.doi.org/10.1111/his.12428.

Journal of Pathology and Translational Medicine 2015; 49: 78-80
http://dx.doi.org/10.4132/jptm.2014.12.15

■ BRIEF CASE REPORT ■

A Rare Case of Tumor-to-Tumor Metastasis of Thyroid Papillary Carcinoma within a Pulmonary Adenocarcinoma

Taebum Lee · Yoon Jin Cha · Sangjeong Ahn · Joungho Han · Young Mog Shim[1]

Departments of Pathology and [1]Thoracic Surgery, Samsung Medical Center, Sungkyunkwan University School of Medicine, Seoul, Korea

Tumor-to-tumor metastasis (TTM) is a rare phenomenon first reported several decades ago in Fried's description of a bronchogenic carcinoma that metastasized to a meningioma.[1] According to previous studies, renal cell carcinoma and meningioma are common recipients, whereas lung and breast cancer are common donors.[2] Thus far, four cases of lung carcinoma harboring papillary thyroid carcinoma (PTC) metastasis have been reported in the English literature.[3-6] Here we present another case of PTC that metastasized to pulmonary adenocarcinoma.

CASE REPORT

A 56-year-old non-smoking male presented with a 3-month history of cough and sputum. On chest computed tomography, a 53-mm-sized ground-glass opacity in the left upper lobe (LUL) of the lung was identified (Fig. 1A left). On positron emission tomography, F-18 fluorodeoxyglucose uptake was detected in the left thyroid accompanied by lymphadenopathy (Fig. 1A right). Histological confirmation was performed for each lesion. Fine needle aspiration of thyroid and bronchoscopic biopsy of the lung lesion revealed PTC with cervical lymph node metastasis and pulmonary adenocarcinoma, respectively. Lobectomy of the LUL was performed prior to thyroid cancer treatment.

A single, well-defined, 0.6×0.6-cm-sized, round, firm, white-tan nodule was found in the peribronchial area within a 3.9×3.1-cm-sized, irregular, soft, grey mass in the anterior segment of the LUL, on gross examination (Fig. 1B) and low-power magnification (Fig. 1C). No other suspicious lesions were detected in the given specimen. The main lung lesion was diagnosed as conventional pulmonary adenocarcinoma and was composed of moderately differentiated adenocarcinoma with an acinar and papillary pattern accompanied by a focal micropapillary pattern (Fig. 1D). The small nodule within the adenocarcinoma (Fig. 1D) was comprised of papillae lined by cuboidal cells with nuclear clearing and grooves suggestive of PTC (Fig. 1E). Additional thyroglobulin immunohistochemical staining (1:1,000, Dako, Glostrup, Denmark) highlighted metastatic PTCs in a total of three foci (Fig. 1F). A metastatic papillary carcinoma was also identified in a separately submitted mediastinal lymph node.

Subsequent total thyroidectomy with central neck node dissection was performed one month after lobectomy. Bilateral PTCs (3.3×3 cm and 0.3×0.3 cm) and metastasis to 17 of 36 regional lymph nodes were identified on histologic examination.

DISCUSSION

Synchronous primary cancers are occasionally observed, but TTM is extremely rare; only about 100 cases have been reported in the English literature. Campbell *et al.*[7] proposed the concept of TTM, which can be distinguished from collision tumor based on following criteria: 1) more than one primary tumor; 2) the recipient tumor may be a true benign or malignant neoplasm; 3) the metastatic neoplasm is a true metastasis with established growth within the host tumor, not the result of contiguous growth (collision tumor) or tumor emboli; 4) primary tumors spreading into the lymphatic system in the setting of general-

Corresponding Author
Joungho Han, M.D.
Department of Pathology, Samsung Medical Center, Sungkyunkwan University School of Medicine, 81 Irwon-ro, Gangnam-gu, Seoul 135-710, Korea
Tel: +82-2-3410-2800, Fax: +82-2-3410-0025, E-mail: hanjho@skku.edu

Received: October 22, 2014 **Revised:** Novembr 25, 2014
Accepted: December 14, 2014

pISSN 2383-7837
eISSN 2383-7845

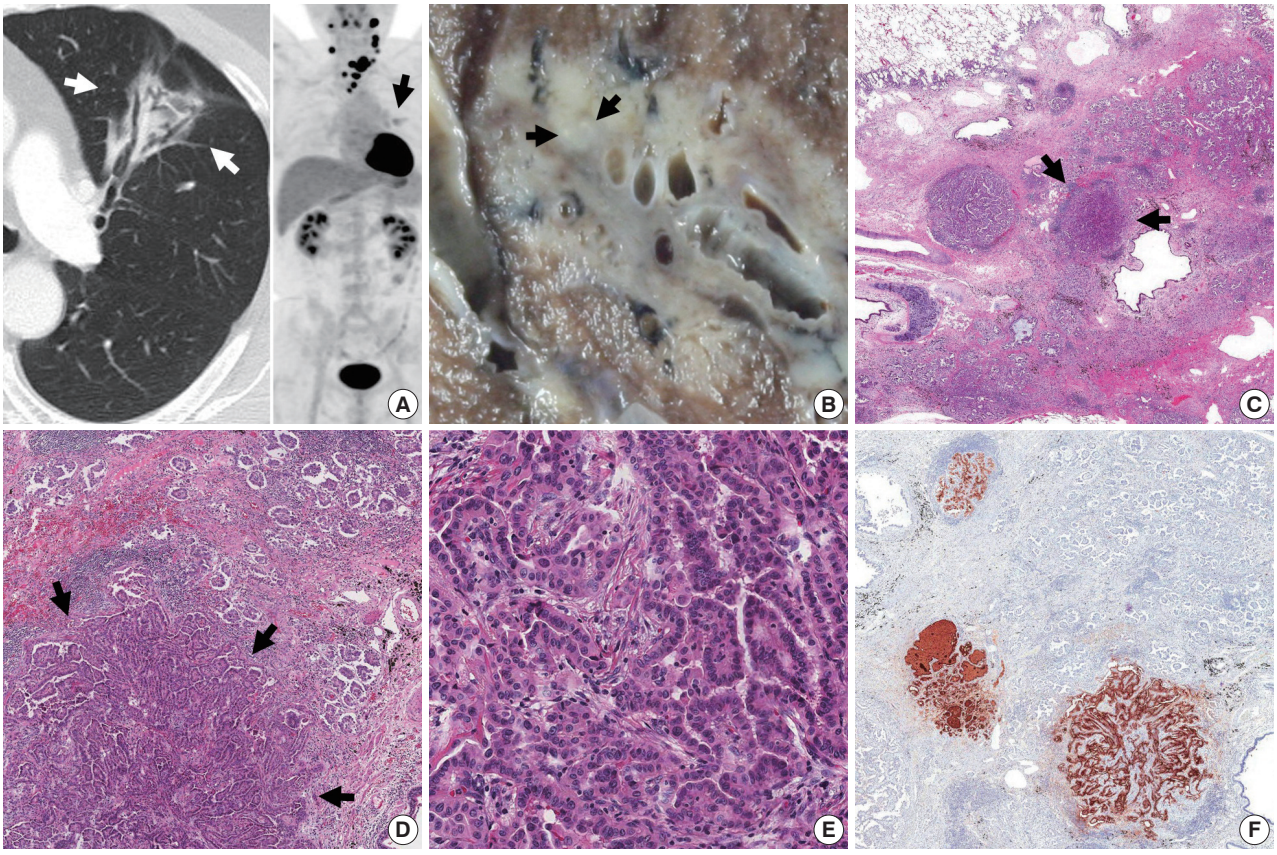

Fig. 1. Metastasis of thyroid papillary carcinoma within a pulmonary adenocarcinoma. (A) Chest computed tomography shows ground-glass opacity (white arrows) in the left upper lobe. Positron emission tomography reveals F-18 fluorodeoxyglucose uptake in the left lobe of the thyroid, multiple cervical lymph nodes and the left upper lung (black arrow). (B) Grossly, metastatic papillary thyroid carcinoma (PTC) is a small, round, firm, white-tan nodule (arrows) located within an irregular, soft, grey lung mass. (C) Under low-power magnification, metastatic PTC (arrows) is distinguished from background pulmonary adenocarcinoma by its localized and compact arrangement of tumor cells. (D) Metastatic PTC (arrows) exhibits a papillary growth pattern and less fibrosis compared to the predominant acinar pattern and large-scale fibrosis of pulmonary adenocarcinoma. (E) Together with well-formed papillae, tumor cells of metastatic PTC have typical nuclear features including nuclear clearing and grooves. (F) Three metastatic PTCs are strongly positive for thyroglobulin on immunohistochemistry.

ized lymphoreticular malignancy are excluded.

According to the 'seed and soil hypothesis'[8] of cancer metastasis, interactions between cancer cells (seed) and specific organ microenvironments (soil) determine the outcome of metastasis. Renal cell carcinoma and meningioma are both highly vascularized tumors, and have high lipid and glycogen content, which can provide a fertile environment for growth. However, pulmonary adenocarcinoma is a less likely candidate recipient tumor because it is often accompanied by fibrosis, rather than the "nutritious components" described above, and is less vascularized than normal lung tissue.[3]

TTM is rare, but with the advent of new diagnostic tools and treatment strategies, reports of such cases are becoming more common. In the current study, despite the challenge of radiologic detection on account of its small size and location, metastatic PTC within pulmonary adenocarcinoma was observed both macroscopically and microscopically. The typical nuclear features and immunohistochemistry along with the patient's history of PTC were helpful in establishing an accurate diagnosis. Regular radiologic follow-up is scheduled for this patient based on the potential for multiple metastases. Pathologists should consider the possibility of TTM when they encounter a histologically unusual component within a typical tumor of the primary organ because appropriate treatment will vary in cases of TTM.

Conflicts of Interest

No potential conflict of interest relevant to this article was reported.

REFERENCES

1. Fried BM. Metastatic inoculation of a meningioma by cancer cells from a bronchiogenic carcinoma. Am J Pathol 1930; 6: 47-52.
2. Petraki C, Vaslamatzis M, Argyrakos T, *et al*. Tumor to tumor metastasis: report of two cases and review of the literature. Int J Surg Pathol 2003; 11: 127-35.
3. Kim KM, Kim YN, Chu HH, Jin HY, Kim MH, Chung MJ. Papillary carcinoma of thyroid metastatic to adenocarcinoma in situ of lung: report of an unusual case. Korean J Pathol 2012; 46: 282-6.
4. Xue L, Luan Z, Liu Y, *et al*. Pulmonary metastasis of a papillary thyroid carcinoma and primary lung adenocarcinoma: two coincident carcinomas at the same location. Diagn Pathol 2013; 8: 26.
5. Roscoe KJ, Raja S, Tronic B, Dou Y. Single F-18 fluorodeoxyglucose positron emission tomography hypermetabolic focus containing metastatic papillary thyroid cancer within a primary scarring adenocarcinoma lung cancer. Clin Nucl Med 2006; 31: 359-60.
6. Nonomura A, Mizukami Y, Shimizu J, Watanabe Y, Kamimura R, Takashima T. Two patients with metastasis of cancer to other neoplasm: a thyroid carcinoma metastatic to a lung carcinoma and a gastric carcinoma metastatic to a thyroid adenoma. Endocr Pathol 1994; 5: 233-9.
7. Campbell LV Jr, Gilbert E, Chamberlain CR Jr, Watne AL. Metastases of cancer to cancer. Cancer 1968; 22: 635-43.
8. Paget S. The distribution of secondary growths in cancer of the breast. 1889. Cancer Metastasis Rev 1989; 8: 98-101.

http://dx.doi.org/10.4132/jptm.2014.12.15

Journal of Pathology and Translational Medicine 2015; 49: 81-84
http://dx.doi.org/10.4132/jptm.2014.06.03

■ BRIEF CASE REPORT ■

Alveolar Rhabdomyosarcoma of the Lip in an Adult with Clear Cell Features

Jae Yeon Seok · Juhyeon Jeong · Young Woo Cheon[1] · Hyun Yee Cho · Seung Yeon Ha · Dong Hae Chung

Departments of Pathology and [1]Plastic Surgery, Gachon University Gil Medical Center, Incheon, Korea

Rhabdomyosarcoma, which occurs in the head and neck, genitourinary tract and deep soft tissue of the extremities and typically presents in childhood or adolescence, is a malignant mesenchymal tumor showing differentiation of skeletal muscle.[1,2] Less than 3% of rhabdomyosarcoma cases present in adults. Although rhabdomyosarcoma frequently occurs in the head and neck region, involvement of the lips is very rare; only 8 cases have been reported in the English literature.[3-10] Conventionally, rhabdomyosarcoma is categorized into embryonal, alveolar and pleomorphic subtypes.[11] We report a case of alveolar rhabdomyosarcoma with clear cell features presenting as a perioral subcutaneous nodule on the upper lip of a 58-year-old woman. A review of the literature and possible differential diagnoses are described.

CASE REPORT

A 58-year-old woman presented with a subcutaneous hard mass on her upper lip (Fig. 1A). A punch biopsy was performed at a local clinic and revealed small round cells infiltrating the dermis. The possibility of a small round cell tumor such as Merkel cell carcinoma or lymphoma was suggested. A wide excision was performed, and a skin-colored 0.7-cm nodule was noted. The cut surface of the mass was white gray and firm. Microscopic findings showed an ill-defined subcutaneous tumor that involved the entire dermis and subcutaneous adipose tissue sparing the epidermis (Fig. 1B, C). Small tumor cells infiltrated dissecting dermal collagen bundles and showed densely packed groups of cells. The cytoplasm was scanty with indistinct borders, and marked clear cell change was noted in most of the tumor cells (Fig. 1D). Some tumor cells had amphophilic cytoplasm. The nuclei were round to oval with focal indentation and finely granular chromatin. Frequent mitotic figures were noted up to 7 per 10 high power fields.

Periodic acid–Schiff stain demonstrated a few intracytoplasmic glycogen particles (Fig. 2A). Immunohistochemical examination of the tumor cells showed strong positivity for desmin, myogenin, and vimentin (Fig. 2B, C). The tumor cells were negative for cytokeratin, smooth muscle actin, human melanoma black 45, S-100 protein, and neuron-specific enolase. Under electron microscopy, the tumor cells showed thin and thick filaments with focal electron density in the cytoplasm, and many vacuoles which corresponds to clear cytoplasm visualized under light microscopy (Fig. 2D). These findings confirmed the diagnosis of rhabdomyosarcoma, alveolar type.

After the diagnosis, head and neck computed tomography and positron emission tomography were performed and revealed no evidence of a primary tumor elsewhere or evidence of a mass in deeper soft tissue. The patient underwent radiation therapy and was free of recurrence or metastasis for four months after surgery.

DISCUSSION

Rhabdomyosarcoma arising in the lip is very rare. Only eight cases have been reported in the English literature (Table 1),[3-10] and the patients ranged in age from 1 to 58 years. Three of nine patients including the current case were adults, and four of nine patients were male. Six patients had a mass in the upper lip. Three

Corresponding Author
Dong Hae Chung, M.D.
Department of Pathology, Gachon University Gil Medical Center, 21 Namdong-daero 774beon-gil, Namdong-gu, Incheon 405-760, Korea
Tel: +82-32-460-3073, Fax: +82-32-460-2394, E-mail: dhchung@gilhospital.com

Received: February 25, 2014 **Revised:** May 30, 2014
Accepted: June 3, 2014

pISSN 2383-7837
eISSN 2383-7845

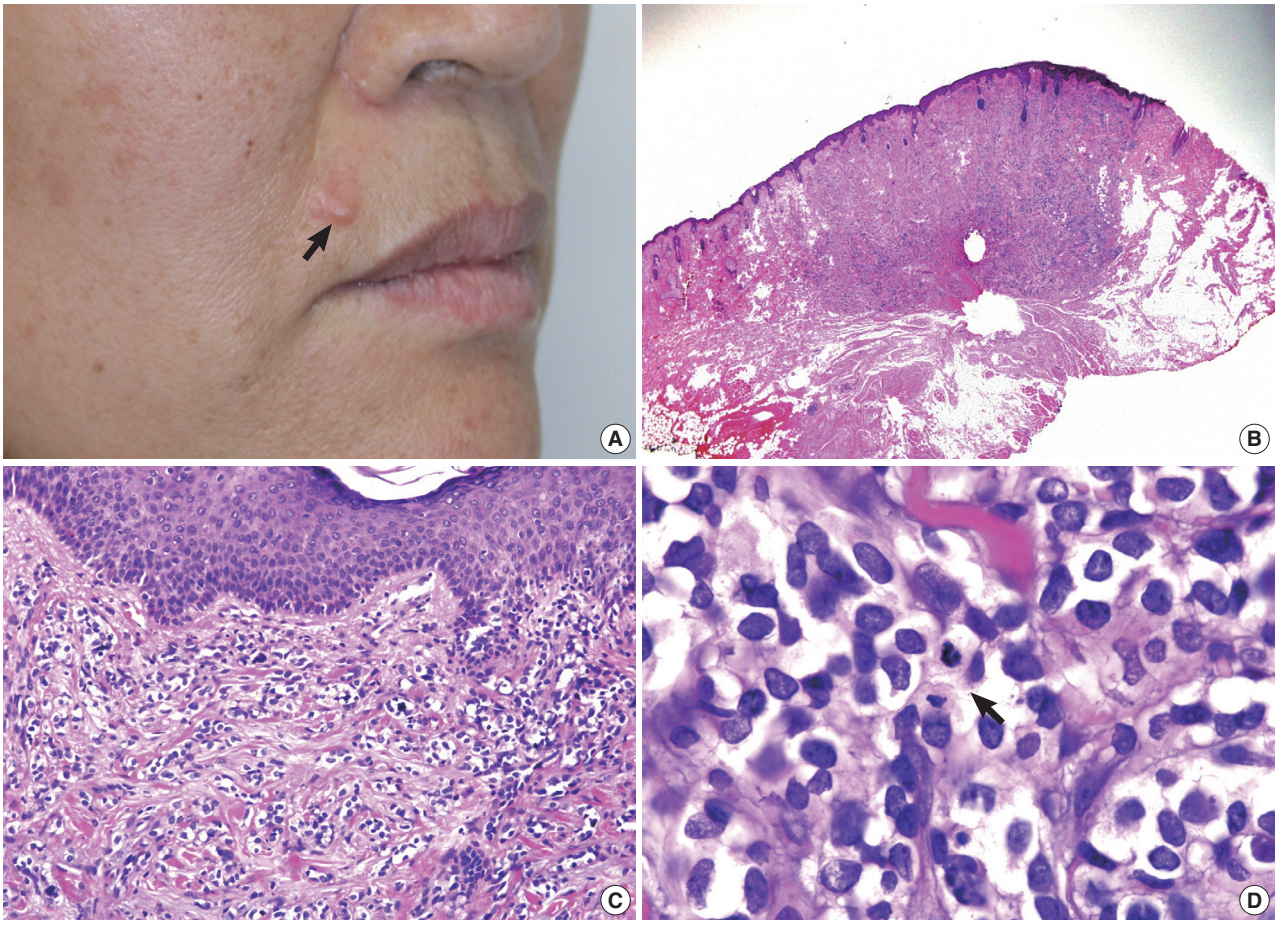

Fig. 1. (A) A skin-colored nodule is noted in the upper lip (arrow). (B) An ill-defined mass involves the dermis and subcutaneous fat tissue. (C) The tumor cells extend to the papillary dermis but do not invade the epidermis. (D) The tumor is composed of densely packed groups of small round cells intersecting collagen bundles with marked clear cell change and frequent mitotic figures (arrow).

of nine patients presented with a congenital mass. The duration of symptoms ranged up to seven months, and the tumor size ranged from 0.7 cm to 10 cm. Five patients were diagnosed as alveolar subtype, three patients as embryonal subtype, and one patient as pleomorphic subtype. The follow-up period ranged from 3 to 71 months. None of the nine patients experienced local recurrence, but two had metastatic lesions. One patient had metastatic lesions at the cervical lymph node and salivary gland. The other patient had metastatic lesions at the lung and bone, who died of the disease within three months.

Rhabdomyosarcoma of the lip as a primary lesion is rare. The previously reported cases showed various clinical features such as ulcerated hemorrhagic soft mass, smooth mobile nodule, firm lobulated erythematous mass, lobulated small raised lesion, painful swelling and tender firm indurated mass. The clinical differential diagnoses include hemangioma, odontogenic tumor, dermoid, solitary fibromatosis, gingival granular cell tumor, neurofibroma and rhabdomyosarcoma. Microscopically, when the tumor shows skeletal muscle differentiation such as a rhabdoid feature, strap cells or cytoplasmic striation, it is easy to reach a diagnosis of rhabdomyosarcoma. However, in the case of a small biopsy or small tumor, the diagnosis may be more obscure. Several tumors including lymphoma, Ewing sarcoma and rhabdomyosarcoma can show the histologic features of a small round cell tumor. Suspicion of this diagnosis and an extensive search for the signs of differentiation on light microscopy are needed in such cases. An immunohistochemical study including desmin and myogenin is helpful if tumor cells do not show characteristic differentiation on light microscopy. Electron microscopy and genetic study are useful when the immunohistochemical staining is not diagnostic. Ultrastructural rhabdomyosarcoma tumor cells show cytoplasmic thick and thin filaments resembling rudimentary sarcomeric structure, cross striation, and glycogen particles.

http://dx.doi.org/10.4132/jptm.2014.06.03

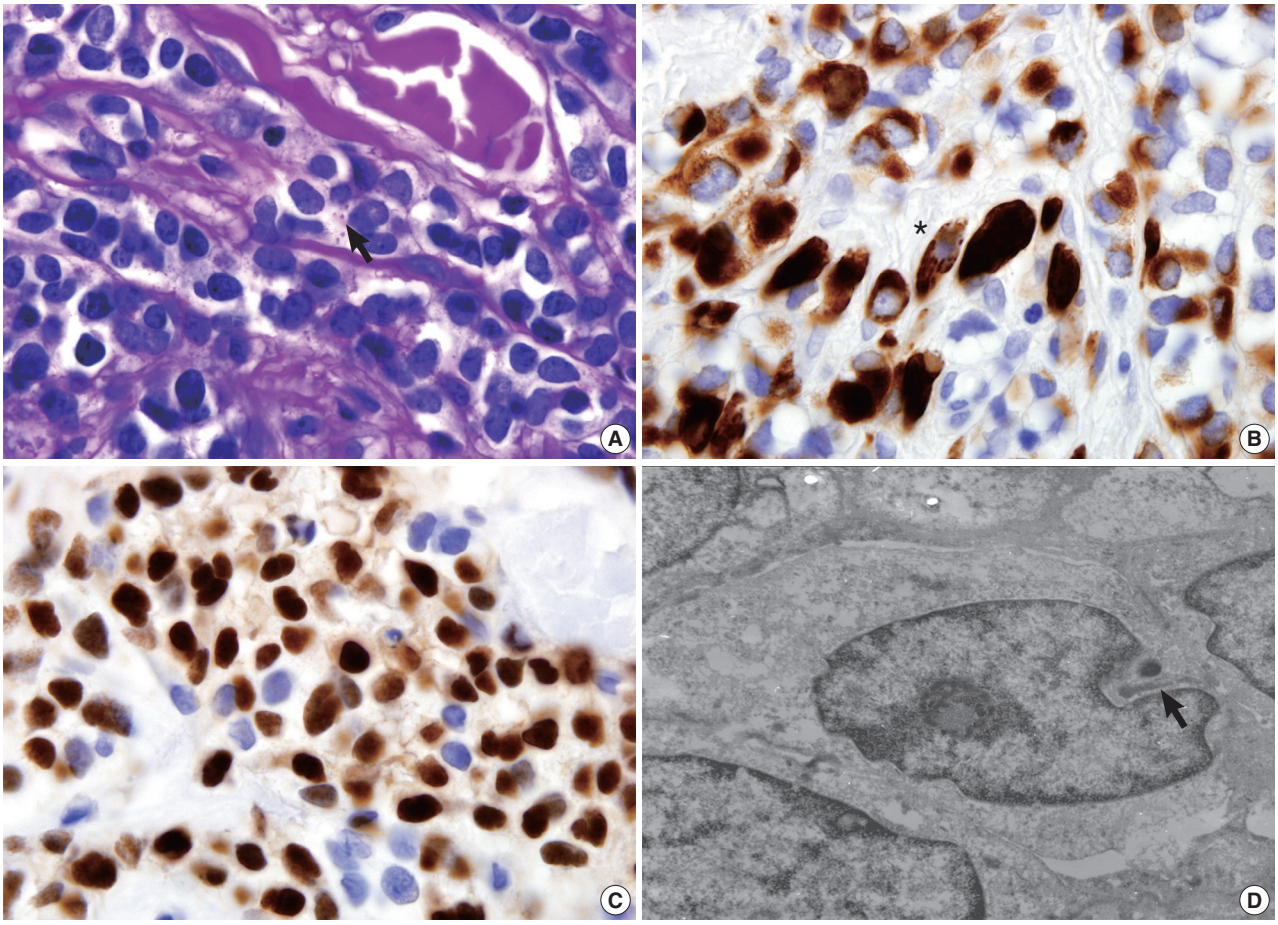

Fig. 2. (A) Periodic acid–Schiff stain shows a few glycogen particles in the cytoplasm (arrow). (B) The cytoplasm is intensively immunoreactive for desmin, and a tumor cell shows striation-like features in the cytoplasm (asterisk). (C) The nuclei are positive for myogenin immunohistochemical stain. (D) Ultrastructurally, the tumor cell shows intracytoplasmic filaments (arrow) (×60,000).

Table 1. Clinicopathologic features of rhabdomyosarcoma of the lip

Author	Year	Age	Sex	Site	Duration	Size (cm)	Type	Treatment	Recurrence/Metastasis/Follow-up (mo)
Smith[3]	1962	49 yr	M	L	8 wk	NA	E	S	–/–/NA
Piattelli[4]	1991	Adult	NA	U	NA	NA	P	NA	NA/NA/NA
D'Amico *et al.*[5]	1996	8 mo	M	U	7 mo	0.8	A	S, C	–/+ (cervical LN, salivary gland)/alive (NA)
Brecher *et al.*[6]	2003	2 wk	M	U	Congenital	4.2	A	S, C	–/–/alive (6)
Seth and Kempert[7]	2004	3 yr	F	L	Congenital	1.5	E	S, C	–/–/alive (60)
Marburger *et al.*[8]	2012	3 yr	M	NA	NA	NA	A	C	–/–/alive (71)
Dhull[9]	2012	5 yr	F	U	3 mo	10	A	R, C	–/–/alive (6)
Singh *et al.*[10]	2013	11 day	NA	U	Congenital	5	E	C	–/+ (bone, lung)/dead of disease (3)
Present case	2014	58 yr	F	U	Few mo	0.7	A	S, C	–/–/alive (3)

L, lower lip; M, male; NA, not available; E, embryonal rhabdomyosarcoma; S, surgical treatment; U, upper lip; P, pleomorphic rhabdomyosarcoma; A, alveolar rhabdomyosarcoma; C, chemotherapy; LN, lymph node; F, female; R, radiotherapy.

Rhabdomyosarcoma with clear cell features has been rarely described in the English literature.[12,13] The clear or vacuolated cytoplasm visible on light microscopy is due to lipid droplets or glycogen particles on electron microscopy. Lipid-rich rhabdomyosarcoma resembles liposarcoma but the tumor cells are immunoreactive to muscle-specific markers such as desmin and myogenin. Variable amounts of glycogen can be observed in rhabdomyosarcoma and can be demonstrated with periodic acid–Schiff stain. The clear cell change itself obscures the definitive diagnosis of rhabdomyosarcoma especially when the clear

cell features are dominant within the tumor. Tumors presenting as a dermal or subcutaneous nodule, which can show clear cytoplasm, are diverse and include balloon cell nevus, balloon cell melanoma, clear-cell sarcoma, Paget's disease, clear-cell basal cell carcinoma, clear-cell syringoid tumors, clear-cell hidradenoma/hidradenocarcinoma, trichilemmoma/trichilemmocarcinoma, sebaceous neoplasm, lipoma/liposarcoma, cutaneous metastasis from renal cell carcinoma and clear-cell dermatofibroma.[14]

Recently, a great advance in the ability to distinguish each of the subtypes of rhabdomyosarcoma has been demonstrated.[11] In alveolar rhabdomyosarcoma, reciprocal translocation of t(2;13)(q35;q14) and t(1;13)(p36;q14) and their associated fusions were identified. In embryonal rhabdomyosarcoma, chromosomal losses (chromosome 9 and 10) and gains (chromosome 8, 2, 7, 11, 12, 13, and 20) occur, as do allelic losses and mutations. Chimeric proteins from the fusion of PAX3 or PAX7 with FOXO1 are expressed in most alveolar rhabdomyosarcoma cases, resulting in the worse prognosis with this subtype.

Due to the rarity of this tumor, the diagnosis of adult rhabdomyosarcoma with clear cell features in the lip may be challenging in daily practice of surgical pathology. If the diagnosis of rhabdomyosarcoma is made in a lip biopsy, clinical investigation should be performed to eliminate the possibility of metastasis from other primary sites. Complete surgical excision and close follow-up are needed because of the possibility of metastasis.

Conflicts of Interest

No potential conflict of interest relevant to this article was reported.

REFERENCES

1. Weiss SW, Goldblum JR, Enzinger FM. Enzinger and Weiss's soft tissue tumors. 5th ed. Philadelphia: Mosby Elsevier, 2008.
2. Jung WH, Kim YJ, Jung SH, Yim H, Yoo CJ. Rhabdomyosarcoma in children: histologic subtypes and prognosis. Korean J Pathol 1992; 26: 573-81.
3. Smith JF. Rhabdomyosarcoma of the lower lip. Oral Surg Oral Med Oral Pathol 1962; 15: 454-7.
4. Piattelli A. Pleomorphic rhabdomyosarcoma of the upper lip in an adult patient: report of a case and review of the literature. Acta Stomatol Belg 1991; 88: 57-64.
5. D'Amico AV, Goldwein J, Womer R. Alveolar rhabdomyosarcoma of the lip in an infant. Med Pediatr Oncol 1996; 26: 409-13.
6. Brecher AR, Reyes-Mugica M, Kamino H, Chang MW. Congenital primary cutaneous rhabdomyosarcoma in a neonate. Pediatr Dermatol 2003; 20: 335-8.
7. Seth T, Kempert P. Embryonal rhabdomyosarcoma of lower lip. Ind Pediatr 2004; 41: 858-9.
8. Marburger TB, Gardner JM, Prieto VG, Billings SD. Primary cutaneous rhabdomyosarcoma: a clinicopathologic review of 11 cases. J Cutan Pathol 2012; 39: 987-95.
9. Dhull AK. Primary alveolar rhabdomyosarcoma: a horrendous presentation with miraculous remission. BMJ Case Rep 2012; 2012: bcr2012007657.
10. Singh GB, Arora R, Kumar D, Jain M, Puri V. A rare case of congenital rhabdomyosarcoma with review of the literature. Case Rep Otolaryngol 2013; 2013: 518952.
11. Parham DM, Barr FG. Classification of rhabdomyosarcoma and its molecular basis. Adv Anat Pathol 2013; 20: 387-97.
12. Bégin LR, Schürch W, Lacoste J, Hiscott J, Melnychuk DA. Glycogen-rich clear cell rhabdomyosarcoma of the mediastinum: potential diagnostic pitfall. Am J Surg Pathol 1994; 18: 302-8.
13. Ahmed AA, Tsokos M. Sinonasal rhabdomyosarcoma in children and young adults. Int J Surg Pathol 2007; 15: 160-5.
14. Lázaro-Santander R, Andrés-Gozalbo C, Rodríguez-Pereira C, Vera-Román JM. Clear cell atypical fibroxanthoma. Histopathology 1999; 35: 484-5.

 http://dx.doi.org/10.4132/jptm.2014.06.03

Journal of Pathology and Translational Medicine 2015; 49: 85-88
http://dx.doi.org/10.4132/jptm.2014.10.28

■ BRIEF CASE REPORT ■

Squamous Cell Carcinoma of the Seminal Vesicle from Zinner Syndrome: A Case Report and Review of Literature

Younghoon Kim · Hae Woon Baek · Eunoh Choi · Kyung Chul Moon

Department of Pathology, Seoul National University College of Medicine, Seoul, Korea

Until now, fewer than 60 cases of tumors originating from the seminal vesicle have been reported. Most of them were adenocarcinoma, cystadenoma, and benign mesenchymal tumor.[1] Among them, only three cases in the English literature have been reported as squamous cell carcinoma.[2-4] Although all three cases had a prolonged history of stone formation or chronic inflammation, none of them were associated with congenital malformation of the urogenital system such as Zinner syndrome. Zinner syndrome is a rare Müllerian duct abnormality consisting of unilateral renal agenesis, ipsilateral seminal vesicle cyst, and ejaculatory duct obstruction. Herein, we report a 41-year-old male with Zinner syndrome, who developed a poorly differentiated squamous cell carcinoma of the seminal vesicle as a result of prolonged inflammation.

CASE REPORT

A 41-year-old male was admitted to our hospital due to gross hematuria for two and a half months. Twelve years previous, the patient underwent transurethral resection, suprapubic cystostomy, and urethral sounds to cure a right seminal vesicle cyst with multiple stones and obstruction of the right ejaculatory duct. At that time, a biopsy diagnosed the seminal vesicle cyst as an epidermal cyst, a benign cyst lined with a thin layer of squamous epithelium. A week after his current admission, perineal and scrotal pains newly developed. Digital rectal examination detected tenderness with a hard and highly elevated posterior prostate compressing the rectal wall. No prostate-specific antigen elevation was detected and urine cytology was negative for malignant cells. Computed tomography (CT) urography revealed hypoplastic change in the right kidney, a 4.9-cm-sized right seminal vesicle cyst with a thickened wall, and benign prostate hyperplasia (Fig. 1A). The patient was diagnosed with Zinner syndrome with a seminal vesicle cyst. Transrectal sonography detected a 3.8-cm-sized hypoechoic lesion at the left transitional zone of the prostate showing a bulging contour and prominent vascularity, which favored chronic prostatitis over malignancy. Treatment included not only palliative medication but also aggressive procedures such as nerve blocking for pain control. Six months after the initial onset of gross hematuria, another transrectal biopsy was done and the specimen was pathologically diagnosed as poorly differentiated carcinoma. CT urography and magnetic resonance imaging demonstrated a bulging mass at the left prostate gland, which had increased in size compared with images taken three months previous (Fig. 1B). The mass showed signs of internal necrosis and anorectal adhesion, but did not show anorectal invasion. A 4.7-cm-sized seminal vesicle cyst at the right side and necrotic lymph nodes at the left external iliac area were also observed. Through surgery, the urinary bladder, prostate, and bilateral seminal vesicles were removed *en bloc*. On gross examination, the specimen consisted of an 11.0×6.0×5.0-cm-sized multinodular mass with a tan-white cut surface accompanied by hemorrhage and necrosis. Adjacent to the tumor, the seminal vesicle cyst had a smooth mucosa measuring 5.0×3.0 cm. Under the microscope, squamous metaplasia was observed in the seminal vesicle cyst lining (Fig. 2A). Microscopically observed, the tumor was a poorly differentiated car-

Corresponding Author
Kyung Chul Moon, M.D.
Department of Pathology, Kidney Research Institute, Medical Research Center, Seoul National University College of Medicine, 103 Daehak-ro, Jongno-gu, Seoul 110-799, Korea
Tel: +82-2-2072-1767, Fax: +82-2-743-5530, E-mail: blue7270@snu.ac.kr

Received: June 30, 2014 **Revised:** October 22, 2014
Accepted: October 24, 2014

pISSN 2383-7837
eISSN 2383-7845

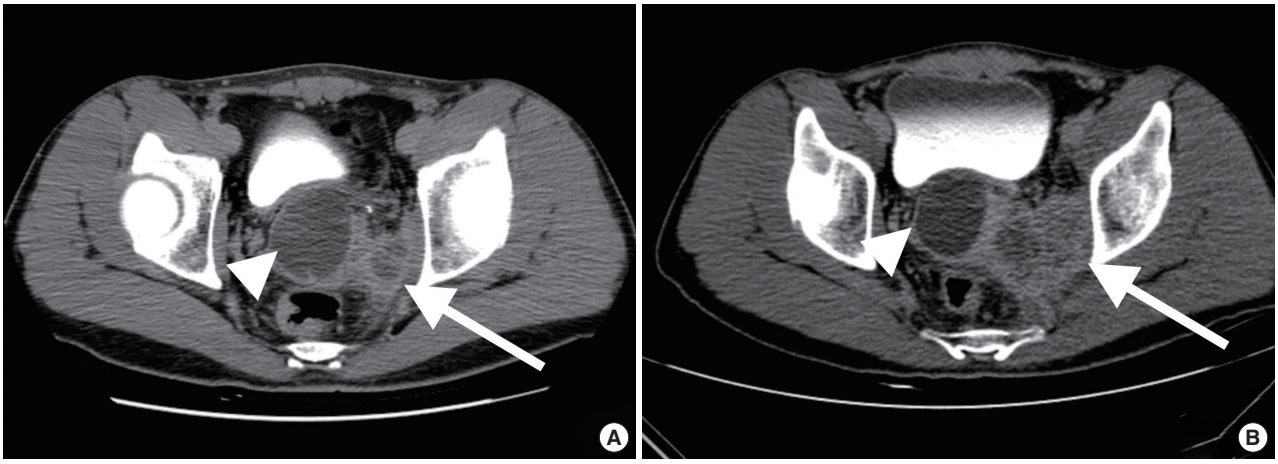

Fig. 1. Computed tomography urography. (A) Images taken three months before the surgery demonstrate a 4.9-cm-sized right seminal vesicle cyst (arrowhead) and an exophytic tumor measuring up to 3 cm (arrow). (B) Images taken three months later show a 4.7-cm-sized seminal vesicle cyst (arrowhead) with an enlarged mass (arrow) bulging to the left prostate gland (6.1 cm).

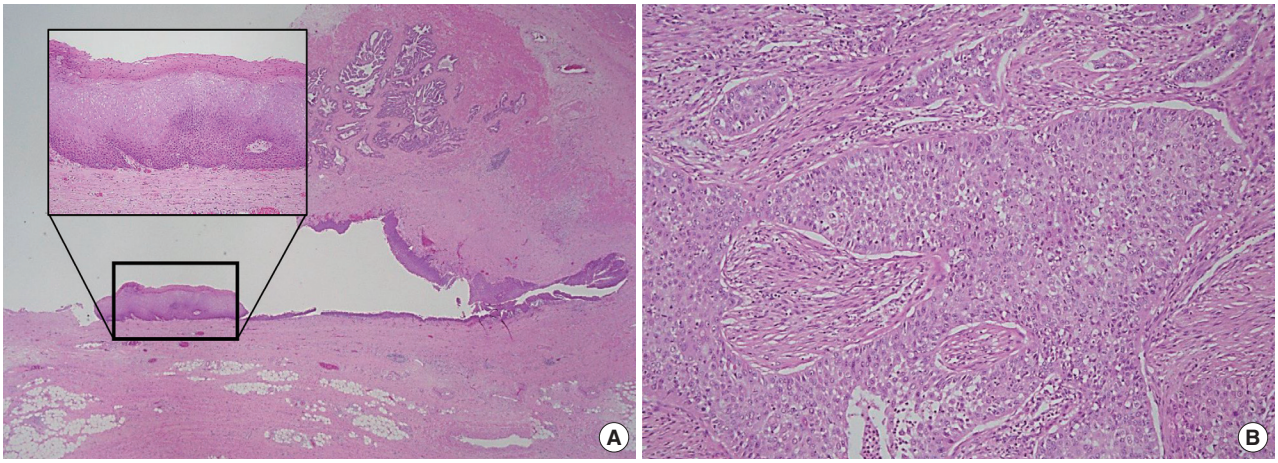

Fig. 2. Histopathologic findings of the right seminal vesicle cyst. The specimen shows squamous metaplasia (insert), glandular tissues (A), and a poorly differentiated carcinoma (B).

cinoma (Fig. 2B). Immunohistochemical analysis of the tumor was positive for p63 (Fig. 3A) and negative for cytokeratin 7 (Fig. 3B), cytokeratin 20 (Fig. 3C), and carcinoembryonic antigen (Fig. 3D). Although the specimen displayed some immunoactivity for vimentin (Fig. 3E), the staining was positive in macrophages, as reported in murine seminal vesicle carcinoma.[5] Histochemical studies (periodic acid–Schiff [PAS] and mucicarmine) were positive for mucin (Fig. 3F). The tumor was pathologically diagnosed as poorly differentiated squamous cell carcinoma arising from the seminal vesicle cyst. The involvement of carcinoma was detected in rectal and right ureter tissues, but no lymph node metastasis was observed. The postoperative course had no further events. The patient was discharged and scheduled for adjuvant concurrent chemoradiation therapy.

DISCUSSION

Our patient suffered from Zinner syndrome, a male counterpart of Mayer-Rokitansky-Küster-Hauser (MRKH) syndrome which occurs in females. MRKH syndrome is reportedly associated with ovarian cancer and renal cell carcinoma in the genitourinary tract.[6,7] Two cases of adenocarcinoma arising from a seminal vesicle cyst in Zinner syndrome patients have been previously reported.[8,9] Table 1 summarizes those cases as well as the present case.

In the current case, no diagnostic tool was able to detecting the hidden malignancy until the inflammation subsided. Moreover, poorly differentiated and wide-spread features of the malignancy made it difficult to determine the exact origin of the

http://dx.doi.org/10.4132/jptm.2014.10.28

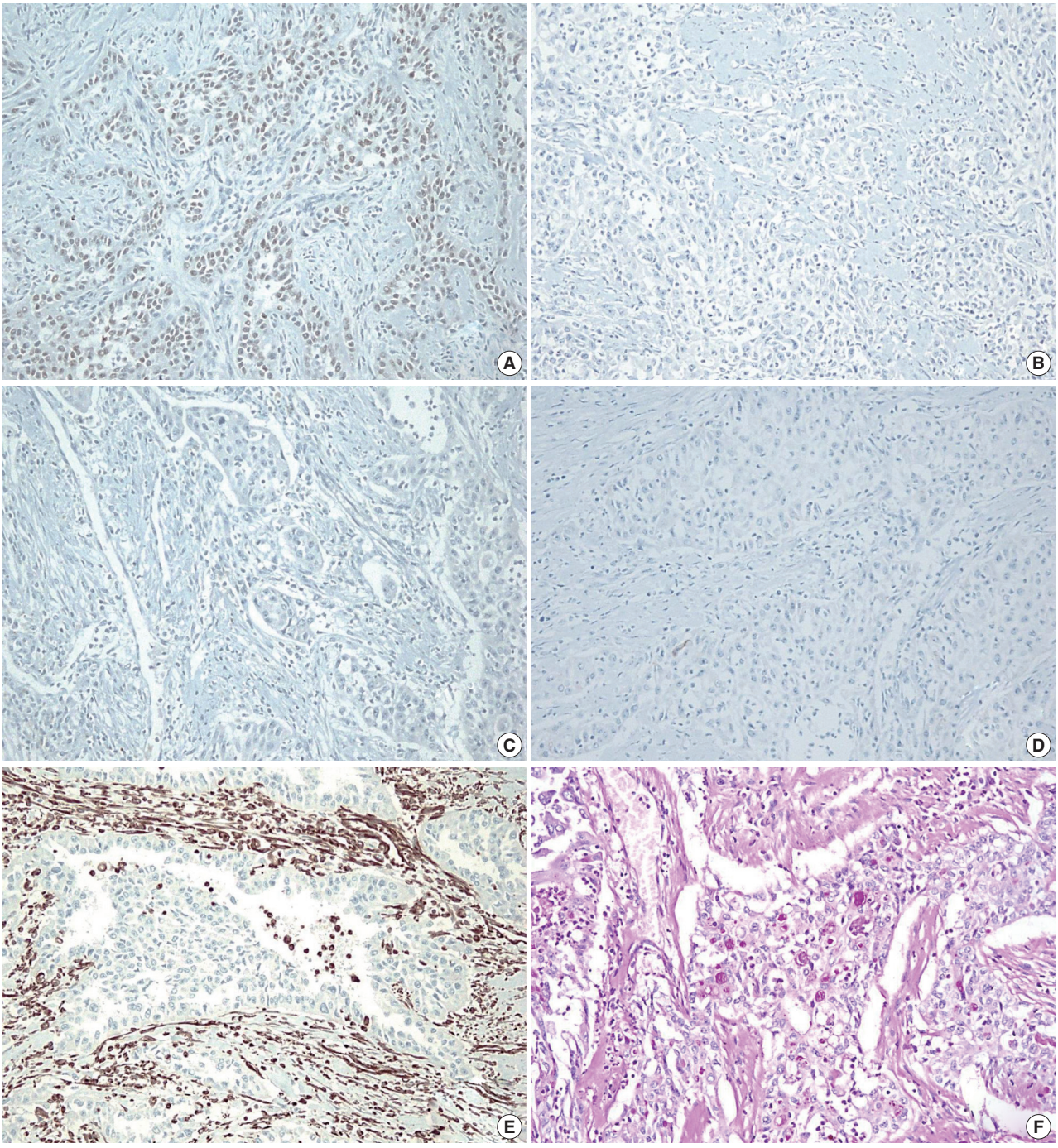

Fig. 3. Immunohistochemistry and histochemical staining for phenotyping of the carcinoma. Tumor cells are positive for p63 (A), and negative for cytokeratin 7 (B), cytokeratin 20 (C), and carcinoembryonic antigen (D). Vimentin shows focal positivity in macrophages (E), and periodic acid–Schiff staining is positive for mucin (F).

tumor before surgery. In this case, squamous metaplasia was pathologically proven 12 years prior to the discovery of the malignancy, which clarifies the origin of the tumor. By contrast, in all three previously reported cases of squamous carcinoma arising from the seminal vesicle, squamous metaplastic foci were diagnosed simultaneously with the carcinoma.[2-4] Although tumor cells in the present case were positive for mucin in PAS and mucicarmine staining, it is not uncommon for a squamous cell carcinoma to express mucin content.[10]

To the best of our knowledge, this is the first report of a squa-

Table 1. Summary of reported cases of carcinomas arising from a seminal vesicle cyst in Zinner syndrome patients

	Okada *et al.* (1992)[8]	Lee *et al*. (2007)[9]	Present case
Age (yr)	17	41	41
Chief complaint	Lower abdominal mass and dysuria	Hematuria	Hematuria
Past medical history	None	Prostatitis	Squamous metaplasia, stone formation and chronic inflammation of the seminal vesicle
Seminal vesicle cyst detection	Latest admission	Latest admission	Twelve years ago
Location	Right seminal vesicle cyst	Left seminal vesicle cyst	Right seminal vesicle cyst
Pathologic diagnosis	Papillary adenocarcinoma	Mucinous adenocarcinoma	Poorly differentiated squamous cell carcinoma
Prostate-specific antigen	Normal	Normal	Normal

mous cell carcinoma of the seminal vesicle developed in a Zinner syndrome patient. Our case indicates that long-term observation and thorough evaluation are mandatory for patients with Zinner syndrome expressing nonspecific but rapid and progressive urogenital symptoms.

Conflicts of Interest

No potential conflict of interest relevant to this article was reported.

REFERENCES

1. Lorber G, Pizov G, Gofrit ON, Pode D. Seminal vesicle cystadenoma: a rare clinical perspective. Eur Urol 2011; 60: 388-91.
2. Tabata K, Irie A, Ishii D, Yanagisawa N, Iwamura M, Baba S. Primary squamous cell carcinoma of the seminal vesicle. Urology 2002; 59: 445.
3. Yanagisawa N, Saegusa M, Yoshida T, Okayasu I. Squamous cell carcinoma arising from a seminal vesicular cyst: possible relationship between chronic inflammation and tumor development. Pathol Int 2002; 52: 249-53.
4. Wang J, Yue X, Zhao R, Cheng B, Wazir R, Wang K. Primary squamous cell carcinoma of seminal vesicle: an extremely rare case report with literature review. Int Urol Nephrol 2013; 45: 135-8.
5. Shoda T, Mitsumori K, Imazawa T, *et al.* A spontaneous seminal vesicle adenocarcinoma in an aged F344 rat. Toxicol Pathol 1998; 26: 448-51.
6. Ghirardini G, Magnani A. Mayer-Rokitansky-Küster-Hauser syndrome and ovarian cancer: report of a case. Clin Exp Obstet Gynecol 1995; 22: 247-8.
7. Mermerkaya M, Burgu B, Hamidi N, *et al.* Mayer-Rokitansky-Küster-Hauser syndrome accompanied by renal cell carcinoma: a case report. J Pediatr Hematol Oncol 2013; 35: e309-10.
8. Okada Y, Tanaka H, Takeuchi H, Yoshida O. Papillary adenocarcinoma in a seminal vesicle cyst associated with ipsilateral renal agenesis: a case report. J Urol 1992; 148: 1543-5.
9. Lee BH, Seo JW, Han YH, Kim YH, Cha SJ. Primary mucinous adenocarcinoma of a seminal vesicle cyst associated with ectopic ureter and ipsilateral renal agenesis: a case report. Korean J Radiol 2007; 8: 258-61.
10. Ocque R, Tochigi N, Ohori NP, Dacic S. Usefulness of immunohistochemical and histochemical studies in the classification of lung adenocarcinoma and squamous cell carcinoma in cytologic specimens. Am J Clin Pathol 2011; 136: 81-7.

 http://dx.doi.org/10.4132/jptm.2014.10.28

Journal of Pathology and Translational Medicine 2015; 49: 89-91
http://dx.doi.org/10.4132/jptm.2014.10.07

■ BRIEF CASE REPORT ■

Biliary Granular Cell Tumor

Changwon Jung · Ilyeong Heo · Sang Bum Kim[1] · Sunhoo Park · Soo Youn Cho

Departments of Pathology and [1]Surgery, Korea Cancer Center Hospital, Korea Institute of Radiological and Medical Sciences, Seoul, Korea

Granular cell tumor (GCT) is a benign neoplasm showing neuroectodermal differentiation and is most commonly found in the head and neck region, including the tongue.[1] This tumor is now believed to occur in virtually any site of the body, including skin, breast, and gastrointestinal tract, with less than 1% developing in the biliary tract.[2] To our knowledge, only one case of GCT of the biliary tract has been reported in Korea, which occurred in the gallbladder.[3] Herein, we present another case of GCT of the biliary tract.

CASE REPORT

A 62-year-old female was referred to our hospital for management of gastric adenocarcinoma that had been found during a periodic health examination. She had been receiving treatment for hypertension and diabetes mellitus for 20 years. Abdominal computed tomography for a diagnostic workup revealed focal dilatation of the right posterior hepatic duct, and subsequent imaging with magnetic resonance imaging and magnetic resonance cholangiopancreatography showed a stricture at the right hepatic duct (Fig. 1A). Laboratory findings were unremarkable.

Under the presumptive diagnosis of synchronous cholangiocarcinoma and gastric carcinoma, she underwent hepatic right lobectomy with radical subtotal gastrectomy. On a resected specimen, a 0.9×0.4 cm sized, ill-defined, nonencapsulated tumor was noted in the extrahepatic portion of the right hepatic duct (Fig. 1B). The bile duct mucosa was grossly intact, and the tumor was located in the submucosal layer. The cut surface of the tumor was gray to whitish, solid, firm, and infiltrative (Fig. 1C). The margins were clear on frozen biopsy. On microscopic examination, the tumor was composed of large polygonal cells with abundant eosinophilic granular cytoplasm, and the nuclei were small, dark, uniform, and centrally located (Fig. 2A, B). The overlying mucosa was atrophic and showed autolysis (Fig. 2A). The tumor cells were diffusely positive for periodic acid-Schiff (PAS), CD68, and S100 protein (Fig. 2C). A diagnosis of GCT was made. The stomach tumor was papillary adenocarcinoma (pT1N0Mx). The patient remains healthy at 20 months after the resection, without any signs of complication.

DISCUSSION

The first case of GCT was reported by Abrikossoff in 1926 in the skeletal muscle of the tongue.[4] Since then, there have been some discrepancies regarding the origin of GCT based on histologic and immunohistochemical findings, including myogenic, histiogenic, neurogenic, and multicentric histogeneses.[5] The exact histogenesis is still unclear, but a neural origin, more specifically Schwannian type neuroectodermal origin, is favored by many authors[1,5,6] because the tumor cells show positivity for S100 protein, which is normally found in the central nervous system and peripherally in Schwann cells.[6,7]

GCT has a distinct histological appearance, being composed of polygonal eosinophilic cells that contain cytoplasmic granules strongly reactive to PAS. The cells also contain small, central, and vesicular nuclei, appear as clusters or sheets, and infiltrate diffusely within the surrounding structures. They commonly show perineural infiltration that might lead to local recurrence after incomplete excision. Immunohistochemically, these tumor cells show positivity for S100 protein, neuron-specific enolase, vimentin, and various other Schwann-cell–related antigens. Mitosis and necrosis are rarely noted. There have been some

Corresponding Author
Soo Youn Cho, M.D.
Department of Pathology, Korea Cancer Center Hospital, Korea Institute of Radiological and Medical Sciences, 75 Nowon-ro, Nowon-gu, Seoul 139-706, Korea
Tel: +82-2-970-2545, Fax: +82-2-970-2430, E-mail: pathsycho@naver.com

Received: August 31, 2014 **Revised:** October 4, 2014
Accepted: October 7, 2014

pISSN 2383-7837
eISSN 2383-7845

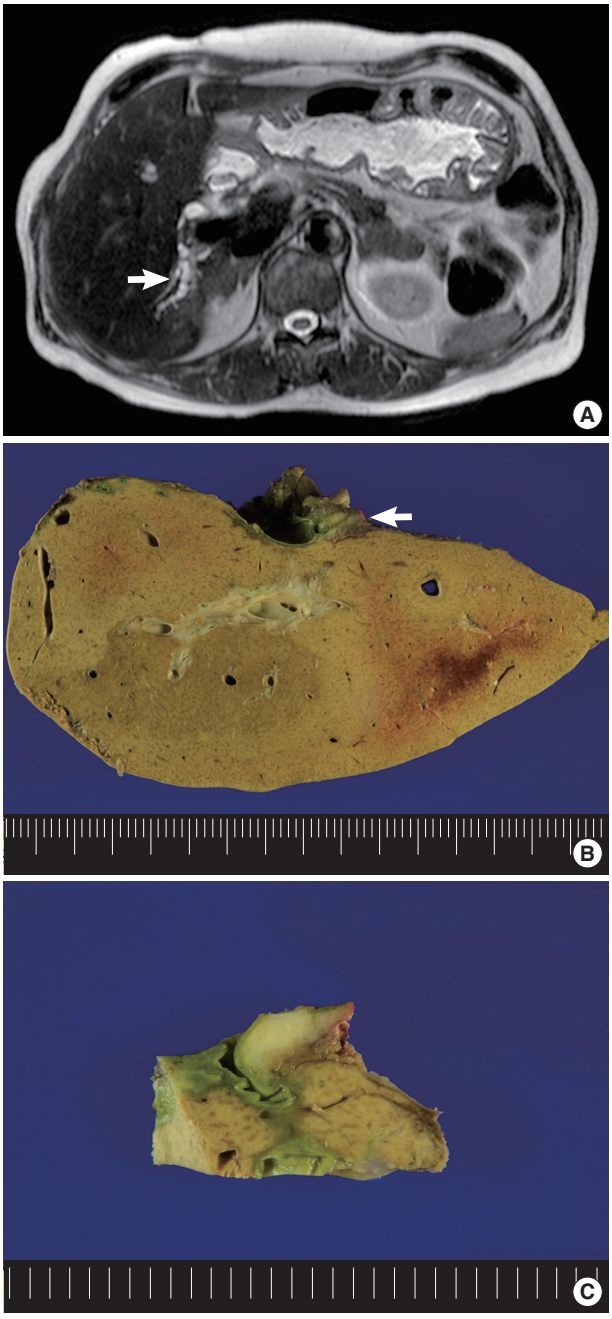

Fig. 1. (A) Magnetic resonance imaging shows focal dilation of the intrahepatic bile duct in the right posterior segment (arrow) with atrophy. (B) The specimen shows a small tumor in the extrahepatic portion of the right hepatic duct (arrow) and dilated intrahepatic bile ducts. (C) A whitish infiltrative tumor is noted in the submucosal layer of the bile duct.

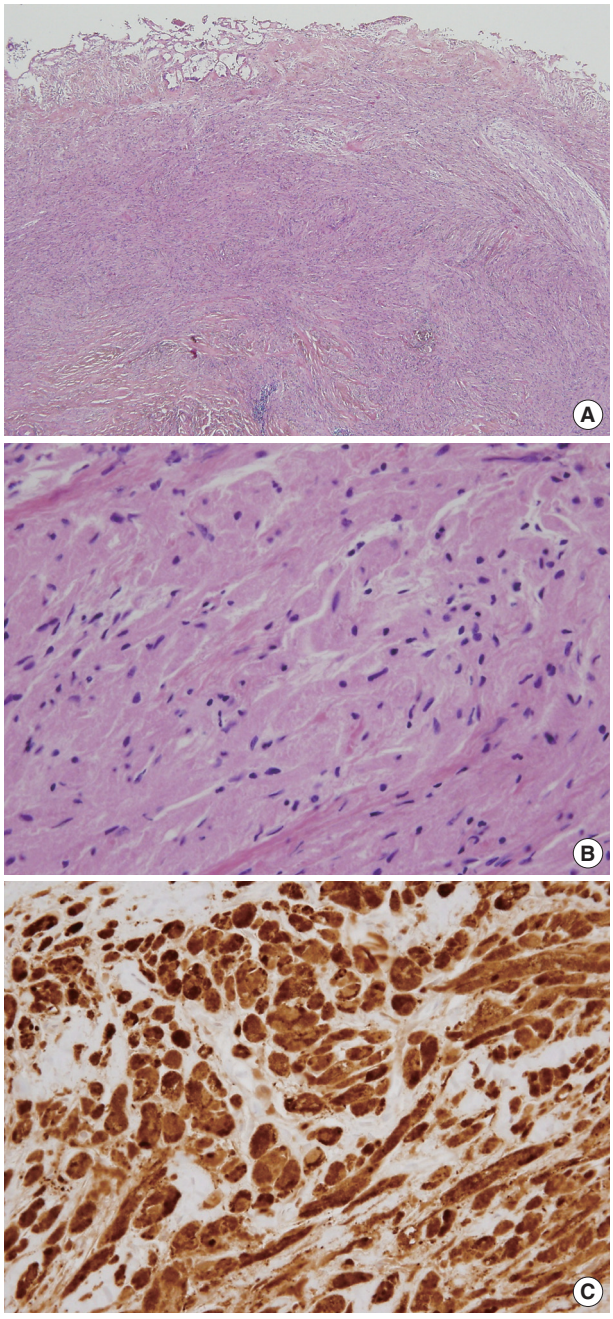

Fig. 2. Histologic findings of the tumor. (A) Diffuse, infiltrative tumor is noted in the submucosa of the bile duct. (B) The large tumor cells show eosinophilic granular cytoplasm. (C) The tumor cells are strongly positive for S100 protein.

reports of malignant GCT; however, there is no report of malignant biliary tract GCT to date.

GCT can develop at any age but is more prevalent in the fifth and sixth decades and shows a slight male predominance. It is typically solitary and smaller than 3 cm in diameter. GCT has been found in almost every part of the body, with the head and neck region being the most commonly affected site, accounting for 45%–65% of cases.[1]

GCT of the biliary tract is very rare, with the first case reported by Coggins in 1952 during autopsy.[8] Since then, 81 cas-

http://dx.doi.org/10.4132/jptm.2014.10.07

es of biliary tract GCT have been reported in the English literature, with only one case reported in a Korean patient. Among reported cases, including our case (n = 82), about 52% (n = 43) of the biliary tract GCT has been observed in black women with a median age of 34 years (range, 14 to 91 years). Interestingly, GCT of the biliary tract is more prevalent in slightly younger age and females (female to male ratio, 5.3:1). The younger age at presentation might reflect a spatial problem due to a narrow lumen of the biliary tract. In the literature review, most patients have complained of jaundice (44.4%), abdominal pain (34.6%), or both (11.1%).[7,9,10] There have been two cases that required liver transplantation due to secondary biliary cirrhosis. In our case, the tumor was incidentally detected during the stage workup for gastric cancer.

Many patients are clinically and radiologically suspected for cholangiocarcinoma preoperatively; thus, they tend to undergo extensive procedures such as Whipple's operation. However, GCT is almost always benign and can usually be cured by complete excision alone, which is associated with a generally good prognosis. Biliary tract GCT can also be treated with surgical excision with tumor-free margins followed by hepaticojejunostomy.

In summary, biliary GCT can cause symptoms related to biliary obstruction and might present with a clinical impression of cholangiocarcinoma. Thus, GCT should be included in the differential diagnosis of biliary tract tumors, even though the incidence is extremely low.

Conflicts of Interest

No potential conflict of interest relevant to this article was reported.

REFERENCES

1. Fletcher CD, Bridge JA, Hogendoorn P, Mertens F. WHO classification of tumours of soft tissue and bone. 4th ed. Lyon: IARC Press, 2013.
2. Karakozis S, Gongora E, Zapas JL, He P, Krishnan J, Kirkpatrick JR. Granular cell tumors of the biliary tree. Surgery 2000; 128: 113-5.
3. Kim DK, Jung YK, Chung DH, *et al.* Granular cell tumor originating from gallbladder. Korean J Med 2012; 83: 624-8.
4. Abrikossoff A. About myomas originating from striated musculature. Virchows Arch A Pathol Anat 1926; 260: 215-33.
5. Caputo R, Bellone AG, Tagliavini R. Ultrastructure of the granular cell myoblastoma: so-called Abrikossoff's tumor. Arch Dermatol Forsch 1972; 242: 127-36.
6. Le BH, Boyer PJ, Lewis JE, Kapadia SB. Granular cell tumor: immunohistochemical assessment of inhibin-alpha, protein gene product 9.5, S100 protein, CD68, and Ki-67 proliferative index with clinical correlation. Arch Pathol Lab Med 2004; 128: 771-5.
7. Patel AJ, Jakate SM. Granular cell tumor of the biliary tract. Gastroenterol Hepatol (N Y) 2010; 6: 331-6.
8. Coggins RP. Granular-cell myoblastoma of common bile duct: report of a case with autopsy findings. AMA Arch Pathol 1952; 54: 398-402.
9. Bilanović D, Borićić I, Zdravković D, Randjelović T, Stanisavljević N, Toković B. Granular cell tumor of the common hepatic duct presenting as cholangiocarcinoma and acute acalculous cholecystitis. Acta Chir Iugosl 2008; 55: 99-101.
10. Saito J, Kitagawa M, Kusanagi H, *et al.* Granular cell tumor of the common bile duct: a Japanese case. World J Gastroenterol 2012; 18: 6324-7.